Aromaticity, Transport and Spin Filter Properties of A Few Molecular Systems

A thesis submitted in partial fulfilment for the degree of

Master of Science

as a part of the

Integrated Ph.D. Programme

(Materials Science)

By

Dibyajyoti Ghosh

Molecules to Materials Laboratory
Theoretical Science Unit
Jawaharlal Nehru Centre for Advanced Scientific Research
(A Deemed University)
Bangalore, India.

Dedicated to My Family

Declaration

I hereby declare that the matter embodied in the thesis entitled "***Aromaticity, Transport and Spin Filter Properties of a Few Molecular Systems***" is the result of investigations carried out by me at the Theoretical Sciences Unit, Jawaharlal Nehru Centre for Advanced Scientific Research, Bangalore, India under the supervision of Prof. Swapan K. Pati and that it has not been submitted elsewhere for the award of any degree or diploma.

_____

Dibyajyoti Ghosh

Certificate

I hereby certify that the matter embodied in this thesis entitled "***Aromaticity, Transport and Spin Filter Properties of a Few Molecular Systems***" has been carried out by Mr. Dibyajyoti Ghosh at the Theoretical Sciences Unit, Jawaharlal Nehru Centre for Advanced Scientific Research, Bangalore, India under my supervision and that it has not been submitted elsewhere for the award of any degree or diploma.

_____

Prof. Swapan K. Pati

Acknowledgments

"**In three words I can sum up everything I've learned about life: it goes on**."
Robert Frost.

Probably, we can't define life better. And in our journey of life we come across some special people who influence us in more ways than one and help us to go ahead by overcoming the hardships. I want to thank them all for being beside me and I take the M.S. thesis as an opportunity to acknowledge their support.

Of all, I want to express my wholehearted love and respect to my parents, without whom I wouldn't have been who I am. They are the constant source of inspiration and motivation for me and helped me in being a good human being. I am fortunate enough to get my elder sister as my best friend, who knows me more than anyone else. From her I learnt to handle problems of life with a smiling face.

This thesis could not have been written without my supervisor Prof. Swapan K. Pati, who not only guided me through the scientific problems but have also been of constant support, encouragement and enthusiasm whenever I needed. His deep love for science motivates me to serve science throughout my life. He has taken pain to go through the project and make necessary correction as and when needed. I also thank Anusooya Ma'am for her love and affection. Sir and Ma'am never allowed me to feel that I am far away from home. I will always remember the weekend parties at their place.

I thank all my course instructors in JNCASR for the brilliant teaching.

I am grateful to my high school and undergraduate teachers to help me in understanding the basics of science and clarifying my doubts.

It is an honor for me to thank Prof. Anna Painelli for her guidance during a month long project in Italy. I also acknowledge her student Dr. Cristina who tried her best to make our stay in Italy comfortable.

I am thankful to all my present and past lab mates, Dr. Sasmita, Prakash, Arun, Alex, Ershaad, Pralok, Dr. Siam, Dr. Ganga, Dr. Meera, Sharma, Wasim Aftab, Wasim Raja, Pallavi, Somananda, Swastika, Arkamita, Bradraj, Nabanita, Divya and Anisha for creating a scientific atmosphere in the lab. Scientific discussions with them really helped me a lot to learn many basic things. I owe my special thanks to Dr. Ganga and Prakash

from whom I learnt how to tackle scientific problems and move forward in the field of research.

I would like to thank my Integrated PhD batch mates Prashant, Anindita, Ajmala and Darshana for their constant support and encouragement.

Thanks to all my friends, Migfar Bhai, Himadri, Sabyasachi, Pranab, Prakash K., Sudip, Partha, Arup, Gautam, Sananda, Debabrata, Suman, Sutapa, Arpan, Ritesh, Rana, Sudeshna, Gayatri, Chidambar, Sisir, Kaushik, Anirban, Ramana, Babru, Bivas, Amrit, Bharath, Dhanya, Srinu, Soumik, Jia, Sougata with whom I really enjoyed my stay here. I would like to thank all my college friends who made my college-life memorable. Special thanks to my closest friends, Javed, Sabina and Mostafizur who gave me moral support when I needed it the most.

I am also grateful to JNCASR for providing a world class environment to peruse research. I am thankful to all the administrative, technical, security, Complab and CCMS staff who try their best to make our life smooth at the campus.

Thank You All.

Synopsis

As low dimension materials exhibit a number of interesting phenomena, they have attracted huge attention of physicists, chemists, material scientists and nanotechnologists. Small aromatic organic molecules and organometallic sandwiched complexes are two important classes of these materials. Aromaticity is a key concept of physical organic chemistry but the main problem with this property is that it is a virtual quantity, not an observable one. Enormous efforts have been given to measure it based on several criteria, which arise essentially due to the presence of cyclic delocalization of π-electrons in the molecular structure. Presently, a considerable interest has been given to study the isoelectronic substitution effect in these aromatic molecules. As boron, nitrogen substituted polyaromatic hydrocarbon molecules can have a huge application in the field of optoelectronic and chemosensor materials, the study related to the effects of B, N substitution in these molecules have massive industrial importance. On the other hand, organometallic sandwiched complexes are quasi-one-dimensional compounds which can be used as an active component of spintronic devices. Half-metallicity which arise in some of these complexes, is a key property for a spintronics material. This thesis is mainly focused on three studies: firstly, boron and nitrogen substitution effects in four six-membered ring containing polyaromatic hydrocarbons, secondly, the nature of spin transports in iron-polyacene and in its BN-analogues and lastly, the structural, magnetic and transport behavior of lanthanide-based organometallic sandwiched complexes.

In this thesis, first chapter begins with a brief discussion about the materials under study. Here, a general introduction about polyaromatic hydrocarbons (PAHs), organometallic sandwiched complexes and lanthanide-based sandwiched complexes have been given. Next, various aromaticity criteria and their corresponding indices are explained briefly. After that, an overview about transport in nanoscale devices has been given. Next in line are the methods such as Density Functional Theory (DFT), quantum transport theory, which are used to calculate various properties of the materials, have been explored. This chapter is concluded with the outline of the rest part of thesis.

In the next chapter, we have studied the topological and local aromaticity of B, N substituted benzene, pyrene, chrysene, triphenylene and tetracene molecules. We have calculated nucleus-independent chemical shift (NICS), harmonic oscillator model of

aromaticity (HOMA), para delocalization index (PDI) and aromatic fluctuation index (FLU) to quantify aromaticity in terms of magnetic, structural and electronic criteria, respectively. We find that charge separations due to the introduction of heteroatoms not only reduce the local delocalization in the six member ring but also affect strongly the topological aromaticity. In fact the relative orders of the topological and local aromaticity strongly depend on the position of the heteroatoms in the structure. In general, more ring shared B, N containing molecules are less aromatic than the less ring shared B, N molecules. In addition, our results provide evidence that the structural stability of the molecule is dominated by the σ bonds rather than the π bonds.

In the third chapter, using density functional theory (DFT), we have investigated the structural, electronic and magnetic properties of infinite chain of Fe_n-bis(n-acene), and BN-analogue of it (Fe_n-bis(n-BNacene)). Our band structure calculations show that, the electronic structure of these two systems are quite dissimilar, i.e., [Fe_∞-bis(polyacene)] shows metallic behaviour while its BN-analogue is a robust half-metal. We have also studied the transport characteristic of finite size Fe_3-bis(3-BNacene) when coupled to gold electrodes on either side. From transport calculations, we predict that Fe_3-bis(3-BNacene) shows efficient spin filter behaviour, which possibly can have a huge application in spintronic devices.

In the last chapter, using density functional theory, the structural, electronic, magnetic and transport properties of [Er(COT)($CpMe_5$)] have been investigated for its possible applications in molecular spintronic devices. Systematic studies show that methyl ($-CH_3$) groups in the Cp ring induce the tilting in the structure. Computed tilting angle and ^1H NMR values are in good agreement with the corresponding experimental values. The charge transfer nature of this complex has proven by using localized natural orbital analysis, where charge transfer occurs from ligands to metal. This molecule is highly stable with paramagnetic spin-ground state of S=3/2, where three unpaired electrons are located at three Er *f*-orbitals, which remain deep inside the energy level. Focusing on transport property, when this molecule gets attached to gold electrodes through appropriate anchoring groups, explicitly shows spin polarized transport behavior in both zero and finite bias limit.

Table of Content

List of Figures

List of Tables

Chapter 1

Introduction

Low-dimensional materials have attracted a huge attention of chemists and physicists in recent years.[1, 2] The appearance of anomalous novel properties in these materials has made them very interesting to investigate. The main reason behind these properties is quantum confinement effects in the low dimension.[3-9] Actually, the motions of microscopic degrees of freedom such as electrons, phonons get constrained due to the reduced length scale for these materials. In such condition, electronic correlations and restricted boundary conditions introduce various exotic properties in these materials.[10-14] To explain these special features of low dimensional systems, one needs some approaches of physics which is different from the three dimensional one. In general, low dimensional systems are treated in fully quantum mechanical way to explain various effects such as Aharonov-Bohm effect[15], persistent currents[16], phase-coherent transport[17] etc. Very recently, metal-insulator transitions,[18] high temperature superconductivity[19, 20] and Kondo effect[21-24] in low dimensions also have created a huge curiosity among the scientists.

Researches on low-dimensional materials have got a huge acceleration with the advancement in the experimental techniques. Improvement in various experimental tools such as molecular beam epitaxy (MBE), scanning tunneling microscopy (STM)[25-27], mechanically controlled break junction[28, 29], atomic force microscopy (AFM)[30-34], transmission electron microscopy (TEM)[35, 36] and angle resolved photoemission spectroscopy (ARPES)[37, 38] have introduced highly sophisticated ways to fabricate and characterize the low-dimensional materials. In this thesis, we have focused on various

types of low-dimensional systems and explored a number of exciting properties which arise due to various kinds of interactions in low-dimensions.

In this general introductory chapter, we briefly discuss about various low-dimensional materials, characteristic properties of which are studied in this thesis. We also include a brief overview of the theoretical and computational methods which are used to study the typical properties of these materials. In this thesis, we mostly focus on the aromatic, electronic, magnetic and transport properties of different types of low-dimensional systems. In the following section, we provide a brief description of the low dimensional systems such as polyaromatic hydrocarbons (PAH), organometallic complexes and lanthanide-based sandwiched complexes, various properties of which have been explored in the thesis. In the following section, we have discussed several criteria of aromaticity and ways to calculate these. Next section is mainly devoted to a brief introduction of transport phenomena in low-dimensional systems. We conclude this chapter by giving a general introduction about the various methods used to calculate the desired properties.

1.1 Low Dimensional Systems

1.1.1 Polyaromatic Hydrocarbons (PAH)

According to National Research Council, "PAHs are neutral, nonpolar organic molecules that comprise two or more benzene rings arranged in various configurations." These compounds are usually hazardous for general health, which is found in petroleum and produced as by-products during fossil fuel utilization and conversion processes. Anxiety about PAHs firstly focused on their toxicity to cause cancer[39], but more recently, it has been discovered that they also interfere with hormone systems and cause fatal effects on reproduction as well as in immune systems.[40-42]

PAHs are pure hydrocarbons i.e. they do not contain any substituent or heteroatoms in their aromatic rings. Therefore, these are lipophilic in nature. Usually, PAHs consist of four-, five-, six- or seven-member rings, but those with five or six are most common[43]. PAHs, having up to six fused aromatic rings are considered as small PAHs while those with more number of rings one called as large PAHs. Although, PAHs

evidently are aromatic compounds, the degree of aromaticity can be different for each ring segment.[44-47] As an example, for anthracene, where three benzene rings are linearly fused, middle ring is far less aromatic than the terminal benzene rings.[48] Such kind of observations about aromatic nature of these compounds can't be explained using well-known Hückel's (4n+2) rule as this is strictly valid for monocyclic conjugated systems. A number of modifications to this rule have been done to extend it for PAHs.[49] A most successful rule among them is Clar's aromatic π-sextet rule [50-53] which states that "*the Kekulé resonance structure with the largest number of disjoint aromatic π-sextet, i.e. benzene-like moieties, is the most important for the characterization of the properties of polyaromatic hydrocarbons (PAHs).*"[53] Recent experimental studies on the delocalization of π-electrons in PAHs[54-56], valance bond-based calculation[57], theoretical magnetic shielding values[52] etc. extensively support the robustness of Clar's rule for PAHs. The isoelectronic substitutions in these molecules have a huge application in optoelectronics and chemosensing properties [58-62].

1.1.2 Organometallic Sandwiched Complexes

Organometallic sandwiched complexes are a special type of low-dimensional organometallic complexes, where metal atoms remain coordinated to two or more arene ligands. The heptacity (i.e. the number of contiguous atoms of the ligand that are bound to the metal) of these ligands can vary depending upon the metal atom sandwiched in the complex. Generally, *d*-block and *f*-block elements are used as metal-center for these complexes [63-65]. In the early 1950s, the discovery of ferrocene [Fe (η^5-C_5H_5)$_2$]

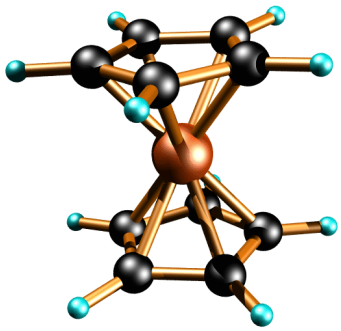

Figure 1.1: Structure of ferrocene molecule, the first discovered organometallic complex.

(see figure 1.1) is considered as the beginning of this field.[66] After that, a number of monometallic, dimetallic, multidecker complexes have been synthesized and characterized successfully.[67-71] One of the difficulties to grow pure cluster of these compounds was incorporation of solvent molecules in the structure. The advancement in laser vaporization, molecular beam methods provides a gentle solution to this problem by introducing gas-phase synthesis process of these complexes.[72-74]

The unique electrical, structural, magnetic and transport properties of these complexes created a considerable interest to explore these materials both experimentally and theoretically.[75-83] The appearance of half-metallicity (i.e. metallic behavior in one spin orientation and semiconducting/insulating in the other) in some of these clusters opens a huge possibility to use these materials as an active component in spintronic devices.[84-87] In spintronic device, spin dependent effects are used for information processing.[88, 89] These devices need materials where one should be able to control and manipulate spin degrees of freedom effectively.[90, 91] As half-metals have very large spin polarization at the Fermi level, it can be used as promising candidates for this purpose.

Another interesting property of these materials is spin-filter property.[90, 92-94] Theoretical investigations have shown that when these half-metallic sandwiched compounds are placed between two non-magnetic electrodes, only one type of spin (majority or minority spin) can migrate from one electrode to another at finite bias.[95-101] Interestingly, experimentally spin-filtering property has been demonstrated only at a very low temperature. But recent advancements in this field are quite promising to increase this critical temperature even up to room temperature.[93, 102]

1.1.3 Lanthanide-based Sandwiched Compounds

In these compounds, lanthanide atoms form coordination bonds with polyhapto anionic organic rings.[103-107] Lanthanides are 4*f*-block elements with electronic configuration $[Xe]4f^{1-14}5d^{0-1}6s^2$. Due to the large size of lanthanides and presence of bulky groups in the cyclic organic ligands, some of these form bent structure rather than proper stacked parallel structure.[103, 107-110] These compounds are dissimilar than the transition metal-based sandwiched compounds in many aspects. Unlike transition metal based compounds, lanthanide-based one shows high ground state magnetic moment and high magnetic anisotropy value at low temperature.[111-113] Due to these phenomena, some of the

lanthanide-based compounds possess long magnetic relaxation time at very low temperature, demonstrating single-molecular magnetic (SMM) properties.[114-119] As these molecules have high spin ground state, they can also be used as dynamic components of spin-polarized transport devices.[120-123]

1.2 Aromaticity

Aromaticity comes from the word "aroma" (means pleasant fragrance), used in 1855 by Hoffman, to represent a phenyl radical containing compounds.[124] Since then, it became one of the key concept and popular word in physical organic chemistry. Aromaticity is strictly a virtual quantity rather than an observable quantity and very hard to accurately define.[125-128] Generally, it arises from the cyclic delocalization of electrons which results in extra stabilization of a system.[129-132] Researcher defines aromaticity using many criteria such as structural, magnetic, energetic, electronic, reactivity etc. As per Schleyer *et.al*, [126] "*Aromaticity is a manifestation of electron delocalization in closed circuits, either in two dimensions or in three dimensions. This results in energy lowering, often quite substantial, and a variety of unusual chemical and physical properties. These include a tendency toward bond length equalization, unusual reactivity and characteristic spectroscopic features. Since aromaticity is related to induce ring currents, magnetic properties are particularly important for its detection and evaluation*."

Aromaticity is not a directly measurable quantity; one should concentrate on some particular criteria which are sensitive to the amount of delocalization of electrons in the molecule. A number of criteria have been put forward in attempts to give a quantitative picture of aromaticity. Among all these criteria, mostly five categories of criteria have been explored.[44, 48, 132, 133] Those are as follows:

- Energetic (improved stability)
- Structural (all bond equalization)
- Magnetic (particular shielding and deshielding)
- Electronic (π-electron delocalization) and
- Reactivity (inertness towards addition reaction).

Among these five types of properties, first four are based on its own nature, while the last one depends on the complete reaction mechanism.[44, 129] As a result, it is not easy to give a quantitative idea about aromaticity based on reactivity criteria. A brief discussion over all these criteria is given below.

1.2.1 Energetic Criterion

The aromatic molecules possess extra thermodynamic stability with respect to structurally analogous chain model system. Cyrański has defined as [44] *"The thermodynamic stability of the system is enhanced with respect to a structurally analogous model system (most often an acyclic system), which has no cyclic π-electron delocalization".* This quantity can be calculated using both experimental and theoretical methods, which is an advantage of this criterion.

Initially, this criterion had been introduced to understand the enhanced stability of benzene. Pauling *et.al* [134]and Kistiakowsky *et.al* [135] numerically estimated this extra thermodynamic stabilization and presented an index called resonance energy (RE). Resonance energy is calculated as the energy difference between the resonance structures. For example, in benzene, RE was calculated as the energy difference between a model Kekulé benzene structure and the real benzene structure. The computed value was 36 $kcal \cdot mol^{-1}$ and was in good agreement with the experimental enthalpy of formation or hydrogenation energy value.[136-138] But in RE index, the effect of strain, hyperconjugation, differences in types of bonds are not taken into account. With the advancement of computational chemistry methods, other developed indices based on this criterion have been employed. Among this, aromatic stabilization energy (ASE) [125, 129, 139, 140] has been explored and used for a wide range of systems.

Aromatic Stabilization Energy (ASE)

ASE is based on assessments of energy relative to the reference systems such as olifins, polyacenes etc. Depending upon the reference systems, two types of reactions are considered[141] (isodesmic[142, 143] and homodesmic[144, 145]) to calculate ASE. Herein, we have considered benzene as an example to show two types of methods.

Isodesmic reaction for Benzene

An isodesmic reaction is a hypothetical chemical reaction and mainly considered in thermodynamic cycle, in which the type of chemical bonds broken in the reactant are the same as the type of bonds formed in the product.[146]

$$C_6H_6 + 6CH_4 \rightarrow 3H_2C{=}CH_2 + 3H_3C\text{-}CH_3$$

Isodesmic Stabilization Energy (ISE) for benzene is 64 kcal·mol^{-1},[146] which is higher than their corresponding experimental value. The reference systems considered for this model does not preserve local bonding pattern of carbon atoms in benzene, which is a major drawback of this criterion. In order to overcome this, we considered homodesmic reactions.

Homodesmic reaction for Benzene

Homodesmic reactions retain the local hybridization of carbon systems or maintain the same number of each type of bonds in the reactant and product.

$$C_6H_6 + 3H_2C{=}CH_2 \rightarrow 3H_2C{=}CH{-}CH{=}CH_2$$

Homodesmic Stabilization Energy (HSE) for benzene comes out as 21.49 kcal·mol^{-1}. [147] As for this type of reactions, purely conjugated π-electron delocalization stabilizes more, HSE turns out to be lesser than ISE for most of the time.[141]

The main drawbacks of the ASE indices are that its value depend largely on the type of reaction scheme (i.e. homodesmic, isodesmic etc.), chemical reaction (i.e. reference system) under consideration and level of theory used to calculate the energies of the chemical species.

1.2.2 Structural Criterion

The aromatic systems try to remain planar with all the cyclic bonds equal, value of which typically remain in between the values corresponding to single and double bonds.[48, 130]

The construction of these criteria essentially arises from the idea that one of the main reasons of aromaticity is π-electron delocalization. For a planar molecule, this type of delocalization is highest as in this geometry, p_π-orbitals which are responsible for delocalization, achieve maximum overlap among them.[48] And as a consequence of the π-electron delocalization in cyclic structure, all the cyclic bonds try to be equal in length. Geometrical indices of aromaticity describe these effects quantitatively. Just like

energetic criteria, these indices are also not independent. They are defined and calculated on the basis of some parameters which are obtained from reference structures, where the π-electrons are completely localized or completely delocalized. The most reliable geometry-based index among all is Harmonic Oscillator Model for Aromaticity (HOMA).[148-151]

Harmonic Oscilator Model for Aromaticity (HOMA)

HOMA can be defined as a normalized sum of squared deviations of the individual experimental or calculated cyclic bond lengths from a reference bond length, which is derived from a fully π-electron delocalized structure. It can be formulated as:

$$HOMA = 1 - \frac{\alpha}{n}\sum(R_{opt} - R_i)^2 \qquad (1.1)$$

where n is the number of bonds taken into the summation and α is an empirical constant chosen in such a way that HOMA becomes equal to 0 for the model nonaromatic systems (e.g. the Kekule´ structure) and equal to 1 for a system with all bonds equal to the reference value R_{opt}. The individual bond lengths are given by R_i.

This model also can be used for the structures including heteroatoms (i.e. atoms other than carbon),[150]

$$HOMA = 1 - \frac{\begin{array}{c}\{\alpha(CC)\sum\left[R(CC)_{opt} - R_i\right]^2 + \\ \alpha(CX)\sum\left[R(CX)_{opt} - R_i\right]^2 + \alpha(CY)\sum\left[R(CY)_{opt} - R_i\right]^2 + \\ \alpha(XY)\sum\left[R(XY)_{opt} - R_i\right]^2\}\end{array}}{n} \qquad (1.2)$$

here X and Y are denoted as heteroatoms. The HOMA can be divided analytically into two parts where one term takes care about the bond elongation (termed as EN) and another term corresponds to bond alteration (termed as GEO) in the structure;

$$HOMA = 1 - \left[\alpha\left(R_{opt} - R_{av}\right)^2 + \frac{\alpha}{n}\sum(R_{av} - R_i)^2\right] = 1 - EN - GEO \qquad (1.3)$$

here R_{av} is taken as the mean bond length. The modified version of this formula can also be extended to hetero-π-electron systems. But this index can't be used as the only criterion to decide the aromaticity in a molecule, because, some nonaromatic or weakly aromatic molecules (e.g. borazine) can have all bonds equal in length, giving a HOMA value (i.e. ~ 1; for example HOMA=0.94 for borazine[152]) which would theoretically

correspond to aromatic systems. The other drawback of this index is the dependence of it over the reference bond length for a particular bond. The choice of reference structure is not unique.[126]

1.2.3 Magnetic Criterion

When an external magnetic field is applied perpendicular to the molecular plane of a planar aromatic molecule, it induces a diamagnetic ring current which gives rise to a secondary field in the system. This secondary field remains antiparallel with respect to the externally present field, giving rise a magnetic shielding or deshielding for some part of the molecule.[126, 129]

The figure 1.2 given below demonstrates the magnetic shielding very clearly. Here the middle of the benzene ring is being shielded from the external magnetic field.

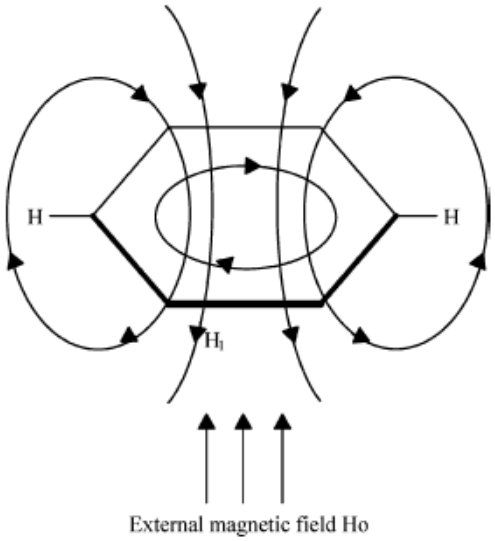

Figure 1.2: Internal ring current induced by external magnetic field (H_0).

The concept of ring current was first introduced by L. Pauling.[153] It can be expected that this aromatic molecules possess free rotation of π-electrons along the closed contour which is in ring plane. In presence of external magnetic field, these freely rotating π-electrons generate diamagnetic ring current which act in opposite direction of the external magnetic field. This ring current (*I*) can be quantified as follows:[154]

$$I = -\frac{2e^2}{9c\hbar^2}\beta S H_0 \qquad (1.4)$$

where β is resonance integral for CC π-bond, S is area of the ring, H_0 is external magnetic field, e is the charge of an electron, ħ is h/2π where h is Plank's constant.

The main problem with this ring current is that it can't be measured experimentally. However, this ring current model can be validated by comparing the experimental values with the ring current-based calculation values of various quantities, like, magnetic susceptibility, exaltation, anisotropy, ^{1}H NMR chemical shift etc. But as ring current is not the only factor which controls these properties, one has to identify all other effects and has to remove them from considerations.

Magnetic Susceptibility Anisotropy

This quantity (Δχ) is a characteristic feature of the aromatic molecules. Therefore, an aromatic index can be introduced based on this quantity. This susceptibility anisotropy can be represented as follows:[155-157]

$$\Delta\chi = \chi_{cc} - 1/2\,(\chi_{aa} + \chi_{bb}) \qquad (1.5)$$

where χ_{aa}, χ_{bb} and χ_{cc} are the diagonal elements of the magnetic susceptibility tensor and c is assumed to be the out-of-plane axis for the planar molecule. Experimentally, Δχ can be obtained from various experiments, like, high-resolution Zeeman microwave spectroscopy[156], high-field NMR spectra of fully deuterated compounds[158] etc. This quantity can be divided into two terms $\Delta\chi^{local}$ and $\Delta\chi^{nonlocal}$, where the first term takes into account about the local contributions (e.g. local paramagnetic currents, anisotropy of σ-bonds of CC and CH etc.) to the susceptibility anisotropy and the last term considers the effect of global ring current. Thus, here it is very important to separate the two terms and to use only $\Delta\chi^{nonlocal}$ term as aromatic index. [157, 159]

Magnetic Exaltation

This is another index where molar susceptibility has been used to quantify aromaticity.[133, 160] This index can be represented as follows,

$$\Lambda = \chi_m - \chi_a$$

where χ_m and χ_a are the measured magnetic susceptibility of a conjugated system and of a hypothetical cyclic system where double bonds are fully localized (i.e. the ring current is

zero). A molecule can be considered as aromatic when $\Lambda > 0$; antiaromatic when $\Lambda < 0$ and nonaromatic when $\Lambda \approx 0$. [129, 160, 161]

Nuclear Magnetic Resonance Chemical Shift

The chemical shift can be defined as "*The fractional variation of the resonance frequency of a nucleus in nuclear magnetic resonance (NMR) spectroscopy in consequence of its magnetic environment*."[162] In fact, when an atom is placed in an external magnetic field, its electrons start circulating (called diatropic circulation) in such a manner that a small magnetic field is generated around nucleus.[163] This newly induced field opposes the external magnetic field causing a shielding for the nucleus. Therefore, the effective magnetic field (B_i) experienced by particular nucleus i is

$$B_i = B_0(1 - \sigma_i)$$

where B_0 is the applied magnetic field and σ_i is shielding constant of that nucleus. These shielding constant values of a particular nucleus can change a lot for different chemical environments. Therefore, depending on the chemical environment, an identical nucleus (hydrogen for ^1H, carbon for ^{13}C) resonates with external magnetic field of different strength.[163] Therefore, if in a molecule, a particular nucleus remains in dissimilar chemical environments, they will resonate in different value of external magnetic field. This separation between the peaks is called chemical shift. Generally, the chemical shift is represented as fraction of the applied external field. To compare the various chemical shifts values which indicate different environment around the nucleus, some reference shift value is needed. So, the chemical shift (δ) can be calculated using the following formula,

$$\delta = \frac{\nu_{comp} - \nu_{ref}}{\nu_{ref}}$$

where ν_{comp} and ν_{ref} are the resonating frequencies for a particular compound and reference compound respectively. Usually, for ^1H and ^{13}C NMR, the tetramethylsilane is used as reference system. [163]

^1H NMR chemical shift is probably the most widely used criteria for characterizing aromatic and antiaromatic compounds, both experimentally and theoretically.[129] The deshielding of outer protons and shielding of inner protons of an aromatic ring is basically a demonstration of molecular ring current induced by an

external magnetic field. Generally, inner protons face stronger effect of field than that of outer protons. In ^{1}H NMR data of an aromatic ring, inner protons are shifted more upfield, whereas outer protons are shifted more downfield with respect to the reference acyclic conjugated system. [163] Essentially, the magnetic shielding value does not merely depend on the ring current. There are several other local effects also which have prominent contributions to the shielding value. [164-166] For heteroatomic ring system, these local effects have very important role and for some of the systems, these effects become the governing factors for aromaticity. [167, 168] Therefore, this index is also not unique to describe about the aromatic character of a ring system quantitatively.

Nucleus Independent Chemical Shift (NICS)

NICS is defined as the negative of magnetic shielding value calculated at some interesting points in the neighborhood of the molecules.[126, 169] Here negative sign is introduced just to get correspondence with well-known NMR chemical shift. It was originally "*computed at ring centers (nonweighted mean of the heavy atom coordinates)*" [169], but with the advancement of the concept, now it can be calculated in some points located above or below the ring or even can be calculated forming some grids in the vicinity of the molecule.[126, 151] A ring with negative, positive and near to zero NICS value is considered as aromatic, antiaromatic and non-aromatic rings, respectively.[169]The magnitude of the NICS directly corresponds to the intensity of aromatic nature of a system i.e. more negative NICS indicates stronger aromaticity than a lesser one. To avoid the local effects originated from σ-electron structure at the ring plane, it is better to calculate the NICS at 1Å above or below the ring, where the local effects are almost negligible.[126, 170, 171]

More recently, it has been advised to consider the susceptibility tensor component corresponding to the principle axis perpendicular to the ring plane ($NICS_{zz}$ if the molecule is in xy-plane) to have a better characterization of π-electron systems.[126, 172] This index has several advantages over the other indices, generally used to quantify aromaticity. The one of the main advantage of it is that it can give a quantitative idea about aromaticity without involving any reference structures or increment scheme or calibrating reactions. Unlike Λ, NICS shows only a little dependence on the ring size. It can also be correlated with the other aromatic indices based on energetic or geometric or other aromatic criterion.[126, 169]

The one of the main disadvantage of NICS is that it is a local descriptor of aromaticity. So, it can't predict anything about global aromaticity in the structure. Other drawback is that this index is completely theoretical, experimental verification is not possible for most of the cases. Despite of these drawbacks, NICS is considered as one of the most successful index to quantify aromaticity in various types of systems.

1.2.4 Electronic Criterion

The cyclic delocalization of π-electrons in an organic system is the most basic criteria for a molecule to show aromaticity. [46, 130] This criterion is principally the foundation of all other criteria mentioned above.

The most well-known rule based on this criterion to determine the aromatic nature of cyclic molecules is Huckel's rule.[173-175] It states that monocyclic, planar and fully π-conjugated molecule that contains (4n+2) π–electrons will exhibit aromatic nature. On the other hand, molecule having 4n π-electrons will be antiaromatic. This rule generally works fine for n=0 to 6.[176] Although the Huckel's rule has demonstrated the importance of electronic criterion long back, there were very few indices based on this. The main drawback to use this criterion as an aromaticity index is that like NICS, it can't be measured experimentally.[130] Recently, a new door in this field has been opened up with the introduction of concept called localization and delocalization indices (δ)[177-179]by Bader *et.al.* These indices can be calculated by performing double integration of the exchange correlation density over the atomic basins which are created based on Bader's atoms in molecules (AIM) theory.[180, 181] After this breakthrough, several indices have been demonstrated to quantify aromaticity based on this criterion. Among all these indices, aromatic fluctuation index (FLU) [182] and *para*-delocalization index (PDI) [46] are the two mostly used indices.

Delocalization Index (DI)

This is defined as the number of electrons delocalized or shared between two atoms in a molecule.[177-179] This can be calculated from AIM theory, using the following equation,

$$\delta(A,B) = -\iint_{A,B} \Gamma_{XC}(\underline{r}_1, \underline{r}_2)\, d\underline{r}_1 d\underline{r}_2 - \iint_{B,A} \Gamma_{XC}(\underline{r}_1, \underline{r}_2)\, d\underline{r}_1 d\underline{r}_2$$

$$\delta(A,B) = -2\iint_{A,B} \Gamma_{XC}(\underline{r}_1, \underline{r}_2)\, d\underline{r}_1 d\underline{r}_2 \qquad (1.6)$$

where δ(A,B) represents the delocalization index between atoms A and B, Γ_{XC} is the exchange-correlation density over the A and B atomic basins as defined by AIM theory. [181]

Para-delocalization Index (PDI)

It is defined as the average of delocalization indices of atoms situated in *para*-position to each other in a six-membered ring.[46] The idea of this index arises from Bader's observation that in a six-membered ring, electron delocalization is more between *para*-positioned atoms than that of *meta*-positioned one.[180, 181] Therefore, PDI for a six-membered ring can be formulated as,

$$PDI = \frac{\delta(1,4) + \delta(2,5) + \delta(3,6)}{3} \qquad (1.7)$$

For an aromatic ring, PDI will show positive value whereas for non-aromatic ring, it will be almost zero. More positive the value of PDI more is the aromatic nature of the ring. The main disadvantage of this index is that as it needs only *para*-positioned atoms, it is applicable for only six-membered rings.[46] And also, as it is entirely a local index of aromaticity, it can't be used to measure the global aromaticity of a system.

Aromatic Fluctuation Index (FLU)

This aromatic index demonstrates the fluctuation of the electronic charge between the adjacent atoms in a ring.[182] FLU value depends on the electron delocalization in some typical aromatic reference molecules. Therefore, essentially FLU measures the divergence in the electron sharing with respect to some typical aromatic systems. It can be calculated using following formula,

$$FLU = \frac{1}{n}\sum_{A-B}^{n} \left[\left(\frac{Flu(A \to B)}{Flu(B \to A)}\right)^{\alpha} \left(\frac{\delta(A,B) - \delta_{ref}(A,B)}{\delta_{ref}(A,B)}\right)\right]^2 \qquad (1.8)$$

where the summation includes all adjacent pairs of atoms in the ring, n denotes the number of atoms of the ring and Flu(A→B) gives the amount of electronic charge transferred from A to B via A−B bond. For an aromatic molecule, amount of electron transfer from A to B and B to A will be almost same. Therefore, first term of the equation (1.8) will be almost 1. Here, α is a number just to ensure that the first term of FLU is always greater or equal to 1 i.e. α=1 if Flu(A→B) > Flu(B→A) or α=−1 if Flu(A→B) ≤ Flu(B→A); and δ(A,B) and δ_{ref}(A,B) are the delocalization indices for atoms A and B and their reference values, respectively. A typical aromatic system used as reference system here. Therefore, an aromatic system will have FLU value near equal to zero when the electronic charge is homogeneously distributed over all the bonds.

The main advantages of this index over other electronic criteria-based indices are (1) this index can be used for any ring or group of rings; (2) it can measure local as well as global aromaticity of a system.[46, 182] But just like HOMA index, the main disadvantage of it is the involvement of reference structure in the calculation. The value of FLU depends strongly upon the choice of reference structure and this choice is not unique.

1.2.5 Reactivity Criterion

Aromatic molecules are generally more intent for substitution reaction than the addition reaction.[44, 133, 176] In other words, these systems always try to retain their initial π-electron structure during chemical reactions. The reason behind this is quite straightforward. As the π-electron delocalization gives extra stability to the aromatic systems, systems will always try to keep this delocalization nature intact, which is possible if systems get involved in a substitution reaction.[133, 176]

However, this criterion depends on the reaction pathways. As a result, it is too difficult to construct a reactivity-based index which can give a quantitative idea about aromaticity in the system. Although a few attempts have been taken to quantify aromaticity using these criteria, success has been achieved mostly up to simple benzenoid hydrocarbons and small heterocyclic rings.[183, 184]

Almost all indices of this criterion are based on the hardness of the system. There can be different types of hardness like absolute hardness[185, 186] (half of the HOMO−LUMO gap) or relative hardness (difference between the hardness of a molecule

and some acyclic conjugated hypothetical reference structure)[187] value of which show direct correlation with the resonance energy of the system. The main reason of this type of correlation is that with the increment of hardness, the systems become more and more stable and less reactive, which is in other way satisfy the criterion to be a strong aromatic system.[188]

All the criteria mentioned above prove unambiguously that aromatic nature of the molecules can be emphasized by computing more than two or three (minimum energetic, magnetic and geometric) criteria. In this thesis, we have considered maximum criteria to prove the aromatic nature of the molecules.

1.3 Electron transport through nanoscale devices

Last decades has experienced a revolutionary development of nanoelectronics. A careful look can reveal that this advancement has just follows the famous "Moore's law" stated by Intel's co-founder Gordon Moore.[189] In 1965, he predicted that number of components in integrated circuits would be doubled by every 18-24 months. This unbelievable advancement has been achieved through the incredible improvement of 'top down' lithography approach where the existing silicon-based chips have been miniaturized in size.[190-197] However, this 'top down' approach undoubtedly will reach its ultimate limit very soon owing to several fundamental difficulties such as leakage of current via direct tunneling through oxide layer, interconnecting delays, excessive power dissipation etc.[198-200] In addition, it is also very difficult to control fabrication procedure via conventional lithography in nanometer scale. Although some of the problems can be solved by developing sophisticated instruments, increment of cost to do so motivates researchers to find alternative direction.

One of the optimistic ways to tackle this problem is to construct integrated circuit at an atomic or molecular level. In 1959, Richard Feynman, in his famous speech "There is Plenty of Room at the Bottom" first introduced the concept of "bottom-up" nanoelectronics.[201] Enormous experimental and theoretical efforts which are continuing for past three decades have made this concept a promising alternative for conventional silicon-based electronics.[202-209] The basic goal of this notion is to replace 'top-down' lithographic approach with 'bottom-up' synthetic chemical approach where nanodevices

and circuits are directly assembled from their molecular ingredients. As this next generation electronics use molecules as basic building block, it is rightly named as 'molecular electronics'.[203, 210]

Certainly one should be inquisitive about the distinctive advantages of molecular electronics over conventional one to believe that molecules can really replace silicon-chips. The typical benefits of using molecules are as follows[211]:

- Molecules are small, of the order of nanometer, which is a desired scale for functional nanodevices.
- Selective recognition ability and favourable thermodynamically controlled self-assembling process provides a cheap fabrication method to produce molecular building blocks.
- Optical and electronic properties of the molecule can differ a lot for various geometric isomers of it.
- Conformational flexibility in some molecules may result in interesting change in transport phenomenon. It gives an opportunity to control the current through the molecule by controlling the external factors such as temperature, pressure, electric field etc.
- One can also tune molecular binding, optical and electronic properties by altering the composition and geometries during synthesis process.

In 1974, Ratner and Aviram's theoretical prediction about the usage of a single molecular structure as molecular rectifier is considered as the first major breakthrough of this field.[212] Therefore, molecular electronics is a newly emerging field, having a history of 38 years. But the enormous efforts of scientists of several interdisciplinary fields such as synthetic and quantum chemistry, physics, electrical engineering etc. have produced an unbelievable development in this field. As a consequence, in this short period of time, several new molecular-electronic systems have been reported demonstrating various electronic functionalities such as transistors,[213, 214] switches, [215, 216] interconnects, [217] memories, [218] photovoltaics, [219] sensors[220] etc.

A sharp advancement in the field of molecular electronics has confirmed its potential to be used as an alternative of conventional electronics. But at the same time, one needs to work on the several road-blocks which limit the application of molecular

electronics to large-scale. Some of the factors which extremely hinder the growth of this field are as follows;

- The temperature effect on stability and robustness of the systems is a major drawback for reliable applications.
- Due to the small size of molecules, it is too difficult to control the molecule-electrode coupling nature in the devices.

To overcome these difficulties, new experimental techniques as well as improvement of existing techniques are desired.

Molecular electronics is receiving vast interest not only for its technological application but also for a number of fundamental issues it possess. It's really challenging to understand the quantum transport of electrons in a device where two large macroscopic electrodes sandwich a nanoscale conductor such as single molecule.[221, 222] At the very beginning, one should ask "What exactly is changing when we go from macro to nanoscale regime?" The most obvious answer is length scale. Some characteristic length scales have been defined to determine the border between two transport regimes (i.e. classical and quantum transport regimes). And these are the Fermi wavelength λ_F, momentum relaxation length L_m and phase relaxation length L_φ.[221]

Fermi wavelength: The confinement of the conductors in one or two direction makes the quantum modes discredited in the directions normal to the electron propagation. The ratio of the width of the two dimensional wire to the de Broglie wavelength (λ_F) of conduction electrons at Fermi energy, E_F, represents number of quantum modes of that 2-D wire. If W is the width of the wire, the number of modes N can be formulated as $N= Int(2W/\lambda_F)$ where right hand side is the integer that is just smaller that ($2W/\lambda_F$). According to Landauer, transmission probabilities of electrons through these modes only can regulate the conduction properties in nanoscale devices, showing a quantized nature of conductance in these systems.[223]

Momentum relaxation length: It is defined as the average distance an electron can travel maintaining its initial momentum. It can be formulated as $L_m= v_F \times \tau_m$ where v_F is Fermi velocity and τ_m is momentum relaxation time. Generally, electrons lose their initial momentum due to the collisions with other electrons, impurities or defects present in the sample. The order of this length is of μm or nm and depends on various factors.

Phase relaxation length: It measures the average distance travelled by electron where it retain its phase. Interaction with fluctuating scatterers such as, phonons, electrons and magnetic impurities causes the randomization of the phase of electrons in the solids. When this length is greater than the sample length, various quantum effects like interference appears in the system.

To study spin transport in the nanoscale devices, one has to consider some other length scale called as spin diffusion length.

Spin diffusion length: The main concept of spintronics is to use the intrinsic spin degrees of freedom which are not considered in conventional electronics.[88, 224, 225] Fundamentally, for spin based electronics, one needs to apply a method to generate and manipulate spin-polarized population of electrons (i.e. there should be an unequal distribution of spin up and spin down electrons) near to Fermi level. The period of time that such a non-equilibrium population can be maintained is known as the spin lifetime, τ. For a diffusive conductor, the distance travelled by spin within spin lifetime, is called as spin diffusion length (λ). Among several mechanisms, spin-flip scattering and spin dephasing are dominating processes for decay of a spin polarized populations.

1.3.1 Factors affecting Transport in nanoscale

There are several factors which extremely affect the transport in nanoscale devices. Some of these factors are discussed here[221]:

Effects of molecule-electrode coupling: Basic difficulty to understand the transport in these systems is to handle the interaction nature between the molecules and macroscopic metallic electrodes, which contain discrete energy levels and possess continuous band structure, respectively.[222] When a molecule is attached to electrodes, depending on the strength of coupling, the discrete levels of molecule would get broadened. This broadening occurs due to the hybridization among the molecular orbitals and delocalized metal wave functions. The lifetime of an electron in the molecular energy level is inversely associated with the broadening of the levels. The rate of electron at which it can escape from molecular level to the contacts, strongly depends on this broadening factor. Therefore, for strong coupling, a higher amount of current can be transported than that for weak coupling.[226] As different experimental set-ups produce metal-molecule coupling of different strengths, the transport characteristics get influenced in different ways.

Position of the contact Fermi energy: For electrode-molecule system, the Fermi energy of electrodes falls somewhere in the HOMO-LUMO gap of the connected molecule. Because of broadening in the molecular states, fractional charge transfer may occur from contact to molecular level, making the molecule charged. The energy level shift in the molecules on injecting the fractional charge greatly depends on the value of charging energy per electron. This provides an idea about the arrangement of energy levels of electrons with respect to Fermi energy of the metal. Generally, the shape of the current-voltage (I-V) characteristics of molecular conductor has huge dependence over this factor.

Electronic structure of the molecule: Molecular orbitals of conductor play a key role for the transport in the molecular electronic devices. Hence, a precise description of electronic structure of molecules is necessary to understand transport in these systems.

Effects of inelasticity and thermal fluctuation: For the nanoscale transport, where a small molecule is attached to the macroscopic electrodes, electron-electron correlations become very dominating factor. To have a complete idea about the transport, one has to consider non-equilibrium situation including electron-molecular vibration, scattering and electronic many-body effects.

1.3.2 Mechanism of molecular transport

With the advancement of electronic devices in nanoscale regime, the conventional theories of electrical transport, applicable for macroscopic system has been improved a lot. Based on the two characteristic lengths, momentum (L_m) and phase relaxation length (L_φ), electron transport can be divided into three regimes, namely, ballistic, diffusive and classical regime.

Ballistic transport regime: When the length of the conductor is much smaller than both of the above mentioned lengths, the electrons can propagate freely from one electrode to another electrode without scattering. As in this regime, the energy of the tunneling electrons resonates with the conduction band of the wires and does not face any scattering process; it is known as coherent resonant tunneling regime. In this regime, rate of electron transport obeys Landauer's formula which states that conductance depends over the transmission probability and is independent of the length of the molecular bridge. The conductance through the wire linearly increases with the increase in transmission probability and number of eigenmodes in it. Due to the resistance at the junction of the

nanoscopic conductor and macroscopic electrodes, conductance for this regime always remains finite. Generally quasi-1D structures such as metallic nanowires, carbon nanotubes show ballistic conductance with quantized conductance ($G=2e^2/h$, where e is the electronic charge and h is Plank constant).[227-229] However, for most of the systems as the molecular eignestates are not delocalized fully, transmission probability through these channels appears less than 1.

Diffusive or Coherent nonresonant tunneling regime: The device where tunneling electrons do not resonate with the energy levels of molecular states, the conduction happens through non-resonating process. [230] Generally, for this case $L_{\varphi} >> L_m$ i.e. electrons retain their initial phase for a long distance although the momentum of them get completely randomized within such a distance. Here, the transport occurs in diffusive manner. The rate of electron transfer for this regime depends strongly on the length of the system. This rate can be formulated as $G=A \exp(-\beta N)$ where A is associated with contact conductance and takes into account the electrode-molecule interactions, β is electronic structure related decay parameter and N is the number of sites in the molecular bridge. This mechanism can be seen for short bridges with large HOMO-LUMO gaps, such as, oligoalkanes.

Classical or Incoherent transfer regime: When the length of the molecular bridge is much larger than both of the characteristic lengths, i.e. $L >> L_{\varphi} >> L_m$, then the electrons get involved into inelastic and incoherent scattering processes losing their interference effect completely. For this case, electronic levels in the molecular bridge use to couple with the vibrational or rotational degrees of freedom. At this point, the molecular system behaves as normal electrical bridge where its resistance is directly proportional to its length. Basically, in this regime, the resistance of molecular bridge changes according to Ohm's law.

These are the general mechanisms; most commonly occur in the molecular electronics. Several parameters such as electronic structure, metal-electrode coupling, environment effects etc. can influence the nature and mechanism of conduction.

1.4 Methods

In this section, we will discuss the theoretical backgrounds of the methods we have used in this thesis. We will first introduce the density functional theory (DFT) –a revolutionary theory to calculate electronic structures of materials. Next, we will briefly describe two approaches: Landauer method and non-equilibrium Green's function (NEGF) method which have been widely used to study transport problem.

1.4.1 Density Functional Theory (DFT)

DFT is one of the most widespread quantum mechanical approaches for calculating the ground state properties of wide range of systems; from molecules to bulk materials, from insulators to metals, from diamagnetic to ferromagnetic materials. DFT can predict various ground state properties such as optimized geometry, vibrational frequency, atomization energy, ionization energy, electronic properties, one-particle magnetic states, optical properties, reaction pathways etc. very reliably. With the advancement of this theory, it has also been modified successfully for several kinds of studies including molecular dynamics, spin dependent study, investigation at non-zero temperature, time dependent phenomena etc.

From elementary quantum mechanics, we know that all the information about a system is stored in its wave function, ψ. The total energy of a system having interacting electrons and nuclei, can be calculated by solving Schrödinger equation,

$$\hat{\mathrm{H}}\,\Psi = E\,\Psi \tag{1.9}$$

where E denotes the total energy eigenvalue and $\hat{\mathrm{H}}$ is the many-body Hamiltonian operator. This operator can be formulated as,

$$\begin{aligned}\hat{\mathrm{H}} = \sum_{i=1}^{N_e} -\frac{\hbar^2}{2m}\Delta_i^2 + \sum_{I=1}^{N_{nuc}} -\frac{\hbar^2}{2M}\Delta_I^2 + \frac{1}{2}\sum_{i\neq j}\frac{e^2}{|\boldsymbol{r}_i - \boldsymbol{r}_j|} \\ - \sum_{i,I}\frac{Z_I e^2}{|\boldsymbol{r}_i - R_I|} + \frac{1}{2}\sum_{i\neq j}\frac{Z_I Z_J e^2}{|\boldsymbol{R}_I - \boldsymbol{R}_J|}\end{aligned} \tag{1.10}$$

where first two terms are kinetic energies of electron and nuclei, respectively; third term takes into account of the electron-electron interactions; fourth terms gives electron-

nucleus interactions and last term is for nucleus-nucleus interactions. Here, ħ is Planck's constant, Z_I is atomic number of I^{th} atom, r_i and R_I are the position of i^{th} electron and I^{th} nucleus, m and M are the mass of electron and nucleus, respectively. It's very complicated to solve this many-body Schrödinger equation. To simplify the equation, we can use Born-Oppenheimer approximation which states that as the nuclei are heavier than electrons and also move much slower than the electrons, the motion of electron and nucleus can be separated. It can be assumed that nuclei are fixed in particular positions, while the electrons are moving in a charged field created by nuclei. Now, entire wave function can be divided into two parts, electronic and ionic part. Therefore, the Schrödinger equation corresponding to electronic part can be written as,

$$H_e(\boldsymbol{r}, \boldsymbol{R})\Psi_e = E_e \Psi_e \tag{1.11}$$

where electronic Hamiltonian is given as,

$$\hat{\mathrm{H}} = \sum_{i=1}^{N_e} -\frac{\hbar^2}{2m}\Delta_i^2 + \frac{1}{2}\sum_{i\neq j}\frac{e^2}{|\boldsymbol{r}_i - \boldsymbol{r}_j|} + \hat{V}_{ext} \tag{1.12}$$

Here $\tilde{V}_{ext}$ denotes the potential acting on the electrons induced by the nuclei and any externally applied field.

After introducing Born-Oppenheimer approximation, the total number of degrees of freedom can be reduced, however still it's very difficult to handle electron-electron interactions part. And also electronic wave function depends on the positions of all electrons. A smart way to treat this situation is to use electron density instead of many-body wave function to describe the system of interest. DFT demands much lesser computational effort and gives a considerably good description of ground state properties of materials.

The Hohenberg-Kohn theorem[231, 232] is the soul of the DFT. As mentioned earlier, the fundamental concept of DFT is to use electron density as an alternative of complicated many-body wave function to handle interacting systems. In 1964, pioneering work by Hohenberg and Kohn considers as the beginning of DFT. [231] There they stated two basic theorems;

- The ground state electron density, ρ_0, of a many electron system can uniquely determine the external potential, V_{ext} ,which is acting on the system. It can be

stated in other way also: the external potential, V_{ext}, can exactly calculate the ground state electron density ρ_0 of the system. Moreover, ρ_0 can uniquely determine the ground state expectation values of any observables.

- To be the true ground-state electron density, it has to minimize the total energy functional of the system. And it can be achieved by following variational principle.

According to this, now one can express the Schrödinger equation in the following way;

$$E[\rho] = \hat{F}[\rho] + \int dr\, V_{ext}\,(r)\rho(\mathrm{r}) \tag{1.13}$$

where F is universal functional of ρ. One can find the ground state density by minimizing the functional, E[ρ], with respect to ρ. But the minimization of the explicit energy functional is still difficult to solve exactly. In 1965, Kohn and Sham proposed an efficient way to replace original many-body problem into an auxiliary one-electron problem. In this approach, interacting electrons are treated as non-interacting electrons which are moving in the effective potential. The many-body effects are included in this through exchange-correlation functional. According to this approach, the total energy functional can be expressed as,

$$\begin{aligned} E[\rho(r)] = T_s[\rho(r)] + \frac{1}{2}\int \frac{\rho(r)\rho(r')}{|r_i - r'_j|} dr dr' + E_{xc}[\rho(r)] \\ + \int \rho(\mathrm{r}) V_{ext}\,(r) dr \end{aligned} \tag{1.14}$$

where $T_s[\rho(r)]$ is the kinetic energy functional for non-interacting electrons, second term is electrostatic energy, third term is exchange and correlation energy and last is the energy due to external potential caused by nuclei and other externally applied potentials. Among these, first and third terms can't be solved in this form. However, if wave functions $\Psi_i(r)$ constructs the electron density, $\rho(r)$, then the first term i.e. the kinetic energy term can be calculated as follows;

$$T_s[\rho(r)] = \frac{1}{2}\sum_{i=1}^{N} \int \Psi_i^*(r)\nabla^2\Psi_i(r)\, dr \tag{1.15}$$

From equation (1.14) we can get a set of differential equations called as Kohn-Sham equations,

$$[\nabla^2 + V_H + V_{xc} + V_{ext}]\Psi_i(r) = \epsilon_i \Psi_i(r) \tag{1.16}$$

where, V_H is Hartree potential, V_{xc} is exchange-correlation term, V_{ext} corresponds to external potential and $\Psi_i(r)$ are the special orbitals called as Kohn-Sham orbitals. The general process to solve these equations is the iterative method and it does continue until self-consistency is reached. Now, we should concentrate on the exchange-correlation potential which can't be found exactly and should be approximated. From equation (1.16), V_{xc} can be expressed as;

$$V_{xc} = \frac{\delta E_{xc}[\rho(r)]}{\delta \rho(r)} \tag{1.17}$$

With the advancement of DFT, several approximations came forward to approximate the exchange-correlation functional more and more accurately. Here, we will discuss about two approximations which are used most extensively in the literature.

Local Density Approximation (LDA): First and simplest approximation of exchange-correlation potential is LDA.[233] It can be defined as;

$$E_{xc}^{LDA}[\rho(r)] = \int d^3r \varepsilon_{xc}\left(\rho(r)\right).\rho(r) \tag{1.18}$$

where $\varepsilon_{xc}(\rho(r))$ denotes the exchange and correlation energy per electron of the homogeneous electron gas with electron density, $\rho(r)$. Here, the electron density smoothly varies in space. Therefore, any area of space can be locally treated as homogeneous electron gas of density, $\rho(r)$. Now, to obtain the total exchange-correlation energy, one has to perform summation of local exchange-correlation energy for all the electrons in every region of space. These functional works nicely for bulk solids but have a poor performance for the systems where the electron density does not vary smoothly in space.

General Gradient Approximation (GGA): In this approximation, the standard LDA has been extended to inhomogeneous systems where electron density varies non-uniformly. This improved approximation not only considers the local charge densities but also more physical parameter i.e. their gradients. Fundamentally, there are three kinds of GGA:

a. **Ab-initio based:** These functionals are derived from exact results. Here exchange and correlation parts are calculated individually. The typical examples of this are PBE (Perdew-Burke-Ernzerhof) [234], PW91 (Perdew-Wang 1991) [235] etc.

b. Atom-based: It has some basic similarities with the previous one such as, these are also based on some exact results and exchange and correlations are treated separately. But for this type, the functional parameters are fitted on close-shell atom properties. Becke's GGA for exchange[236] and Lee Yang and Parr functional for correlation[237] are some example of this.

c. Empirical: In this case, exchange and correlation terms are treated as a whole. Functional parameters are obtained by fitting the results on a set of atomic and molecular properties. Well-known example of this is HCTH (Hamprecht-Cohen-Tozer-Handy) functional.[238]

The one of the most important steps to achieve accurate results for electronic structure calculation is to choose suitable basis sets. One needs to expand the one-particle wave functions in the following manner:

$$\Psi_i(r) = \sum_{j=1}^{N_b} C_{i,j}\, g_i(r) \tag{1.19}$$

where $C_{i,j}$ denotes the coefficients of expansion, $g_i(r)$ is the basis functions and N_b is the size of the basis. In this way, the Kohn-Sham equations convert to one-particle matrix equations. Now, one has to diagonalize this one particle Hamiltonian matrix to obtain the eigenvalues and eignevectors. Here, the Kohn-Sham equations are solved in self-consistent manner. The procedure is to begin with some initial guess of density and keep on improving density and potential in each iteration until the self-consistency is achieved.

Next, we will focus on another vital concept of DFT, called pseudopotential. Usually, it is quite normal to assume that the core electrons remain unaffected during any kind of change in chemical environments of the system. Using this analogy, one can freeze all the core electrons of an atom and can construct an effective external potential which acts on the valance electrons on each atom. Consequently, the oscillatory nature of valance wave function in the core region can be substituted by a smooth wave function. [239, 240] Pseudo wave function and all electron (where core electrons are free) wave function should match exactly with each other beyond a specific value of radial distance, called "cutoff radius". This "cutoff radius" should be chosen in such a way that the value will be greater than the distance where last node of all electron wave function appears. A good pseudopotential should give accurate results of studies for various systems, having

different chemical environment. This particular property is called transferability of pseudopotential.

In the past few decades, a number of packages have been developed where self-consistent calculations for electronic structure using various methods such as Hartree-Fock, post Hartree-Fock and DFT have been implemented. Among all these, some of the packages like Gaussian,[241] General Atomic and Molecular Electronic Structure System (GAMESS),[242] Amsterdam Density Functional (ADF)[243] are used extensively for molecular systems. As these packages use localized orbital basis functions, it can't handle large systems. However, the concept of numerical orbitals and pseudopotential come into play to study large periodic systems. Spanish Initiative for Electronic Simulations with Thousands of Atoms (SIESTA)[244] is an example of such kind of packages, where combination of numerical orbitals and norm-conserving pseudopotentials have been implemented successfully. Another way is to use plane augmented wave basis sets for calculations. Examples of this approach are Quantum-Espresso (PWscf), Vienna Ab-initio Simulations Packages (VASP)[245-247] etc.

1.4.2 Quantum Transport Theory

In this section, we will focus on the Landauer approach to describe non-interacting electron transport which corresponds to the transport at ballistic regime. Next, we will briefly discuss Non-Equilibrium Green Function (NEGF) approach, a more sophisticated method to study electron transport in low-dimensional system.

Landauer approach

In 1957, Landauer in a seminal paper asked the question: Is the conductance of a ballistic wire with a finite width infinite? [223] To give a reasonable answer to this question, he derived the conductance of a ballistic conductor and showed that the conductance is actually finite. In the late 80's onwards, there have been many experiments which clearly showed Landauer's prediction to be correct.[206, 248]

It is one of the most promising approaches to describe the transport through low-dimensions. Fundamentally, the transport in nano-junctions differ from macro-junctions in two aspects: (1) here interface resistance which is independent of sample length dominates over the resistance of the conductor, and (2) the conductance does not increase linearly with the width of the sample.[221]

According to this approach, the total system consists of three regions, central region, left and right regions. The central region which is basically made up of various types of low-dimensional conductors such as molecules, conducting polymer, remains in a sandwiched condition between two macroscopic leads (see figure 4). In this system, leads act as electron reservoirs. The leads remain in two electrochemical potentials, μ_L

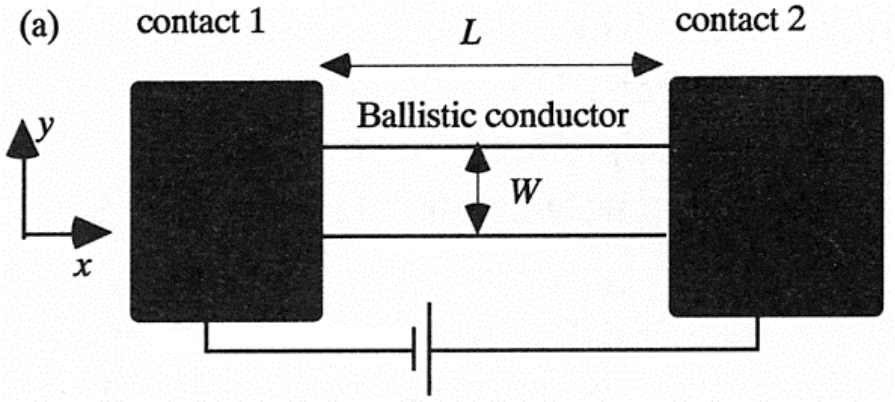

Figure 1.3: A ballistic conductor is sandwiched between two contacts. External bias is applied across this device. Adopted from *Electronic Transport in Mesoscopic Systems* by Supriyo Datta.

and μ_R. At zero-bias, these potentials remain same i.e. $\mu_L = \mu_R$. The electrochemical potentials differ under finite bias and this difference is the driving force for current flow through the system. In such condition, the transport problem can be treated as scattering problem. [221] To give a physical picture of this process, we can consider that leads are having infinite number of modes to transport electrons but conductors have a finite number of channels through which electrons can transmit to the other lead. Therefore, the electrons with its wave function propagate through the leads and get scattered when it reaches the contact region of lead and device conductor. According to Landauer, the current through this conductor can be expressed as the probability of an incident electron to transmit through it. In this thesis, we will derive the Landauer formula in a simple way.

Let us assume that two leads are connected through an ideal one-dimensional wire of length L (see figure 1.3). It is assumed that the transport through this wire is ballistic in nature. In this 1D-wire, the transmitting states are discrete in the direction normal to the propagation of electrons. For a uniform electron gas, current carried by electrons is I=env where n is the number of electrons per unit length and v is the velocity of moving

electrons with charge e. Now, the electron density per unit length for transverse state in the momentum range between *k* and *k*+*dk* can be formulated as,

$$\mathrm{n}(k)dk = 2\frac{1}{L}\frac{L}{2\pi}\,dk = 2\,\frac{1}{2\pi}f(k)dk \tag{1.20}$$

Here, the total function has been multiplied by 2 to consider spin. *f(k)* denotes Fermi distribution function. When bias is applied, the leads develop chemical potential and the device goes into non-equilibrium situation. When current flows through the device a steady state is reached. Now, the flow of current through the system can be viewed as,

$$I = 2\int_0^\infty ev(k)n(k)dk = 2\int_0^\infty e\frac{\hbar k}{m_e}\left(\frac{f_L(k)}{2\pi} - \frac{f_R(k)}{2\pi}\right)dk \tag{1.21}$$

where, $f_L(k)$ and $f_R(k)$ are the Fermi distribution functions for the left and right leads respectively, m_e is the electron effective mass. At zero temperature, as the Fermi functions become step functions, the equation (1.21) can be written as,

$$I = 2\int_{\sqrt{2m_e\mu_R}/\hbar}^{\sqrt{2m_e\mu_L}/\hbar} e\frac{\hbar k}{m_e}\frac{1}{2\pi}dk = 2\,\frac{e^2}{h}\frac{\mu_L - \mu_R}{e} = 2\frac{e^2}{h}V_B \tag{1.22}$$

Here, μ_L and μ_R are the electrochemical potential of the left and right electrodes, respectively. V_B represents the voltage created due to the difference in electrochemical potentials of leads, $\mu_L - \mu_R = eV_B$.

Now, from equation (1.22), we can calculate the maximum conductance of one conduction channel with two spin states, G_0.

$$G_0 = \frac{I}{V_B} = \frac{2e^2}{h} = (12.9k\Omega)^{-1} \tag{1.23}$$

This is called quantum of conductance. Therefore, in ballistic regime, conductance for a conductor is never infinite and it shows discrete nature under finite bias (see figure 1.4). This is because of the presence of contact resistances arising in the nano-junctions. Landauer expressed the conductance of a low-dimensional system in terms of the transmission probability for this scattering phenomenon. In general, it can be formulated as,

$$G = \frac{2e^2}{h}MT \tag{1.24}$$

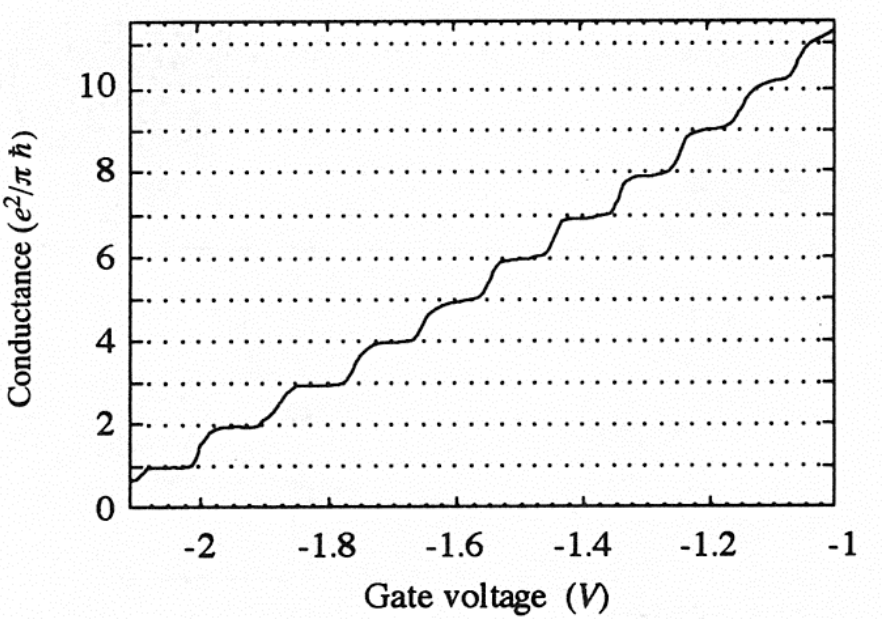

Figure 1.4: Conductance vs. Gate voltage plot for 2-D electron gas, showing quantization of conductance. Adopted from Phys. Rev. Lett. 60, 848 (1988).

where, T is the average of probability of transmission of electrons from one lead to another lead and M is the number of transverse modes which are transport-active. Generalized form of the Landauer formula for bias-induced current can be written as,

$$I(E) = \frac{2e}{h}\int_{-\infty}^{\infty} T(E, V_b)[f(E-\mu_L) - f(E-\mu_R)]dE \qquad (1.25)$$

In 1988, Buttiker extended the Landauer formula for multiple terminals by demonstrating the current I_i as

$$I = \frac{2e}{h}\sum_j T_{i,j}\left[\mu_i - \mu_j\right] \qquad (1.26)$$

where, $T_{i,j}$ is the average transmission when current transmit from terminal j to i.

Therefore, from the above equation, it is clear that to compute current at any bias, one has to calculate energy dependent transmission function. One way to derive this is to use Green's function of the central region which is connected to both leads.

Non-equilibrium Green's Function (NEGF)

For a nano-dimensional study of electron transport, the combination of DFT and NEGF demonstrate a much more efficient method than others.[221] In this section, we briefly discuss the NEGF formalism. At first, we will describe screening approximation, where

the whole system can be divided into three parts: left and right leads and central region. Then we will focus on the self-energy and NEGF formalism.

Screening Approximation: In this thesis, we will consider two-probe setup as our system of interest. As we mentioned earlier, in this setup two semi-infinite leads remain connected through a contact region. There is no direct coupling between the orbitals of atoms present in two different leads (see figure 1.5(a)). Now, the situation is bit tricky; as the semi-infinite leads are periodic in the transport direction, the Hamiltonian becomes infinite-dimensional. We can handle this situation applying screening approximation. Considering this approximation, we can separate the effective potential and density into three parts: left lead (L), central region (C) and right lead (R) (see figure 1.5(b)). The atoms in L/R only interact with the C. The L and R have all the electronic properties same as bulk materials. Therefore, C and two contact regions i.e. C-L and C-R only have different Hamiltonian, overlap matrices and density than the bulk system. On the other hand, various surface effects such as charge transfer, atomic relaxation and disturbance in potential appear due to the perturbation of the central region, making the situation complicated to handle. To eliminate these surface effects, a few layers of atoms of the leads can be included in the central region which now effectively gets screened from the bulk of electrodes.

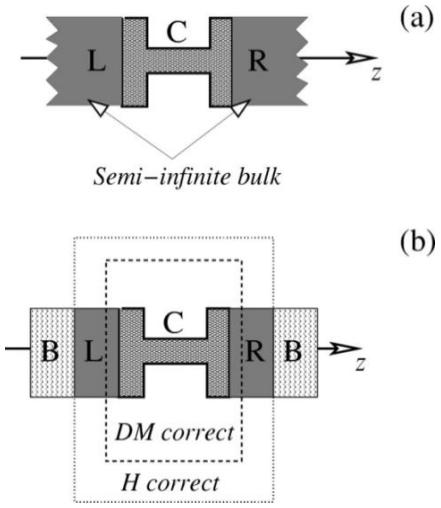

Figure 1.5: Schematic of model for transport calculation. (a) Contact region (C) coupled to two semi-infinite left (L) and Right (R) electrodes. (b) Infinite electrodes are considered as finite system; the Hamiltonian matrixes of L and R have bulk electrodes value. Outside of it i.e. B is not directly taken into account for calculation. The transport direction is assumed to be z-direction. Adopted from Phys. Rev. B, 65, 165401 (2002).

Now, using the screening approximation, the total Hamiltonian can be represented as,

$$\begin{pmatrix} H_L & \tau_L & 0 \\ \tau_L^\dagger & H_C & \tau_R^\dagger \\ 0 & \tau_R & H_R \end{pmatrix} \tag{1.27}$$

where H_L, H_C and H_R represent the Hamiltonian matrix for left, central and right part, respectively. τ_L and τ_R denotes the matrices which include the interaction terms between leads (left and right respectively) and central region. Next step to proceed is to solve the Schrödinger equation using Non-equilibrium Green's function.

Green's functions and self-energies: To continue according to this approach, we have to introduce Green's function of Hamiltonian. The retarded Green's function, G, for this problem can be expressed as,

$$[E^+S - H]G = I \tag{1.28}$$

where, $E^+=\lim_{\eta\to 0+} E+i\eta$, S denotes overlap matrix and I is an infinite dimensional identity matrix. Now, substituting equation (1.27) to equation (1.28), we obtain the equation,

$$\begin{pmatrix} E^+S_L - H_L & -\tau_L & 0 \\ -\tau_L^\dagger & E^+S_C - H_C & -\tau_R^\dagger \\ 0 & -\tau_R & E^+S_R - H_R \end{pmatrix} \begin{pmatrix} G_L & G_{LC} & 0 \\ G_{CL} & G_C & G_{CR} \\ 0 & G_{RC} & G_R \end{pmatrix} = \begin{pmatrix} I & 0 & 0 \\ 0 & I & 0 \\ 0 & 0 & I \end{pmatrix} \tag{1.29}$$

Considering the three equations in the second column, the Green's function for the molecule can be expressed as,

$$G_C = (E^+S_C - H_C - \sum_L - \sum_R)^{-1} \tag{1.30}$$

where, Σ_L and Σ_R are the self-energies of the left and right leads respectively. These can be formulated as,

$$\sum_L = \tau_L^\dagger G_L \tau_L \; and \sum_R = \tau_R^\dagger G_R \tau_R \tag{1.31}$$

where, G_L and G_R are Green's functions for the isolated leads. Fundamentally, the interaction between the leads and molecule are taken into account by these self-energies. It is interesting to notice that this matrix dimension is in molecular basis only. But still the Green's function of the leads formulated as the inverted form of an infinite-dimensional matrix. This quantity can also be derived analytically. For example, if the metallic leads

are denoted by a continuous spectrum of states m and n, the Hamiltonian can be written as,

$$H_{(L,R)} = \begin{pmatrix} E_{(m,n)1} & & 0 \\ & \ddots & \\ 0 & & E_{(m,n)\infty} \end{pmatrix} \tag{1.31}$$

Clearly it's a diagonal matrix which can be manipulated to express self-energies as,

$$\sum\nolimits_{ij}^{L}(E) = \sum_{l} \frac{\tau_{il}\tau_{lj}}{E - E_l + i\epsilon} \tag{1.32}$$

This total term can be split into two parts, one will be real and another will be imaginary. It can be expressed as,

$$\begin{aligned} Re\left[\sum\nolimits_{ij}^{L}(E)\right] &= \Lambda_{ij}^{L}(E) = \sum_{l} \frac{\tau_{il}\tau_{lj}}{E - E_l} \\ Im\left[\sum\nolimits_{ij}^{L}(E)\right] &= -\Delta_{ij}^{L}(E) = -\pi \sum_{l} \tau_{il}\tau_{lj}\delta(E - E_l) \end{aligned} \tag{1.33}$$

For this separation, we have used identity, lim ε→0 1/(b+iε) = 1/b – iπδ(b). These real and imaginary parts represent energy level shift and the energy level broadening, respectively. Additionally, the lifetime of electronic states on central region is associated with the broadening of its level. The lifetime of a state is inversely proportional to the broadening of the particular state. For an isolated system, the electronic states are discrete in nature giving an almost infinite lifetime. When it is coupled to electrodes, the electron can go to the electrodes with a certain probability with a finite lifetime.

Using NEGF formalism, the density matrix can be expressed as follows:

$$\rho = \frac{1}{2\pi} \int_{-\infty}^{\infty} dE[f(E,\mu_L)G\Gamma_L G^{\dagger} + f(E,\mu_R)G\Gamma_R G^{\dagger}] \tag{1.34}$$

here, total number of electrons can be given as N=$Tr[\rho S]$. And the total current through the device can be formulated as

$$I = \frac{2e}{h} \int_{-\infty}^{\infty} dE\, Tr[\Gamma_L G \Gamma_R G^{\dagger}]\ (f(E,\mu_L) - f(E,\mu_R)) \tag{1.35}$$

where, $\Gamma_{L,R}$ represent the imaginary part of the self-energies. As mentioned earlier, these imaginary parts correspond to the broadening of the energy levels. In the absence of incoherent scattering processes, this formalism is exactly merged with Landauer's

formalism which we have discussed earlier. Therefore, for coherent transport, we can compare equation (1.25) and (1.35) and obtain the expression for transmission coefficient as,

$$T(E) = \left[G_C^{\dagger}\Gamma_R G_C \Gamma_L\right] \tag{1.36}$$

These equations are the building blocks of NEGF formalism and can be solved in a self-consistent manner with the potential profile which gets improved by the charge distribution in the device region. The real benefit of using NEGF formalism is that, it can successfully demonstrate some of the scattering processes.

To obtain the current-voltage characteristics of devices, NEGF formalism has been combined with Hartree-Fock methods. With the advancement of DFT, a number of packages have been developed which combine NEGF with the DFT method. Some of the examples of these packages are TranSIESTA,[249] Smeagol,[250] Atomistix Toolkit (ATK), McDCal[251] etc.

In TranSIESTA, SIEATA is the DFT code which has been combined with the NEGF formalism. It can treat full spin-polarized systems. All the transport calculations of this thesis have been done using TranSIESTA code.

1.5 Outline of Thesis

As discussed so far, reduction in dimensions of materials impose a number of interesting properties. The experimental developments in this field of research have demonstrated various unique phenomena. In this thesis, we have mostly focused on aromatic and electronic properties of a few molecular systems.

In the next chapter, we have investigated the aromatic nature of boron and nitrogen substituted four benzene ring containing polyaromatic hydrocarbons. In this study, we have shown that the aromatic properties in these molecules can vary significantly by substituting carbon with heteroatoms in appropriate position. In the third chapter, we have discussed the electronic and magnetic properties of [$Fe_{\propto}$(polyacene)$_2$] and boron-nitrogen analogous of it. Our calculations evidently demonstrate metallic and half-metallic properties for [$Fe_{\propto}$(polyacene)$_2$] and [$Fe_{\propto}$(BNpolyacene)$_2$], respectively. We have also explored transport property of finite cluster of [$Fe_{\propto}$(BNpolyacene)$_2$] which under finite bias comes out as an efficient spin-filter. In the chapter 4, we have explored

the structural, electronic, magnetic and transport properties of a lanthanide-based organometallic sandwiched molecule. The presence of unpaired electrons in the ground state of this molecule gives rise to spin polarized electronic structure. It also shows spin polarized transport when attached to two non-magnetic gold electrodes.

Chapter 2

The aromatic nature of the BN substituted Benzene and four ring polyaromatic hydrocarbons

2.1 Introduction

Quantum mechanical approaches have proved extremely valuable to understand the electron delocalization[252-254] or aromatic nature of various organic[151, 255-262] inorganic[263-267] and hybrid systems[268-272] from lower dimensions[273] to higher dimensions[45, 274-277]. Various computational tools have been proposed to define aromaticity based on structural,[48, 130] magnetic,[132, 278, 279]energetic[44] and reactivity criteria[280]. However, as mentioned in the introductory chapter, all methods have its own limitation to predict the degree of aromaticity, since there is no single definition for this concept. Hence, this is necessary to prove the aromatic nature of the molecule by computing more than one aromatic criterion. In addition, the delocalization nature of the molecules could be studied by analyzing the similarities (or dissimilarities) between related systems that enhance the connections of this approach with general concepts. In this chapter, we present investigations of the delocalization nature of polyaromatic hydrocarbons (PAHs) and also how it get affected due to the presence of electron rich nitrogen and hole rich boron heteroatoms.

Boron and nitrogen substituted PAHs have attracted huge attention recently, since they have shown wide applications as optoelectronic materials and colorimetric chemosensors.[58-62, 281-290] Thus, the replacement of carbons in PAHs by B and N heteroatoms might significantly alter the electronic and photophysical properties, while

maintaining the existing structural features. For example, the experimental studies have shown that the electron poor p-type semiconductor material of all-carbon triphenylene core can be switched to electron rich n-type material by replacing one C-C by isoelectronic B-N unit.[59] The bond polarization due to B-N units in the molecule can affect the delocalization of the ring as in the inorganic benzene $B_3N_3H_6$.[268, 283, 284, 286] These natures make the new classes of hybrid organic/inorganic-based PAH materials interesting. Previous experimental and theoretical studies suggested that the number of B and N atoms and their positions (internal/periphery) in PAH ring are important to determine its electronic nature.[60] However, till now, only a very few computational studies[61, 152, 283, 284, 288, 291, 292] are devoted to understand the effect of various B, N substitution towards the periphery (topological) and local aromaticity of the PAH molecules. In addition, there exists a number of possibilities of having B-N at different positions of the PAH ring, which can affect both local and topological aromaticity. Therefore, it is necessary to understand electronic, delocalization nature of the various BN substituted PAHs molecules using computational tools.

In this chapter, the Nucleus Independent Chemical Shift (NICS),[126, 132, 169, 278] Harmonic Oscillator Model of Aromaticity (HOMA),[48, 148], Para Delocalization Index (PDI)[46, 293] and Fluctuation Index (FLU)[130, 182] were used as tools to compute the electron delocalization nature of the all-carbon and BN substituted PAHs. Among these, NICS and PDI values can predict only local aromaticity of the six member ring in PAH's, while HOMA and FLU values measure both the local and topological/periphery aromatic nature of the systems. The HOMO-LUMO gaps [294-296] are also considered in order to understand the kinetic stability of the systems.

All the four methods have been applied for the series of all carbon and B_xN_y (x and y =0-3) substituted benzene, pyrene, chrysene, triphenylene and tetracene compounds and their relative aromatic nature were compared in order to avoid any discrepancy in the methods. These four six member ring PAHs have wide application in organic light emitting diodes (OLEDs), solar cells and organic field-effecting transistors due to their low concentration excimer formation ability and high charge carrier mobility.[297] In addition, these molecules can be a good model to describe the effect due to BN substitution in the 2D[277]and 3D[275, 289] aromatic systems. Few computational and experimental studies have been reported on pyrene[60, 284, 287] and triphenylene[59]

molecules with one B, N atom pair. Up to our knowledge, there are no report on the BN substituted chrysene and tetracene. This is a first report, which explains both periphery/topological and local aromaticity of the complete series of these molecules. Specifically, the topological aromaticity is necessary to compute, since it has a fundamental influence on its physical and chemical properties.[48]

2.2 Computational studies

All the geometry optimizations were performed with the Density Functional Theory (DFT) using three–parameter hybrid functional B3LYP (Becke exchange with Lee, Yang and Parr correlation)[298-300] with 6–31+G(d,p) basis set for all the atoms as implemented in the Gaussian 03 program package.[301] We choose the B3LYP functional, because, it has been found to be one of the most appropriate functional for the prediction of electronic structure for the PAH systems.[136, 152, 259, 262, 282, 285, 286, 302] Stationary structures are characterized as minima on the basis of the calculations of their harmonic vibrational frequencies. The zero point corrected energy values are reported in this paper. The HOMO-LUMO gaps are calculated using the equation,

$$\Delta = \epsilon_{HOMO} - \epsilon_{LUMO} \qquad (2.1)$$

NICS values are calculated using Gauge Including Atomic Orbital (GIAO) method[303-306],[307] at the same level of theory. NICS proposed by Schlyer et.al.,[169] is the magnetic indices of aromaticity and defined as the negative value of the absolute shielding computed at the ring centers or at some other interesting point of the system. Herein, NICS values have been calculated at the ring center (NICS(0)) and 1.0 Å above (NICS(1)) the ring that one is probing. HOMA, which is the structural based measures of aromaticity,[148] rely on the equalization of the bond lengths and symmetry. HOMA term is analytically divided into two terms, EN and GEO, where EN expresses the spread of the bond lengths between the atoms in the aromatic system and GEO expresses the bond length alteration calculated as in the equation:

$$HOMA = 1 - \alpha\left(r_{opt} - r_{av}\right)^2 - \frac{\alpha}{N}\sum_{i=1}^{N}(r_{av} - r_i)^2 \; for \; r_{av} > r_{opt}$$

$$HOMA = 1 + \alpha\left(r_{opt} - r_{av}\right)^2 - \frac{\alpha}{N}\sum_{i=1}^{N}(r_{av} - r_i)^2 \; for \; r_{av} < r_{opt} \qquad (2.2)$$

$$r_{av} = \frac{1}{N}\sum_{i=1}^{N} r_i$$

where N is the number of bonds taken into summation, α is an empirical constant chosen to give a value of HOMA=0 for a nonaromatic system and 1 for aromatic system with all bonds equal to an optimum value r_{opt} and r_i is the computed bond length. The r_{opt} and α values used in this thesis are shown in the table 2.1. Para Delocalization Index (PDI) proposed by Poater *et.al.*,[46] is based on the Bader *et.al.*,[293] delocalization index δ(A,B) where the average of delocalization indices of *para* related atoms in a given six member ring is calculated. This can be formulated as:

$$PDI = \frac{\delta(1,4) + \delta(2,5) + \delta(3,6)}{3} \qquad (2.3)$$

where δ(A,B) is calculated using atom in molecule (AIM) package and (1,4), (2,5) and (3,6) are *para* positions of the six member ring.[293, 308] The wave function file has been created at the Hartree-Fock (HF) level of theory with 6-31+G(d) basis set for the optimized geometry using B3LYP with 6-31+G(d,p) functional as implemented in the Gaussian 03 package. The aromaticity fluctuation index (FLU),[130, 182] which is also calculated from the δ(A,B) values, describes the fluctuation of electronic charge between adjacent atoms in a given ring. The FLU is based on the comparison of cyclic electron delocalization of typical aromatic molecules and calculated using the equation:

$$FLU = \frac{1}{n}\sum_{A-B}^{n}\left[\left(\frac{Flu(A \rightarrow B)}{Flu(B \rightarrow A)}\right)^{\alpha}\left(\frac{\delta(A,B) - \delta_{ref}(A,B)}{\delta_{ref}(A,B)}\right)\right]^2 \qquad (2.4)$$

where n is the number of the atoms in the ring. Flu(A→B) gives the amount of electronic charge gets transferred from A to B via A−B bonds and δ(A,B) and δ_{ref}(A,B) are the delocalization indices for atoms A and B and their reference values, respectively. The reference values of some typical bonds are given in table 2.1.

Table 2.1: The $\alpha(Å^{-2})$ and $R_{opt}(Å)$ values used for the HOMA calculation and $\delta_{ref}(A,B)$ values used for FLU index calculation for the respective bonds.

S.No	Bonds	α	R_{opt}	$\delta_{ref}(A,B)$
1.	C–C	257.70[48]	1.388[48]	1.40[182]
2.	C–N	93.52[48]	1.334[48]	1.20[182]
3.	C–B	138.06*	1.561*	0.44#
4.	B–N	72.0[152]	1.564[152]	0.40#
5.	N–N	130.33[48]	1.309[48]	0.90#

'' α and R_{opt} values are calculated based on H_3B-CH_3 and $(^iPr)_2N=B=C(SiMe_3)_2$ molecules. '#' δ_{ref} values are taken from $C_2B_2N_2H_6$ molecules.*

2.3 Results and discussion

In order to understand the effect of isoelectronic B, N substitution in tetracyclic PAH's, the well-known benzene ring was studied first with various B and N ratio (figure 2.1). Although 1,2-dihydrido-1,2-azaborine derivatives are experimentally synthesized,[283] very little is known about its aromatic nature. All the aromatic index calculations were performed in ground state equilibrium geometry of all the systems.

2.3.1 Six member rings

Replacement of two carbon atoms in a benzene ring by one boron and one nitrogen atoms can produce three isoelectronic structural isomers. They are 1, 2-dihydrido-1, 2-azaborine (b), 1, 4-dihydrido-1, 4-azaborine and (c) 1, 3-dihydrido-1, 3-azaborine (d) (see figure 2.1). The studies of these isomers provide clear correlation between the charge separation and electron delocalization. The delocalization differences among these three isomers were calculated using NICS, HOMA, FLU and PDI criteria (see table 2.2 and figure 2.1) and compared with the benzene molecule. Computed HOMA, NICS, PDI and FLU values for benzene is in good agreement with the already reported values at various level of theory.[291] All computed aromatic index values (see table 2.2) clearly show that the benzene is more aromatic than B, N containing molecules 1, 2-dihydrido-1, 2-azaborine (b), 1, 4-dihydrido-1, 4-azaborine (c) and 1, 3-dihydrido-1, 3-azaborine (d). Among the B, N substituted benzene isomers, d (1, 3-dihydrido-1, 3-azaborine) is most aromatic with –24.9 ppm $NICS(1)_{zz}$, 0.74 HOMA, 0.07 PDI and 0.014 FLU values (aromatic order d > b

> c). The charge separations at three isomers and their corresponding orbital nodal plane changes are clearly reflected in three occupied π MO's (see figure 2.2). The predicted aromaticity order is in good agreement with the aromatic order reported using isodesmic equation.[291] In addition, this is clear that the less aromatic 1, 2-dihydrido-1, 2-azaborine (b) is energetically more stable than 1,4-dihydrido-1, 4-azaborine (c)

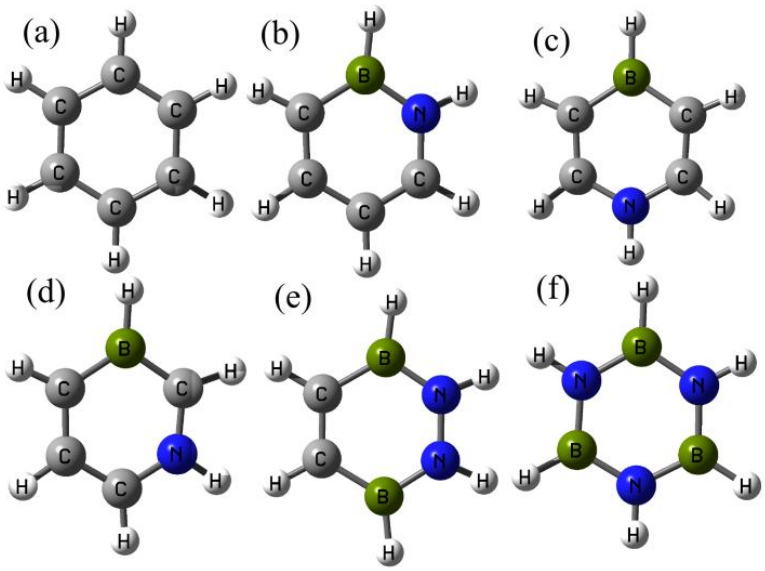

Figure 2.1: Optimized geometry of six member (a) C_6H_6, (b)1, 2-dihydrido-1, 2-azaborine,(c) 1, 4-dihydrido-1, 4-azaborine and (d)1, 3-dihydrido-1, 3-azaborine (e) $C_2B_2N_2H_6$ and (f) $B_3N_3H_6$ rings.

and 1, 3-dihydrido-1, 3-azaborine (d) by 22 and 29.6 kcal·mol^{-1} respectively. The computed relative energy differences for these isomers are in good agreement with the already reported values (c) 23.1 and (d) 29.9 kcal·mol^{-1} at MP4 level,[291] which validates the functional and the basis set that we have used. The energetic stability of the molecule is referred in the HOMO –LUMO gap. The low negative NICS(0)$_{zz}$ (see table 2.2) values of BN-substituted six member rings (see figure 2.1) provide the evidence for the larger σ contribution at the molecular plane. This σ contribution dominates to determine the structural stability order of various isomers.

To elaborate these studies, four carbon atoms in benzene ring were swapped by two boron and two nitrogen atoms which results in $B_2N_2C_2H_6$ molecule (see figure 2.1e). The replacement increases NICS, FLU values, decreases PDI and HOMA values than the benzene, which reflect its less aromatic nature. In addition to very low negative -2.72 *ppm*

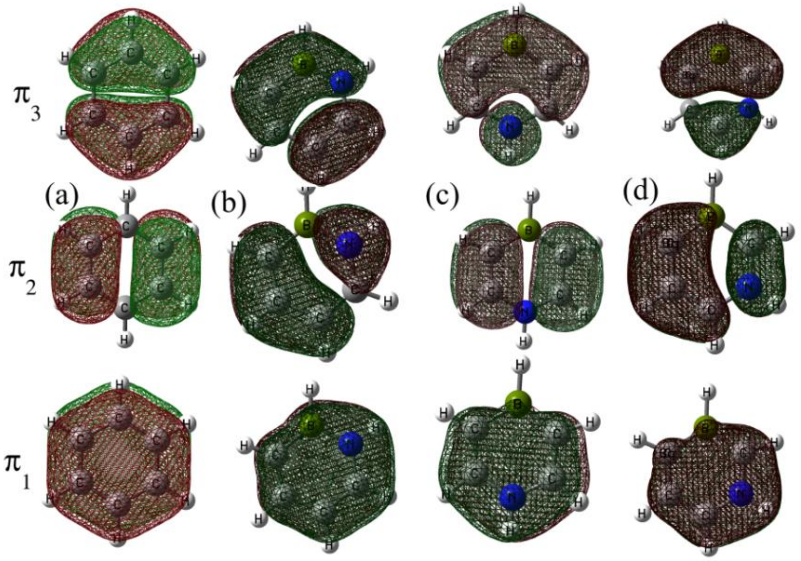

Figure 2.2: The occupied π molecular orbitals (MO's) of (a) benzene, (b) 1, 2-dihydrido-1, 2-azaborine, (c) 1, 4-dihydrido-1, 4-azaborine and (d)1, 3-dihydrido-1, 3-azaborine. The charge separations due to the B, N positions are clearly reflected in the π_2 and π_3 molecular orbitals.

NICS(0) at molecular plane and its positive 3.73 $NICS(0)_{zz}$ components expose the considerable amount of σ orbital contribution. These σ orbital contributions are more prominent in the inorganic benzene $B_3N_3H_6$, which has very large positive $NICS(0)_{zz}$ value (+12 *ppm*) (see table 2.2). These results provide evidence that increase in the number of charge separated B and N hetero atoms in the benzene ring enhance its σ contribution. However, larger HOMA value, less FLU value and negative $NICS(1)_{zz}$

Table 2.2: Computed NICS (ppm) at the plane and 1 Å above the plane, HOMA, Δ (eV) ,PDI (e) and FLU aromatic indices for six member (a) C_6H_6, (b)1, 2-dihydrido-1, 2-azaborine,(c) 1, 4-dihydrido-1, 4-azaborine and (d)1, 3-dihydrido-1, 3-azaborine (e) $C_2B_2N_2H_6$ and (f) $B_3N_3H_6$ molecules (figure 2.1).

molecule	NICS(0)	$NICS(0)_{zz}$	NICS(1)	$NICS(1)_{zz}$	HOMA	Δ	PDI	FLU
a	-8.20 *-8.07*[309]	-14.51	-10.25 *-10.21*[45]	-28.85	0.97 *0.979*[48]	6.59 *6.55*[283]	0.10	0.00
b	-5.08 *-5.62*[283]	-4.28	-7.00 *-7.27*[283]	-20.08	0.71	5.33 *5.32*[283]	0.06	0.015
c	-4.85	-3.54	-7.24	-19.46	0.51	5.93	0.04	0.019
d	-6.36	-9.86	-8.55	-24.90	0.74	4.69	0.07	0.014
e	-2.72	3.83	-4.81	-12.22	0.69	5.36	0.04	0.022
f	-2.06 *-2.02*[283]	12.04	-2.78 *-3.01*[283]	-5.07	0.94 *0.942*[152]	7.81 *7.91*[283]	0.01	0.000

The values in italic are reported using DFT method.

values (see table 2.2) proves the aromatic nature of the $B_3N_3H_6$ molecule. The computed value for inorganic benzene is comparable with already reported value[152] (see table 2.2) which again certifies our method for B, N containing molecules.

2.3.2 Polycyclic aromatic hydrocarbons

Following the monocyclic molecules, tetracyclic PAHs, which are attractive because of their structural simplicity and high symmetry, were studied. Six molecules are possible in the 4 ring arrangement and among these, four molecules; pyrene, chrysene, tetracene and triphenylene are highly stable and have been well characterized. The four molecules are unique and could mimic wide range of 2D material because of their different shapes. All these four molecules have been studied in detail using both experimental and theoretical methods.[48, 126, 182, 259, 295, 297, 306] Previous computational studies [126, 131, 259] have shown that the chrysene is most stable and tetracene is least stable among these four. The above-mentioned properties make them fascinating and comparison between pyrene, chrysene, triphenylene and tetracene and also with the various BN substituted analogues will be informative. Among these, pyrene is known for its distinctive nature that the aromatic molecule with 4n π electrons.

Pyrene

Pyrene is the PAH with $C_{16}H_{10}$ molecular formula and 16 π electrons. The computed NICS, HOMA, FLU and PDI values of pyrene are in good agreement with the already reported values,[126, 131, 259, 295] where R2 and R4 are more aromatic than R1 and R3 (see figure 2.3 and table 2.3). Substitution of two carbon atoms by one boron and one nitrogen leads to five different isomers as shown in the figure 2.3(p-b to p-f), which strongly refrain their local six member ring and topological 14 member ring delocalization nature. The five different isomers lead to five different topologies, which are all-carbon with internal BN entity (p-b), one B (p-c), one N (p-d), *o*-BN (p-e) and *p*-BN (p-f) in the topological rings (see figure 2.3). Topological aromaticity is the one, which determines the electronic, chemical and physical nature of the molecules. The computed HOMA and FLU values show the trend as p-b > p-d > p-f > p-c > p-e for topological aromaticity. The HOMA values are dominated by EN rather than GEO (see table 2.3), which provide evidence for the bond elongation due to BN substituent making the structures less

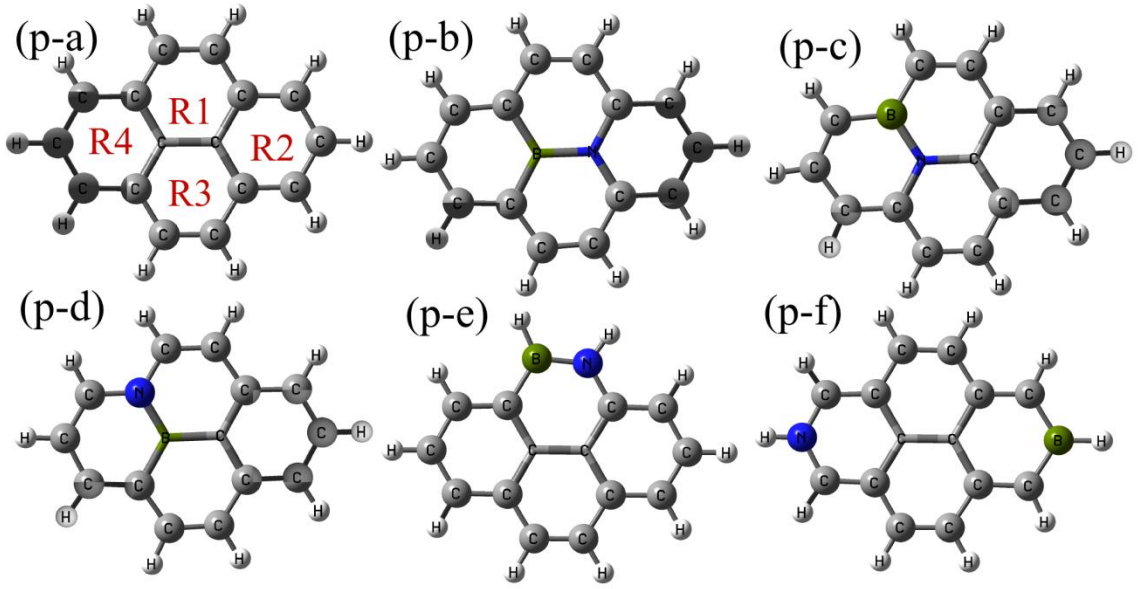

Figure 2.3: Optimized geometry of pyrene and BN substituted pyrene. Ball sticks represent a periphery ring which is used to compute topological aromaticity and R1, R2, R3 and R4 are the labels of six-membered rings of which local aromaticity is been calculated.

aromatic. The studies show that all-carbon topologies (pyrene (p-a) and BN-pyrene (p-b)) are more aromatic in nature than the substituent containing topologies. Moreover, comparing with all-carbon pyrene (p-a) (0.96 HOMA and 0.013 FLU), the internal heteroatom containing structure p-b (see figure 2.3), decreases (0.93 HOMA and 0.014 FLU) its topological aromatic nature (see table 2.3). The electron rich N alone in topological ring (p-d) is more aromatic than electron deficient B (p-c) in topological ring. This is due to the empty *p*-orbitals in the B atom, which contribute less to the π molecular orbitals. Both B and N atoms in topological rings (p-e and p-f) lead to two isomers, which are B, N hetero atoms at the adjacent position and B, N at the opposite position of the topological ring. First isomer is less aromatic than another one. This is similar to the trend observed for 1, 2-dihydrido-1, 2-azaborine (b) and 1, 4-dihydrido-1, 4-azaborine (c) molecules (see figure 2.1). In addition, the MO pictures undoubtedly show that the clear correlation between the orbital shapes and aromaticity. The π MOs of internally substituted pyrene (p-b) is similar to the all carbon pyrene (see figure 2.4), which explains its more aromatic nature. However, the MOs of p-e molecule (containing both B and N heteroatoms in the topological ring) have a completely different orientation due to the charge separation within heteroatoms which is the reason for its less aromatic nature (see

figure 2.4). The effect of BN charge separation in pyrene is similar to that in *o*-,*p*-,*m*- BN substituted benzene ring (see figure 2.2). However, like benzene, topologically more aromatic BN-substituted pyrene is energetically less stable. The energetic stability order of BN-substituted pyrene isomers are p-e (0) > p-c (17.68) > p-d (20.51) > p-b (21.55) > p-f (56.70 kcal·mol^{-1}), which is also reflected in their Δ values (see table 2.3). This

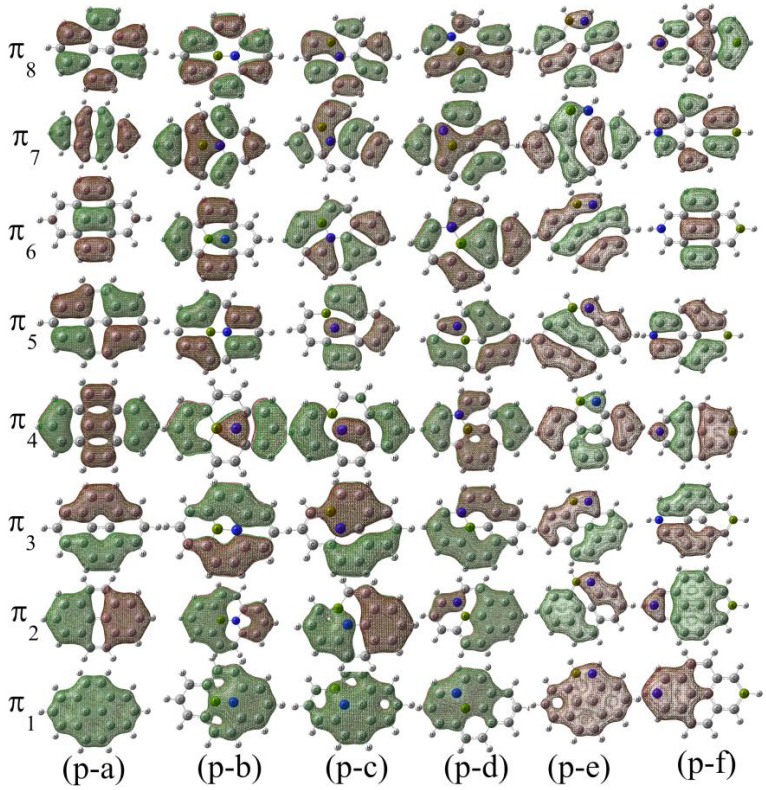

Figure 2.4: The occupied eight π molecular orbitals (MO's) of all carbon and BN substituted pyrene isomers shown in the figure 2.3. The charge separation due to the B and N position reflects in the MOs.

follows similar trend as in the six member heterocyclic systems, where the less aromatic 1, 4-dihydrido-1, 4-azaborine (c) is energetically more stable than more aromatic 1, 3-dihydrido-1, 3-azaborine (d) isomer (see figure 2.1). To understand the change in local aromaticity of each ring due to BN substitution in the structure, NICS, HOMA, PDI and FLU have been calculated for four rings separately. The labeling scheme of the pyrene molecules are shown in figure 2.3. The order of local aromaticity based on NICS(1), NICS(1)$_{zz}$, HOMA, PDI and FLU are, (p-b) R4 >R2> R3=R1; (p-c) R2 > R4 > R1 > R3;

(p-d) R2 > R4 > R1 > R3; (p-e) R4 > R2 > R3 > R1 and (p-f) R4 > R1=R3 > R2 . The general observations from these orders are as follows:

- Computed values clearly show that all the rings are aromatic
- Increase or decrease in the degree of aromaticity for BN-substituted molecule depends on the position of heteroatoms in the structure. The ring which contain only one three-ring-shared heteroatom is less aromatic than the other rings (R3 of p-b and p-e are more aromatic than R3 of p-c and p-d, figure 2.3).
- Ring which solely contain two heteroatoms are less aromatic than other rings (R1 of p-e, figure 2.3).
- However, one electron rich or electron poor hetero atom containing single ring is more aromatic than other rings in the same molecule (R2 and R4 of p-f, figure 2.3).

Table 2.3: Computed NICS (ppm) at the plane and 1 Å above the plane, HOMA, Δ (eV), PDI and FLU aromatic indices for pyrene (p-a) and BN pyrene (p- b – p-f).

Molecules	NICS(0)	$NICS(0)_{zz}$	NICS(1)	$NICS(1)_{zz}$	HOMA(EN/GEO)	Δ	PDI	FLU
p-a R1	-3.92	3.13	-7.01	-16.7	0.70(0.28/0.02)		0.04	0.022
R2	-11.28	-20.00	-12.92	-35.41	0.86(0.12/0.02)	3.79	0.07	0.005
R3	-3.92	3.13	-7.01	-16.7	0.70(0.28/0.02)		0.04	0.022
R4	-11.28	-20.00	-12.92	-35.41	0.86(0.12/0.02)		0.07	0.005
TP					*0.96(0.03/0.01)*			*0.013*
p-b R1	-7.09	-5.97	-9.05	-23.22	0.65(0.30/0.05)		0.03	0.051
R2	-11.83	-19.29	-12.51	- 35.36	0.78(0.22/0.00)	3.56	0.06	0.002
R3	-7.09	-5.05	-9.05	-23.22	0.65(0.30/0.05)		0.03	0.051
R4	-13.42	-28.39	-14.80	-41.33	0.64(0.27/0.09)		0.05	0.066
TP					*0.93(0.07/0.00)*			*0.014*
p-c R1	-2.18	8.85	-4.89	-10.92	0.49(0.45/0.06)		0.03	0.074
R2	-10.35	-15.00	-11.31	-30.62	0.90(0.10/0.00)	3.67	0.08	0.005
R3	1.17	20.56	-2.11	-3.46	0.68(0.31/0.01)		0.03	0.092
R4	-8.11	-9.72	-9.60	-25.85	0.59(0.33/0.08)		0.05	0.074
TP					*0.64(0.31/0.05)*			*0.048*
p-d R1	-3.16	6.31	-5.16	-12.43	0.72(0.24/0.04)		0.03	0.059
R2	-9.72	-16.11	-11.6	-32.6	0.89(0.11/0.00)	3.70	0.08	0.002
R3	-1.02	7.88	-4.02	-10.07	0.61(0.34/0.05)		0.02	0.022
R4	-8.83	-12.38	-10.11	-27.55	0.73(0.2/0.07)		0.05	0.036
TP					*0.80(0.18/0.02)*			*0.038*
p-e R1	-0.08	16.07	-2.78	-5.04	0.48(0.45/0.07)		0.02	0.027
R2	-10.78	-16.44	-11.55	-31.92	0.87(0.12/0.01)	4.09	0.07	0.007
R3	-4.4324	1.53	-7.05	-18.00	0.69(0.30/0.01)		0.04	0.021
R4	-10.14	-16.56	-12.19	-33.08	0.86(0.12/0.02)		0.08	0.003
TP					*0.61(0.36/0.03)*			*0.056*
p-f R1	-4.75	1.5	-7.43	-18.29	0.68(0.32/0.00)		0.03	0.022
R2	-10.38	-20.44	-13.48	-36.27	0.51(0.44/0.07)	3.27	0.03	0.094
R3	-4.73	1.55	-7.42	-18.28	0.65(0.32/0.03)		0.03	0.023
R4	-9.31	-8.20	-9.60	-25.35	0.84(0.14/0.02)		0.04	0.022
TP					*0.72(0.24/0.04)*			*0.020*

R1, R2, R3 and R4 indicate the local aromaticity of the mentioned ring in the figure 2.3. TP represents topological aromaticity.

Chrysene

Chrysene is second example of four rings containing PAH and having chemical formula $C_{18}H_{12}$, with 18π electrons. For chrysene, NICS, HOMA, FLU and PDI values predict that R1 and R4 as more aromatic than R2 and R3 (see figure 2.5 and table 2.4). The computed NICS, HOMA, PDI and FLU values indicate that chrysene is less aromatic than the pyrene molecule, which is in good agreement with the already reported results using 6-311++G(d,p).[126, 131, 259, 295] Five isomers are possible for one boron and one nitrogen substituted chrysene (see figure 2.5, c-b to c-f). Unlike the pyrene molecule, all

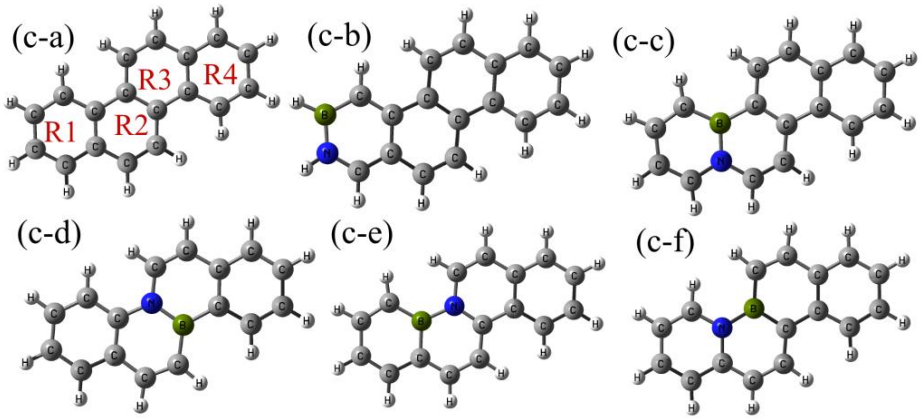

Figure 2.5: Optimized geometry of all carbon (c-a) and BN (c-b – c-f) substituted chrysene. Ball stick is a periphery ring used to compute topological aromaticity and R1, R2, R3 and R4 used to calculate the local aromaticity.

the carbons contribute to the topological ring, which makes both substituents important. According to HOMA and FLU values, the order of topological aromaticity is c-b > c-f > c-c ≈ c-e > c-d, where the energetic order is c-d >c-c >c-b >c-f >c-e. Comparatively, substitution of the B and N atoms in more aromatic R1 or R4 ring (c-b) of chrysene results in more aromatic topology. Similar to pyrene, σ bonds have more effect than π bonds to determine the stability order of BN substituted chrysene isomers. Like pyrene, of the ring makes all carbon six member rings more aromatic than the BN substituent containing ring of this molecule (R4 in figure 2.5, c-b - c-f). The local aromaticity orders for six member rings are as follows: c-b (R4 > R1 > R3 > R2) > c-f (R4 > R3 > R1 > R2) >c-c (R4 > R3 > R1 > R2) ≈ c-e (R4 > R3 > R1 > R2) > c-d (R4 > R1 > R3 > R2).

Table 2.4: Computed NICS (ppm) at the plane and 1 Å above the plane, HOMA, Δ (eV), PDI and FLU aromatic indices for chrysene (c-a) and BN chrysene (c-b – c-f).

Molecules		NICS(0)	$NICS(0)_{zz}$	ICS(1)	$NICS(1)_{zz}$	HOMA (EN/GEO)	Δ	PDI	FLU
c-a	R1	-8.79	-11.85	-10.7	-28.31	0.89(0.09/0.02)	4.20	0.078	0.007
	R2	-6.40	- 3.38	- 8.78	-22.38	0.67(0.28/0.05)		0.051	0.017
	R3	-6.40	-3.38	-8.78	-22.38	0.67(0.28/0.05)		0.051	0.017
	R4	-8.79	-11.85	-10.7	-28.31	0.89(0.09/0.02)		0.078	0.007
	TP					*0.85(0.1/0.03)*			*0.014*
c-b	R1	-6.83	-6.71	-8.76	-23.31	0.78(0.15/0.07)	3.58	0.058	0.031
	R2	-2.67	8.416	-5.63	-12.50	0.50(0.43/0.08)		0.036	0.029
	R3	-6.91	-4.10	-9.19	- 22.90	0.74(0.25/0.00)		0.057	0.015
	R4	-8.44	-10.85	-10.93	-28.71	0.90(0.1/0.01)		0.077	0.007
	TP					*0.83(0.15/0.02)*			*0.028*
c-c	R1	-5.55	-3.2	-7.42	-19.71	0.60(0.29/0.11)	4.19	0.054	0.046
	R2	-4.09	3.70	-6.38	-15.13	0.49(0.43/0.08)		0.034	0.052
	R3	-6.69	-5.17	-9.34	-24.18	0.74(0.26/0.00)		0.059	0.014
	R4	-8.76	-11.77	-10.67	-28.37	0.89(0.1/0.01)		0.077	0.008
	TP					*0.58(0.38/0.4)*			*0.111*
c-d	R1	- 8.02	-11.09	- 10.39	-28.12	0.91(.08/.01)	4.32	0.088	0.002
	R2	- 2.97	7.1	- 5.36	-11.96	0.39(0.46/0.14)		0.029	0.062
	R3	- 3.23	6.52	- 5.66	-12.55	0.43(0.44/0.12)		0.031	0.078
	R4	- 9.36	-11.55	- 10.50	-27.48	0.93(0.07/0.00)		0.083	0.005
	TP					*0.46(0.48/0.05)*			*0.159*
c-e	R1	- 5.87	-6.73	- 8.13	-21.81	0.59(0.33/0.07)	3.40	0.053	0.015
	R2	- 7.37	- 6.95	- 9.02	-23.37	0.56(0.36/0.07)		0.044	0.024
	R3	- 2.20	11.78	- 4.68	-10.17	0.66(0.26/0.07)		0.034	0.081
	R4	- 7.95	- 8.44	- 10.08	-25.70	0.92(0.07/0.00)		0.083	0.004
	TP					*0.58(0.38/0.04)*		\	*0.129*
c-f	R1	- 3.74	4.3	- 6.06	-15.64	0.59(0.33/0.8)	3.40	0.056	0.044
	R2	- 7.66	- 7.25	- 9.34	-24.08	0.56(0.36/0.07)		0.044	0.06
	R3	- 3.42	3.13	- 6.28	-14.50	0.66(0.27/0.07)		0.032	0.035
	R4	- 8.10	-9.94	- 10.17	-26.85	0.93(0.07/0.00)		0.082	0.004
	TP					*0.57(0.39/0.04)*			*0.029*

R1, R2, R3 and R4 indicate the local aromaticity of the mentioned ring in the figure 2.5. TP represents topological aromaticity.

Triphenylene

Triphneylene ($C_{18}H_{12}$) is the third member of this family, where one extra benzene ring is attached to the central ring of phenanthrene. This makes the central ring shared by all three other benzene rings. Computed NICS, HOMA, PDI and FLU values provide evidence that the central ring (R4 of tr-a) is much less aromatic than the other rings (R1, R2 and R3 of tr-a, figure 2.6). HOMA and FLU values clearly indicate that topologically triphenylene is less aromatic than pyrene and chrysene. (see table 2.5). Isoelectronic BN substitution in the triphenylene ring, gives six isomers. Among these isomers, the order of topological aromaticity is as follows tr-d > tr-f ≈ tr-g > tr-e > tr-c > tr-b. This order can also be explained considering the position of substituent atoms in the structure, which

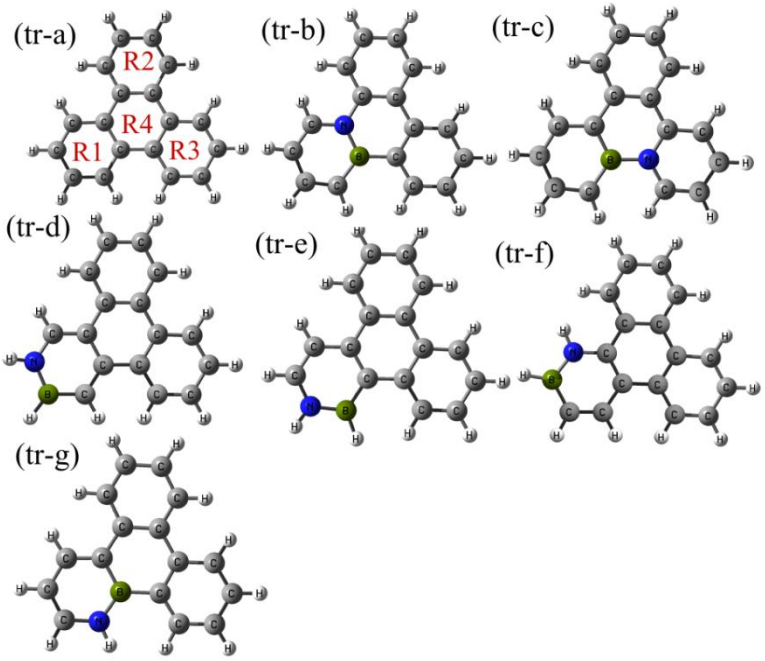

Figure 2.6: Optimized geometry of all-carbon (tr-a) and BN (tr-b – tr-g) substituted triphenylene. Ball sticks represent a periphery ring which is used to compute topological aromaticity and R1, R2, R3 and R4 are the labels of six-membered rings of which local aromaticity is been calculated.

dramatically affects the bond distances. Herein, we have studied the aromaticity change due to the BN substitution at the more aromatic ring. On that way, three different isomers (see figure 2.6, tr-d - tr-f) are possible. Among these, the tr-d is topologically more aromatic (see table 2.5), due to the less effect of BN substitution to the other three rings (R2-R4 of tr-d, figure 2.6). However, in tr-e and tr-f, the R4 ring is directly coordinated to heteroatom which makes them topologically less aromatic than tr-d. Similarly, tr-c for which BN-substituents are shared by R1, R3 and R4 rings, become topologically less aromatic and it reflects in the HOMA and FLU values (see table 2.5). Similar to chrysene, the six member ring with more substituent are locally less aromatic than all carbon six member ring. The local aromaticity orders for the BN substituted molecules are, tr-d (R2 > R3 > R1 > R4) > tr-f (R2 > R3 > R1 > R4) ≈ tr-g (R3> R2> R1 > R4) > tr-e (R2 > R3 > R1 > R4) > tr-c (R2 > R3 > R1 > R4) > tr-b (R2 > R3 > R1 > R4).

Table 2.5: Computed NICS (ppm) at the plane and 1 Å above the plane, HOMA, Δ (eV), PDI and FLU aromatic indices for all-carbon (tr-a) and BN (tr-b – tr-g) substituted triphenylene.

Molecules		NICS(0)	$NICS(0)_{zz}$	NICS(1)	$NICS(1)_{zz}$	HOMA(EN/GEO)	Δ	PDI	FLU
tr-a	R1	-7.83	-8.90	-9.76	-25.84	0.92(0.06/0.02)	4.83	0.054	0.001
	R2	-7.83	-8.90	-9.76	-25.84	0.92(0.06/0.02)		0.087	0.003
	R3	-7.83	-8.90	-9.76	-25.84	0.92(0.06/0.02)		0.091	0.072
	R4	-2.25	12.35	-5.65	-10.07	0.15(0.83/0.02)		0.017	0.077
	TP					*0.81(0.14/0.05)*			*0.015*
tr-b	R1	-4.05	-1.12	-6.69	-16.71	0.62(0.28/0.10)	4.53	0.054	0.001
	R2	-8.35	-8.81	-9.08	-24.05	0.94(0.06/0.00)		0.087	0.003
	R3	-7.07	-8.26	-9.80	-26.05	0.93(0.06/0.01)		0.091	0.072
	R4	-0.52	16.07	-3.51	-5.63	0.22(0.72/0.06)		0.017	0.077
	TP					*0.46(0.50/0.04)*			*0.111*
tr-c	R1	-6.68	-7.46	-8.51	-22.74	0.64(0.24/0.12)	2.98	0.062	0.065
	R2	-7.01	-6.36	-9.18	-23.90	0.88(0.11/0.01)		0.073	0.104
	R3	-4.75	0.89	-7.12	-18.53	0.87(0.11/0.02)		0.068	0.009
	R4	-5.12	0.41	-7.24	-18.20	0.41(0.55/0.04)		0.027	0.038
	TP					*0.60(0.37/0.03)*			*0.118*
tr-d	R1	-5.46	-2.15	-7.54	-19.82	0.8(0.13/.07)	4.04	0.058	0.026
	R2	-7.11	-6.28	-9.17	-23.68	0.94(0.06/0.00)		0.087	0.002
	R3	-7.15	-6.83	-9.39	-24.35	0.93(0.07/0.00)		0.088	0.033
	R4	0.07	20.22	-3.54	- 3.20	0.00(1.00/0.00)		0.018	0.007
	TP					0.82(0.15/0.03*)*			*0.034*
tr-e	R1	-3.82	3.19	- 5.83	-14.86	0.65(0.26/0.09)	4.25	0.046	0.05
	R2	-8.06	-9.66	-10.22	-26.89	0.91(0.07/0.02)		0.084	0.004
	R3	-7.75	-9.22	- 9.94	-26.39	0.91(0.07/0.02)		0.083	0.026
	R4	-3.55	-7.92	-6.88	-13.98	0.25(0.72/0.03)		0.034	0.012
	TP					*0.67(0.29/0.04)*			*0.058*
tr-f	R1	-4.23	3.26	-6.38	-15.24	0.74(0.20/0.06)	3.99	0.048	0.055
	R2	-8.35	-9.38	-10.21	-26.52	0.92(0.08/0.02)		0.083	0.022
	R3	-8.09	-9.22	-10.15	-26.60	0.91(0.07/0.00)		0.083	0.041
	R4	-3.51	7.02	-5.90	-13.68	0.29(0.26/0.03)		0.031	0.004
	TP					*0.75(0.22/0.03)*			*0.011*
tr-g	R1	-5.55	-2.42	-7.30	-19.39	0.73(0.19/0.08)	3.94	0.056	0.026
	R2	-6.79	-6.44	-9.04	-23.86	0.89(0.08/0.02)		0.087	0.002
	R3	-6.95	-7.91	-9.49	-25.47	0.91(0.07/0.02)		0.091	0.030
	R4	0.90	17.55	-3.06	- 3.27	0.02(0.96/0.02)		0.016	0.000
	TP					*0.75(0.22/0.03)*			*0.048*

R1, R2, R3 and R4 indicate the local aromaticity of the mentioned ring in the figure 2.6. TP represents topological aromaticity.

Tetracene

Tetracene is unique from others for its linear structure with chemical formula, $C_{18}H_{12}$ with 18 π electrons. For this structure, R2 and R3 are more aromatic than R1 and R4 rings (see figure 2.7 and table 2.6), which is in good agreement with the previous results.[130] Nine isomers (te-b to te-j) are possible for one boron and one nitrogen substituted tetracene. Topologically all-carbon tetracene is more aromatic than BN-substituted structures. Considering HOMA and FLU values, topological aromaticity order of BN-

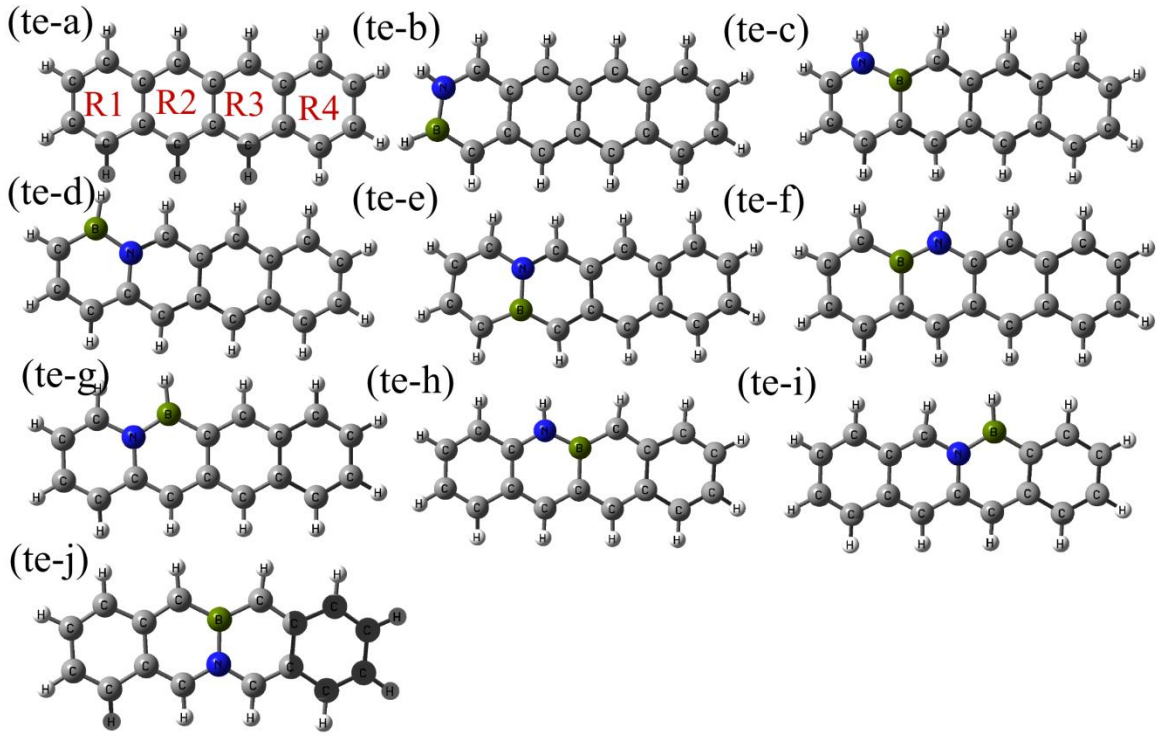

Figure 2.7: Optimized geometry of all-carbon (te-a) and BN (te-b – te-j) substituted tetracene. Ball sticks represent a periphery ring which is used to compute topological aromaticity and R1, R2, R3 and R4 are the labels of six-membered rings of which local aromaticity is been calculated.

substituted structures are as follows: te-b > te-c ≈ te-d > te-h ≈ te-j ≈ te-i > te-e > te-f > te-g. This order can be explained considering the position of the heteroatoms in tetracene molecule. When both boron and nitrogen atoms substitute two carbons of terminal ring (te-b, figure 2.7), the structure remain almost as aromatic as all-carbon tetracene (see table 2.6). However, presence of heteroatoms in middle rings (te-i ,te-j) make the structure topologically less aromatic. In addition, BN substitution in the terminal aromatic ring (R1 of te-b) does not affect the other rings (R4 or R3) in the molecule. Like chrysene and triphenylene, for tetracene, all-carbon six member rings are more aromatic than the BN substituted one. In tetracene, always some discrepancies were observed in the local aromaticity order considering the NICS, PDI and HOMA, FLU values. Note that, NICS and PDI values are without any reference point and calculated at the center of the ring while the HOMA and FLU values strongly depend on the reference values and are calculated as the average of all bonds of the ring. So herein, we consider only NICS and

Table 2.6. Computed NICS (ppm) at the plane and 1 Å above the plane, HOMA, Δ (eV), PDI and FLU aromatic indices for all-carbon (te-a) and BN (te-b – te-j) substituted tetracene.

Molecules		NICS(0)	$NICS(0)_{zz}$	NICS(1)	$NICS(1)_{zz}$	HOMA(EN/GEO)	Δ	P I	FLU
te-a	R1	-6.72	-5.97	-8.84	-23.17	0.72(0.25/0.03)	2.7	0.055	0.024
	R2	-11.01	-18.30	-12.39	-34.42	0.75(0.23/0.02)		0.062	0.012
	R3	-11.01	-18.30	-12.39	-34.42	0.75(0.23/0.02)		0.062	0.012
	R4	-6.72	-5.97	-8.84	-23.17	0.72(0.25/0.03)		0.055	0.024
	TP					*0.92(0.08/0.00)*			0.015
te-b	R1	-9.13	-14.39	-10.28	-29.09	0.73(0.21/0.06)	2.13	0.056	0.028
	R2	-9.01	-13.78	-10.59	-30.57	0.66(0.33/0.01)		0.060	0.018
	R3	- 7.76	- 9.19	- 9.62	-26.83	0.69(0.3/0.00)		0.054	0.015
	R4	-4.42	0.80	-6.73	-17.44	0.76(0.22/0.02)		0.049	0.086
	TP					*0.84(0.13/0.02)*			0.015
te-c	R1	-9.14	-13.68	-10.16	-28.07	0.56(0.32/0.1)	2.10	0.048	0.030
	R2	-9.16	-17.06	-11.05	- 32.01	0.50(0.42/0.07)		0.053	0.018
	R3	-8.10	-11.29	- 9.95	-28.28	0.64(0.35/0.0)		0.053	0.027
	R4	- 4.60	0.15	-6.83	-17.91	0.76(0.21/0.01)		0.049	0.007
	TP					*0.83(0.14/0.02)*			0.024
te-d	R1	-9.51	-15.28	-11.01	-30.44	0.63(0.33/0.03)	2.05	0.044	0.030
	R2	-8.24	-8.36	-9.38	-26.24	0.77(0.21/0.01)		0.053	0.018
	R3	-6.93	-5.25	-8.82	-23.57	0.72(0.27/0.00)		0.054	0.060
	R4	- 3.87	2.44	-6.51	-16.11	0.75(0.22/0.02)		0.049	0.013
	TP					*0.80(0.18/0.02)*			0.024
te-e	R1	-6.44	-5.85	-8.17	-21.79	0.45(0.42/0.11)	2.54	0.046	0.030
	R2	-10.80	-17.02	-11.82	-32.17	0.63(0.29/0.07)		0.055	0.020
	R3	- 8.50	-10.84	-10.23	-27.99	0.67(0.32/0.00)		0.054	0.072
	R4	- 4.54	-0.16	-7.02	-17.94	0.75(0.22/0.02)		0.049	0.082
	TP					*0.75(0.22/0.02)*			0.143
te-f	R1	-2.07	4.09	-5.13	-12.57	0.38(0.53/0.08)	2.09	0.041	0.015
	R2	-5.23	- 0.30	-6.98	-18.07	0.46(0.42/0.12)		0.028	0.012
	R3	-11.17	-16.48	-12.01	-32.30	0.79(0.19/0.01)		0.063	0.025
	R4	-7.93	-10.00	-9.79	-26.49	0.84(0.14/0.01)		0.064	0.045
	TP					*0.66(0.29/0.03)*			0.065
te-g	R1	-0.32	14.97	-2.80	-6.28	0.80(0.16/0.03)	2.96	0.042	0.016
	R2	-5.56	-1.20	-7.25	-18.90	0.54(0.41/0.04)		0.024	0.009
	R3	-10.21	-15.96	-12.03	-32.78	0.77(0.21/0.01)		0.066	0.055
	R4	-7.74	-9.53	- 9.78	-26.26	0.83(0.15/0.01)		0.063	0.107
	TP					*0.68(0.28/0.03)*			0.096
te-h	R1	-9.46	-13.09	-10.63	-28.42	0.86(0.10/0.04)	2.50	0.072	0.033
	R2	-8.63	-9.79	-9.83	-25.86	0.52(0.37/0.11)		0.035	0.022
	R3	-6.13	- 7.18	-8.37	-23.09	0.33(0.49/0.18)		0.047	0.042
	R4	-2.97	3.9	- 5.7	-14.36	0.69(0.29/0.02)		0.045	0.008
	TP					*0.78(0.18/0.02)*			0.049
te-i	R1	-8.46	-12.05	-10.54	-28.63	0.83(0.12/0.05)	2.45	0.076	0.033
	R2	-8.62	-10.67	-9.98	-27.16	0.59(0.38/0.03)		0.031	0.086
	R3	-4.19	4.60	-5.99	-15.74	0.73(0.26/0.01)		0.048	0.060
	R4	-1.76	9.37	-4.55	-10.42	0.66(0.22/0.02)		0.045	0.008
	TP					*0.76(0.20/0.04)*			0.040
te-j	R1	-4.96	-1.92	-7.39	-19.62	0.74(0.23/0.03)	2.88	0.047	0.030
	R2	-10.24	-15.08	-11.35	-30.47	0.59(0.33/0.09)		0.052	0.071
	R3	-10.24	-15.08	-11.35	-30.47	0.59(0.33/0.09)		0.052	0.071
	R4	-4.96	-1.92	-7.39	-19.62	0.74(0.23/0.03)		0.047	0.030
	TP					*0.77(0.19/0.04)*			0.090

R1, R2, R3 and R4 indicate the local aromaticity of the mentioned ring in the figure 2.7. TP represents topological aromaticity.

PDI values of the tetracene to compare the local aromaticity between the rings. The order of local aromaticity of the rings of BN substituted tetracene are as follows: te-b (R2 > R1 > R3 > R4) > te-c (R2 > R3 > R1 > R4) ≈ te-d (R1 > R2 > R3 > R4) > te-h (R1 > R2 > R3 > R4) ≈ te-j (R2 ≈ R3> R1 ≈ R4) ≈ te-i (R1 > R2 > R3 > R4) > te-e (R2 > R3 > R1 > R4) > te-f (R3 > R4 > R2 > R1) > te-g(R3 > R4 > R2 > R1).

2.4 Conclusion

In conclusion, density function theory based five aromatic criteria are applied to the series of B, N substituted six member ring, pyrene, chrysene, tetracene and triphenylene molecule. Our studies show that BN containing six member rings are always less aromatic than the all-carbon containing six member rings. The charge separation due to the hetero atoms in the rings are the reason for its less aromatic nature, which is clearly reflected in their π molecular orbitals. Among the four tetracylcic molecules, pyrene is most aromatic with 16 π electrons. The computed topological aromaticity order based on FLU index for all tetracyclic PAH is pyrene > tetracene > chrysene > triphenylene which is in good agreement with previously reported results based on HOMA.[126, 131, 259, 295] NICS, HOMA, PDI and FLU methods follow the same trends as in local aromaticity in the case of BN-substituted pyrene, chrysene and triphenylene. While for tetracene, HOMA, FLU indexes follow different trends than the NICS, PDI indexes. The topological aromaticity depends largely upon the position of B and N atoms. In general, more ring shared BN containing molecules are less aromatic than the less ring shared BN molecules. The highly aromatic molecule is always energetically less stable than their less aromatic isomers which provide evidence that energetic order of isomers always largely influenced by σ orbital contribution than the π orbital one. Energetic stability is in good correlation with HOMO-LUMO energy gaps.

Chapter 3

Electronic and magnetic structure of Fe_n-bis(n-acene) and its BN-analogue: A theoretical study

3.1 Introduction

As we are in the final stage of the silicon-device era [198, 199], a huge attention has been given to develop new devices where charge as well as intrinsic spin of electrons can be used to store informations.[3] Actually, spin based devices are very efficient than the charge based ones in terms of energy, size, response time, etc.[88, 204, 310, 311] In the early hours of spintronic research, metals and inorganic semiconductors were mainly explored to have efficient spintronic devices.[204] However, very soon, organic materials came into the limelight for its certain advantages like long spin-relaxation length and time, cost, portability, flexibility, etc. compared to other materials [204, 312-316]. And for such kind of organic spintronic devices, half-metals [317] which have nearly 100% spin polarization at Fermi surfaces can be used as a prefect ingredient.[318]

The search for organic half-metallic system got an enormous success when some of the one-dimensional organometallic sandwich molecular wires (SMWs), exhibited half-metallicity and spin filter effect.[85, 315, 319] A number of SMWs, having same [100] or different types [320] of transition metals (TM) which are sandwiched between the layers of organic molecules have been well investigated theoretically. The development of laser vaporization technique brings a new possibility to synthesize finite size clusters of these SMWs.[73, 74] Several properties of these SMWs have also been investigated extensively. [77-79, 321] These systematic studies illustrate the importance of presence of aromatic

ligands to determine the stable structure [322] as well as nature of magnetic interaction between metal atoms [81, 99]. Also, some attentions have been given to replace all carbon systems by their BN-analogues [323, 324]. Experimental as well as theoretical findings illustrate that system properties can be changed abruptly by changing all carbon systems to their BN-analogue. [325-327]

In all these previous studies, SMWs are periodic along the direction of sandwich, i.e., along the direction [ligand-metal-ligand-metal]$_\infty$. As reported earlier, in case of [TM-cyclic aromatic ligand]$_\infty$, the size of the ligand can even be varied from Cp (a five membered ring) to anthracene [81, 99] (three fused six membered rings). Among all this, TM-benzene sandwiched complexes are one of the most extensively studied class of complexes. But a major problem with this type of organometallic sandwiched complexes is that late 3*d* transition metals (Fe-Zn) cannot form proper stacked complexes. Basically, their large number of valence electrons (much greater than 18 [328]) hinders to form parallel stacked complexes. A possible way to overcome this problem and to make a proper stacking of the sandwich complexes of these late TM is, to decrease the number of valence electrons in the system. And that can be done by constructing a structure, where the ligands can have less coordination (possibly less than η^6).

To this regard, it is interesting to ask a question: can the aromatic ligand, benzene, be extended to polyacene to realize a properly stacked wire considering late 3d transition metal, which is periodic along the direction of polyacene instead of the direction of sandwich? In this context, we consider a Fe-based sandwiched complex consisting of two infinite chains of acene (i.e. polyacene) and an infinite chain of Fe atoms, in which Fe-chain remains sandwiched between two polyacene chains (see figure 3.1). By this way, we would be able to create an η^4 coordination between Fe and each polyacene chain where the complex cling to 16 valance electrons (16-electron system), which assists for proper stacking. We have explored the structural, electronic, magnetic and transport properties of Fe_n-bis(n-acene) and its BN-analogues (Fe_n-bis(n-BNacene)). For further discussion, we have nomenclatured the infinite Fe_n-bis(n-acene) and Fe_n-bis(n-BNacene) as Fe_∞-bis(polyacene) and Fe_∞-bis(BNpolyacene), respectively. From band structure calculations, it can be found that Fe_∞-bis(polyacene) is metallic in nature while its BN-

analogue is a half-metal. The transport calculations show the efficient spin-filter property of Fe_3-bis(3-BNacene).

3.2 Computational Details

We have used spin-unrestricted density functional theory (DFT) as implemented in the SIESTA [244] package for geometry optimizations and electronic structure calculations. We have used a double-ζ polarized (DZP) basis set for all atoms and real mesh cut-off is chosen as 300 Ry. For exchange-correlations, we have used Perdew-Burke-Ernzerhof (PBE) functional within the Generalized Gradient Approximation (GGA).[234] For one-dimensional sandwich molecular wire (SMWs), a unit cell of 20×20×c Ang^3, where c is the length of unit cell in periodic direction, has been used to avoid spurious interaction in non-periodic directions. To find magnetic ground state of the molecular wire, we have taken a supercell with two unit cells. For periodic calculations, we have used Monkhorst-Pack 1×1×60 k-point grid (total number of k-points is 31) to sample the 1D Brillouin zone. For all the geometry optimizations, inter-atomic forces are relaxed up to 0.04eV/ Å. To validate the results obtained using localized basis, we have also done a few electronic structure calculations within plane wave basis set using PWscf package as implemented in the Quantum-ESPRESSO.[329] For transport property calculation, we have used non-equilibrium Green function methodology extended for spin-polarized systems as implemented in TranSIESTA package.[330] The transmission function is calculated using the formula:

$$\mathrm{T(E)} = Tr[\Gamma_L(E)G^a(E)\Gamma_R(E)G^r(E)] \qquad (3.1)$$

where the retarded Green's function, $G^r(E)$ is calculated from the Hamiltonian and self-energies of the central region, $\Gamma_\alpha(E)$ is (-2 times) the imaginary part of the self-energies of the left and right electrodes (α=L,R). The current is calculated by the Landauer-Buttiker formula:

$$I = (e/h)\int_{\mu_L}^{\mu_R} T(E, V_b)dE \qquad (3.2)$$

where μ_L and μ_R are the chemical potential of left and right electrode respectively and V_b is the source drain bias voltage.

3.3 Results and Discussion

In Figure 3.1, we present optimized geometries of Fe_∞-bis(polyacene) and Fe_∞-bis(BNpolyacene). For Fe_∞-bis(BNpolyacene), we have considered two tautomeric eclipsed structures: eclipsed-1, the structure in which B atoms are on top of B atoms of two BN-polyacene and eclipsed-2 (see figure 3.1(b)), the structure in which B or N atoms is on top of counter atoms (i.e. N or B atoms respectively). We find that, eclipsed-2 is more stable than eclipsed-1. This stabilization can be explained on the basis of favorable charge transfer between B and N atoms. In the rest of our discussions, we have considered the stable conformation eclipsed-2 (see Fig 3.1(b)). Separation between Fe

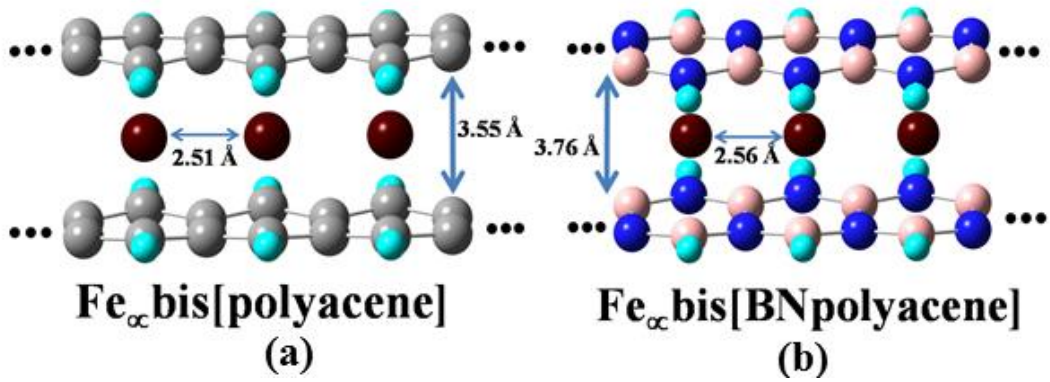

Figure 3.1: Optimized structure of infinite chain of (a) Fe_∞-bis(polyacene) and (b) Fe_∞-bis(BNpolyacene)

chain and BNpolyacene is found to be 1.88 Å while for Fe_∞-bis(polyacene), this value is 1.77 Å. The Fe-Fe distance in these two, are 2.56 Å and 2.51 Å, respectively. To examine the stability of this sandwiched TM-polyacene chain, we have calculated binding energy (BE) of the corresponding unit cell using following formulas,

$$E_b\ ([Fe(C_4H_2)_2]_\infty) = E([Fe(C_4H_2)_2]_\infty)) - E(Fe) - 2E(C_4H_2)$$

$$E_b\ ([Fe(B_2N_2H_2)_2]_\infty) = E([Fe(B_2N_2H_2)_2]) - E(Fe) - E(B_2N_2H_2)_2)$$

The binding energy for unit cell of Fe_{∞}-bis(polyacene) and Fe_{∞}-bis(BNpolyacene) are found to be -2.99 eV and -0.97 eV respectively. The less BE for Fe_{∞}-bis(BNpolyacene) is due to the charge separated state between boron and nitrogen atoms, where π-electrons get less delocalized in BNpolyacene. This less availability of π electrons causes weak η^4 interaction of Fe chain with BNpolyacene chain compared to polyacene chain.[99] To investigate the type of magnetic interaction acting among Fe atoms, we have taken a supercell of 1×1×2 and have calculated the local magnetic moment. We have found out all the systems to be ferromagnetically stabilized and thus have a magnetically polarized ground state. In order to estimate the ferromagnetic stability, we have calculated the energy difference (ΔE) between the ferromagnetic (FM) and the anti- ferromagnetic (AFM) state. Note that, the negative sign of ΔE indicates the stabilization of the FM state over the AFM state. This stabilization energies are, ΔE = -527.1 meV for Fe_{∞}-bis(polyacene) and ΔE = -36.7 meV for Fe_{∞}-bis(BNpolyacene).The large magnitude of ΔE designates the high stability of the FM state even at room temperature. From our calculation, we find that net magnetic moment of the unit cell is 1.66 μ_B for Fe_{∞}-bis(polyacene) and 2.00μ_B for Fe_{∞}-bis(BNpolyacene). To get a quantitative picture of magnetic moment distribution, we have calculated local magnetic moment on Fe atoms and the ligands. A large positive magnetic moment of 1.924 μ_B and 2.224 μ_B are found on Fe atom in Fe_{∞}-bis(polyacene) and Fe_{∞}-bis(BNpolyacene), respectively. A small negative moment of -0.264 μ_B and -0.224 μ_B are localized on polyacene and BN-polyacene chains, respectively. Because of the charge separated states in BN-polyacene chain, magnetic moment which arises from the ligand, is non-uniformly distributed over B and N atoms, while for polyacene chain, magnetic moment is homogeneously distributed over all edge carbon atoms. Like graphene nanoribbons [331], we find that, C and B atoms at edges (atoms with hydrogen passivation) mainly contribute to the magnetic moment of polyacene and BN-polyacene, respectively.

To get a better picture of orbitals which contribute to net magnetic moment of the unit cell in these structures, we present spin polarized band structure along with the respective wave function of the bands in figure 3.2. Due to strong hybridization, 4s levels are pushed well above the Fermi level. As a result, the effective electronic configuration of Fe becomes $3d^8 4s^0$. For both systems, the bands (band 1 and band 2) derived from d_z^2 and

$d_{x^2-y^2}$ orbitals, remain far below the Fermi energy and hence are completely filled up for majority as well as minority spin electrons. Hence, these two orbitals do not contribute to the net magnetic moment and even remain silent in both transport and magnetic behaviors. The bands (band 3, band 4 and band 5) derived from d_{xy}, d_{yz} and d_{xz} remain close to Fermi level and the dispersion of these bands mainly determines the transport and magnetic properties of these systems. For Fe$_\infty$-bis(polyacene), the top of the valence band

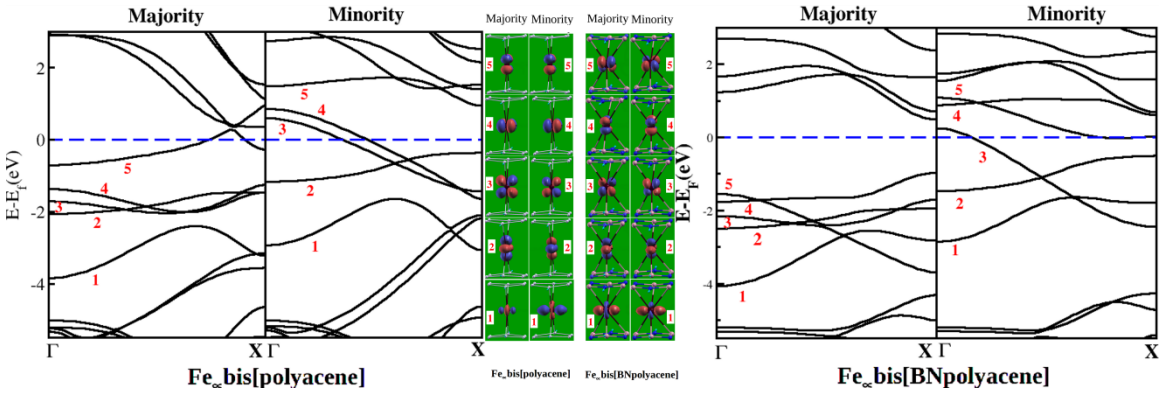

Figure 3.2: Spin resolved band structure of Fe$_\infty$-bis(polyacene) and Fe$_\infty$-bis(BNpolyacene) and the wave functions of some selected bands. The plot is scaled for E_F to lie at 0 eV.

(band 5) which has a major contribution from $3d_{xz}$ orbital, just crosses the Fermi level in majority spin channel, while the band 3 and band 4 which comes from $3d_{yz}$ and $3d_{xz}$, cross the Fermi level in minority spin channel, leading to the metallic behavior of Fe$_\infty$-bis(polyacene). As the band 5 is (almost) filled for majority spin electrons and is completely empty for minority spin electrons, it contributes 1μ_B/per magnetic ion to the net moment. The remaining moment of 0.92 μ_B originates from the partially filled band 3 and band 4. In case of Fe$_\infty$-bis(BNpolyacene), all the five d-bands are completely filled for majority spin and consequently it opens up a semiconducting gap of 1.5 eV(at X point) in majority spin channel. The dispersive bands, band 3 and 4, which are in a mixed characters between d_{xz} and d_{yz}, just cross the Fermi energy, making the system metallic in minority spin channel. The important point here is that we have a coexistence of the metallic and insulating nature for electrons in minority and majority spin channels, respectively, leading to a half-metallic behavior for the Fe$_\infty$-bis(BNpolyacene). As the

band 5, which is derived from $d_{xy,}$ orbital, is completely filled for majority spin and is completely empty for minority spin channel, it contributes 1 μ_B/magnetic ion to the total moment (2.22 μ_B). Also band 4 which is completely filled for majority spin and (almost) empty for minority spin channel, contributes a moment of 1μ_B/magnetic ion. The remaining moment of 0.22 μ_B arises from the small unoccupied portion of top of the valence band (band 3) in the minority spin channel.

To analyze further the metallic and half-metallic character of Fe$_\infty$-bis(polyacene) and Fe$_\infty$-bis(BNpolyacene) respectively, in figure 3.3 we have presented total Density of States (DOS) and projected Density of State (pDOS) for Fe atoms. As can be seen clearly that, the density of states near Fermi level mainly arise from Fe atoms. For Fe$_\infty$-bis(polyacene), a finite density of states for both the spin channels at Fermi level makes the system metallic in nature. Whereas, for Fe$_\infty$-bis(BNpolyacene), a finite number of states at Fermi level are available to take part in transport for minority spin channel, while a semiconducting gap of 1.5 eV opens up for majority spin channel, making the system half-metallic.

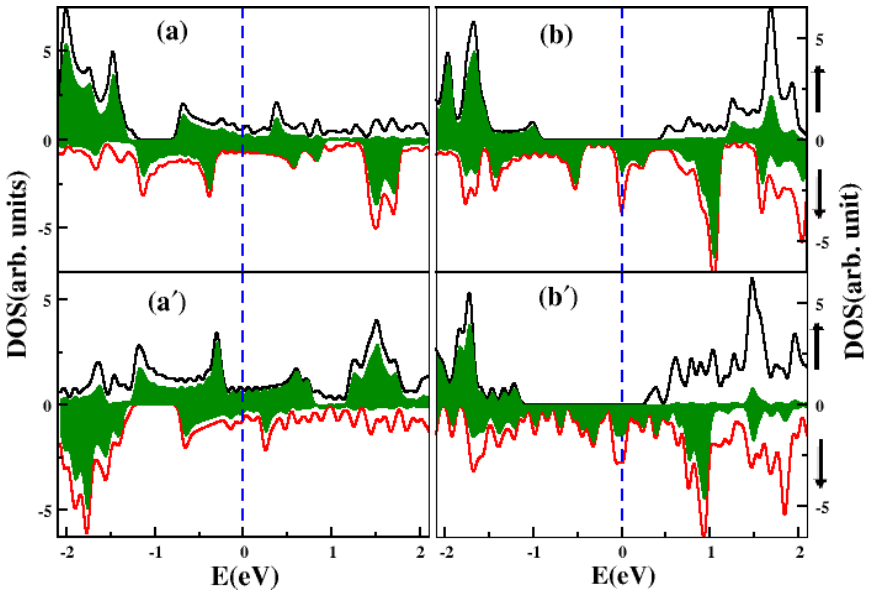

Figure 3.3: Spin resolved DOS for Fe$_\infty$-bis(polyacene) and Fe$_\infty$-bis(BNpolyacene). Solid green represents the pDOS of Fe ion.Top panel shows the results for localized basis (SIESTA) and bottom panel shows results for plane wave basis (Quantum Espresso). Up-arrow and down-arrow show the results for majority spins and minority spins, respectively.

As SIESTA uses localized basis, in principle one should verify the obtained electronic structures using plane wave basis set. For that, we have calculated the electronic density of states of both the systems using plane wave basis and have plotted in figure 3.3a′ and figure 3.3b′. It can be seen clearly that both the basis sets show qualitatively similar behavior with same conclusion about the overall electronic states of the systems. Especially, our main findings of half-metallicity retains true irrespective of the types of basis sets used for calculations. Although the position of peaks and energy gap are not same with different basis set calculations, the overall electronic nature of the systems is robust against the details of the calculations.

To explore the possibility of device applications, we have investigated the transport properties of these systems. As the band structure of Fe_{∞}-bis(BNpolyacene) shows half-metallic behavior, we have chosen a finite fragment of Fe_{∞}-bis(BNpolyacene) for our transport study. A finite fragment of Fe_3-bis(3-BNacene) consisting of three Fe atoms, coupled with gold electrodes on either sides are modeled as electrode-molecule-electrode (EME) system. We consider a non-magnetic 4×4×4 bulk gold electrode (Au (111) plane), containing 48 gold atoms for our transport calculations. To have a strong coupling between molecular fragment and Au electrodes, we have used thiol (-SH) as an anchoring group.[332] First, we have optimized the geometry of molecular fragment (with thiol groups), Fe_3-bis(3-BNacene)$(SH)_4$. Then we have removed hydrogen atoms of -SH groups and placed the molecule between the two gold electrodes and optimized the whole system freezing coordinates of the gold electrodes. In figure 3.4, we have plotted the spin polarized DOS and zero-bias transmission functions. It is quite clear that, within a small energy window near Fermi level (-2 eV to 2eV), only minority spin electrons show strong transmission peak at Fermi level and hence take part in transport while a transport gap opens up for majority spin electrons. To understand this, we have plotted total DOS and its projection onto the molecular states. As can been seen, the transmission spectra shows a series of peaks with strong correlation between transmission and pDOS spectra, especially with regard to the location of their peaks (see figure 3.4). These transmission peaks correspond to the resonant transmission through molecular states. Transmission shows a peak only when molecular states resonate with the states of the electrodes. In a low energy window around the Fermi energy, the vanishing contribution of molecular states to the eigenstates of the system leads to a case of weak resonance, which in turn

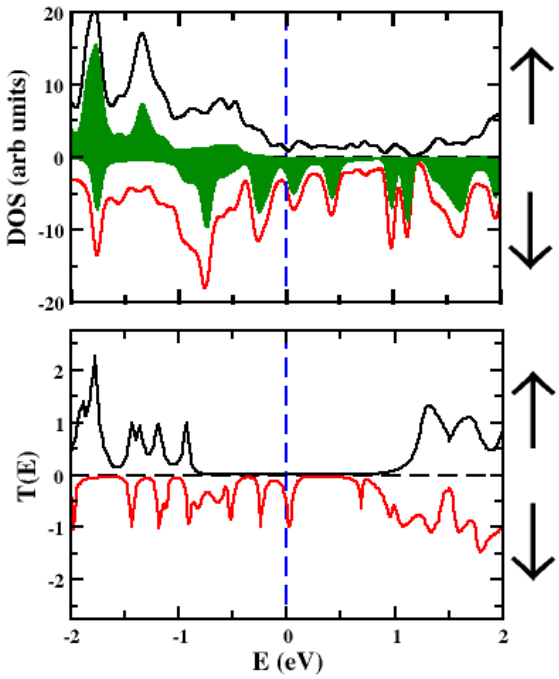

Figure 3.4: Spin resolved DOS and T(E) plot for Au-[Fe_3-bis(3-BNacene)(S_4)]-Au. Solid green represents the pDOS of Fe ion. The plot is scaled for E_F to lie at 0 eV.

makes the transmission almost negligible for majority spin electrons. While due to strong resonance, minority spin electrons show strong transmission peaks near the Fermi level.

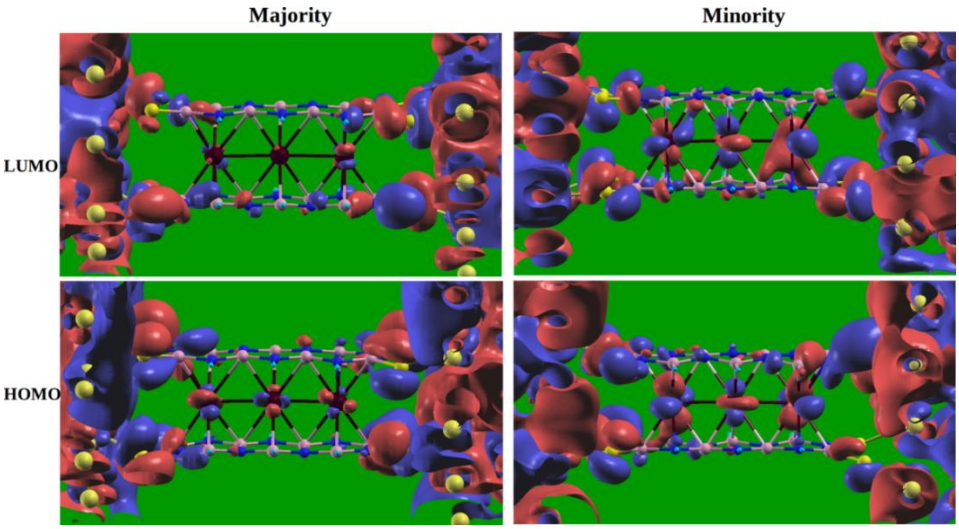

Figure 3.5: Wave function plot of HOMO and LUMO orbitals for majority and minority spin channels.

Looking once again at the plots of HOMO and LUMO for majority and minority spin electrons in figure 3.5, it can be seen that due to weak coupling of molecular orbitals and

incident states from the electrode, the HOMO and LUMO rarely contribute to the transmission for majority spin. While the HOMO and LUMO for the minority spins show a strong transmission peak because of the strong resonance of molecular states with the electrode.

As actual device works at a finite bias, in figure 3.6 we have presented I-V characteristic of the system. When bias is applied, the currents reaches up to several μA for minority spin component, however, remains almost zero for majority spin component. Importantly, as Fe_{∞}-BNpolyacene allows only one kind of spin to pass through, it can possibly be realized as a good candidate for spin filtering component in spintronics.

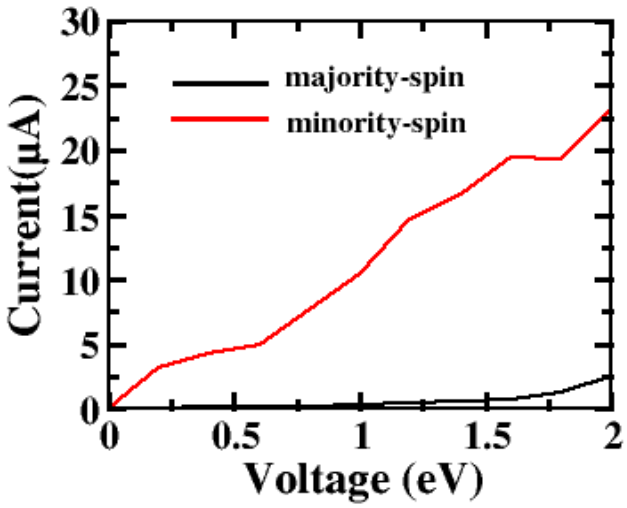

Figure 3.6: I-V characteristics for Au-[Fe_3-bis(3-BNacene)(S_4)]-Au . Code: black and red solid lines show I-V for majority and minority spin respectively.

3.4 Conclusion

In conclusion, theoretically we have investigated the electronic and magnetic properties of Fe_{∞}-bis(polyacene) and Fe_{∞}-bis(BNpolyacene). Here we have described a possible way to make the proper stacking of these Fe-based sandwiched complexes. We have argued that Fe_{∞}-bis(polyacene) is a ferromagnetic metal while Fe_{∞}-bis(BNpolyacene) is a ferromagnetic half-metal. We also find that Fe_3-bis(3-BNacene) can be realized as a 100% efficient spin filter system which can have a huge significance in the future spintronic devices.

Chapter 4

Structural, Electronic, Magnetic and Transport Properties of Lanthanide-based Single Ion Magnet

4.1 Introduction

Modern electronics is facing a revolution at the present time because of contemporary development of two interdisciplinary fields called as spintronics [88, 224, 333-336] and molecular electronics [337-342]. Molecular magnetic materials can form a bridge between these two promising fields and can produce a more efficient field called molecular spintronics[90, 92, 204, 225, 343, 344]where both macroscale and nanoscale properties can be assembled together. In spintronics, one should be able to manipulate charge as well as spin of the magnetic molecule (one or more molecules) in the electronic device.[91, 225] Single molecular magnet (SMM)[345-347] possesses extremely long magnetization relaxation time[348, 349](can be several years at very low temperature) because of which it becomes one of the intriguing group of elements, utilized for the molecular spintronics[123, 343, 350-352] This slow magnetization relaxation rate makes them a potential candidate for efficient storage material as well. SMMs are fundamentally organometallic molecules containing one or several metal centers with unpaired electrons.[353-358] At low temperature, these molecules act like nanomagnets with large spin ground states together with huge magnetic anisotropy.[359] Generally, transition metals or transition metal–lanthanide hybrids are used to form magnetic core of SMMs.[360-367] However, in recent years mononuclear lanthanides are also used as magnetic core for SMMs, which are called as single ion magnets (SIMs).[368-378] In comparison to transition metal complexes,

lanthanides have huge magnetic anisotropic energy barrier, which is a key decisive factor for SMMs.[116, 379] Moreover, the relaxation mechanisms of SIMs can be tuned by choosing the appropriate ligands, which can directly influence axial and rhombic terms.[380-382] Cyclic organic ligands with the delocalized π-electrons (which form η^n coordination with metal atoms) are one of this type of ligands which can induce a single-axial magnetic anisotropy.[368, 373, 383] Erbium(III) ion, sandwiched between cycloctatetraene($C_8H_8^{2-}$,COT) dianion and pentamethylcyclopentadienide ($C_5Me_5^-$, Cp*) anion molecule is one of the appealing example of this type of SIMs.[373] Although recent experiment by Jiang *et al.* [373] demonstrates the longer magnetization relaxation natures of this molecule, the origin of spin, charge transfer and a detail role of ligands are not known. Moreover, the possible functions of this molecule for molecular spintronics applications have not been explored. To understand these properties using the experimental methods may be very expensive, while it can be predicted quickly and reliably using the computational methods. The [Er(COT)(Cp*)] is one of the example of the small SIMs,[373] which can be considered for the ultimate miniaturization of storage-materials.

In this chapter, we have studied the molecular, electronic and magnetic properties of [Er(COT)(Cp*)] SIM using density functional theory (DFT). Moreover, the transport properties in zero- as well as in finite bias are computed for this sandwiched molecule (–S-CH_2-Cp*-Er-COT-CH_2-CH_2-S-) using gold (Au(111)) as electrodes. The non-equilibrium Green's function (NEGF) method has been used to calculate transmission function for this system.

4.2 Computational Details

Unrestricted Density Functional Theory (DFT) calculations have been performed for geometry optimization and electronic structural calculations as implemented in the SIESTA package.[384] Perdew-Burke-Ernzerhof (PBE) exchange-correlation functional within the Generalized Gradient Approximation (GGA)[385] has been used with the double-ζ polarized (DZP) basis sets for all atoms. The real mesh cut-off is chosen as 300 Ry. For geometry optimizations, all structures have been relaxed until the average force on the each atoms reduced down to 0.05 eV/Å. Geometry optimization of molecule has

been done by considering only Γ-point. The optimization of the molecule with the electrodes on either side has been done using 3×3×3 k-point grid. The transmission functions have been calculated at various bias using Non-equilibrium Green's function (NEGF)[386] methodology extended for spin-polarized systems as implemented in the TranSIESTA package.[387] The transmission function has been formulated as:

$$T(E) = Tr[\Gamma_L(E)G^a(E)\Gamma_R(E)G^r(E)] \quad (4.1)$$

where the retarded Green's function, $G^r(E)$ is calculated from the Hamiltonian and self-energies of the central region, $\Gamma_\alpha(E)$ is (-2 times) the imaginary part of the self-energies of the left and right electrodes (α=L,R). The current is calculated by the Landauer-Buttiker formula:

$$I = (e/h)\int_{\mu_L}^{\mu_R} T(E, V_b)dE \quad (4.2)$$

here μ_L and μ_R are the chemical potential of left and right electrode respectively and V_b is source drain bias voltage. Further, the optimized structure in the SIESTA package is characterized as minima on the basis of their harmonic vibrational frequencies as implemented in the Gaussian 09 package.[241] ^1H and ^{13}C NMR chemical shielding values have been computed using Gauge Including Atomic Orbital (GIAO) method.[388] The population analysis has been carried out using natural bonding orbital (NBO)[389] method.

4.3 Results and Discussion

The optimized structure of [Er(COT)(Cp*)] molecule is shown in figure 4.1. Here, Er atom remains sandwiched between the planar Cp* and COT cyclic π-electronic ligands. COT ring stays much closer (1.958 Å) to Er than the Cp* ring (2.382 Å), which are in a good agreement with experimental values, 1.73 Å and 2.27 Å respectively.[373] COT ligand possess total 10 π-electrons with extra 2 negative charges, while Cp* holds 6 π-electrons with one extra negative charge. Both the ligands follow (4n+2) π-electrons Huckel's rule, where the average C-C bond distances are 1.428 Å and 1.439 Å for COT and Cp*, respectively. The computed C-C bond-distances are in good agreement with their corresponding experimental values (1.41 Å for COT and 1.42 Å for Cp*).[373] The steric environment created by the methyl groups are the reason for the longer distance

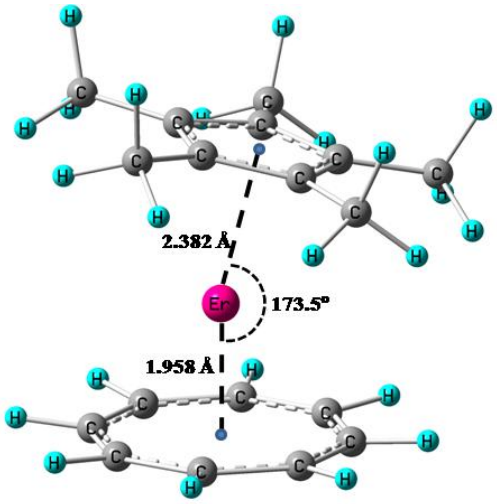

Figure 4.1: Optimized geometry of [COT-Er-Cp*] molecule. Important bond distances (Å) and angles (°) are given. The centers of the rings (represented as blue circles) are considered to measure the distances between the Er and ligands.

between the Cp* and Er atom. Moreover, this steric crowding makes the Cp* ring to be tilted from its plane by an angle of 6.5°. In order to prove this fact, the strain energy has been calculated in the presence and absence of $-CH_3$ groups in the Cp ring. Strain energy (E_{strain}) is defined as the amount of extra energy, needed to make the rings parallel to each other ($E_{strain}=E_{parallel}-E_{tilted}$; where $E_{parallel}$ and E_{tilted} are the total energies of the molecule when two rings make an angle of 180° and 173.5° between them, respectively). The strain energy for the [Er(COT)(Cp*)] (with $-CH_3$ groups) and [Er(COT)(Cp)] (without $-CH_3$ groups) molecules are 0.94 eV and 0.09 eV, respectively. The huge strain energy difference provides the evidence that the presence of methyl groups is the reason for the tilting angle.

The absence of imaginary frequency in the harmonic vibrational spectra confirms the stability of this complex. The structures are further validated by computing ^{1}H and ^{13}C NMR values. The computed ^{1}H NMR chemical shift value (5.9 ppm) of COT in the complex is comparable with the experimental value (5 ppm).[390] The slight dissimilarity between the computed and experimental values is due to the absence of solvent environment in the computational model. In addition, ^{13}C-NMR chemical shift value of Cp^{*-} (116.32 ppm) presents in the downfield than the COT^{2-} (89.94 ppm) carbons, which indicates that the Cp^{*-} is more aromatic than other ligand. In order to realize its aromatic nature, the chemical shift values are compared with the bare ligands (COT^{2-} and Cp^{*-})

chemical shift values. For COT^{2-}, the complex formation makes upfield shift in the ^{13}C-NMR value compared to the bare ligand (94.33 ppm), while for Cp^{*-}, it is downfield shifted compared to bare Cp^{*-} ring (103.54 ppm). The predicted variation in the chemical shift values are due to the change in electron density of the ligands in the complex.

In order to prove this, the charge distribution has been studied using NBO.[389] NBO is one of the localized atomic orbital method,[389] which can give a clear picture about the charge distributions. The reliability of this method has been proved already by applying to the similar kind of complexes.[391-393] Generally, the bare COT and Cp* ligands are stable with their dianionic and anionic form, respectively, while, in the [Er(COT)(Cp*)] complex, they collectively transfer 1.64 e^- of charge to the metal cation (Er^{+3}). This charge transfer is the driving force for the stability of this organometallic complex. The molecular electrostatic potential has been mapped in order to show this charge distribution over the molecule (see figure 4.2). It clearly shows that both COT and Cp* rings are negatively charged while Er atom is highly positively charged. Further, the natural atomic charge calculations have been carried out to obtain the quantitative value

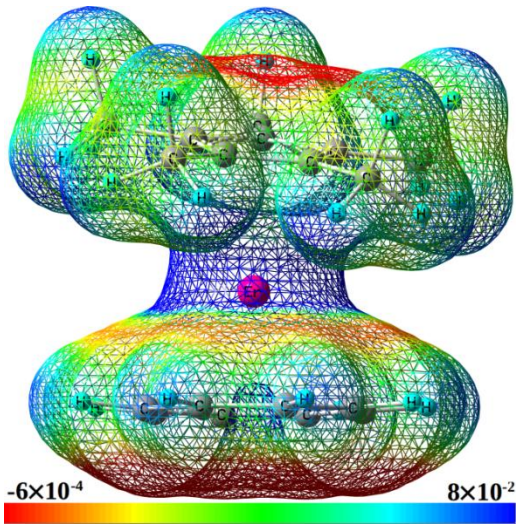

Figure 4.2: Mapping of the molecular electrostatic potential (MEP) on an isocontour (0.02) of the electron density taken to be 0.009 e^- $bohr^{-3}$

of the charge transfer. Overall, Er^{3+} ion, after receiving ~1.64 e^- amount of charge, shows valence electronic configuration as [$6s^{(0.11)}4f^{(11.05)}5d^{(1.16)}$ $6p^{(0.28)}$]. These transferred charges mostly get accommodated in its 5*d*-orbitals. COT^{2-} and Cp^{*-}contribute 1.11 e^- and 0.53 e^- charge respectively to the total amount of transferred charge, 1.64 e^-. After

the charge-transfer, valance electronic configurations of ring carbon atom becomes ($2s^{(0.95)}2p^{(3.43)}3p^{(0.03)}$) for COT and ($2s^{(0.87)}2p^{(3.27)}3p^{(0.01)}$) for Cp^{*-} ligand. Note that, the COT^{2-} ligand donates extra charge about 0.58 e^- to the Er^{3+} ion than the Cp* ligand. The concurrence between the computed and experimental structural parameters and chemical shift values validate the molecular structure of the [Er(COT)(Cp*)] complex. The next task is to understand its SIMs nature. For that, first step is to realize the distribution of unpaired electron, which is reflected in the computed spin density plot of the complex (see figure 4.3). The ground state of the complex has 3 unpaired electrons (S=3/2), where

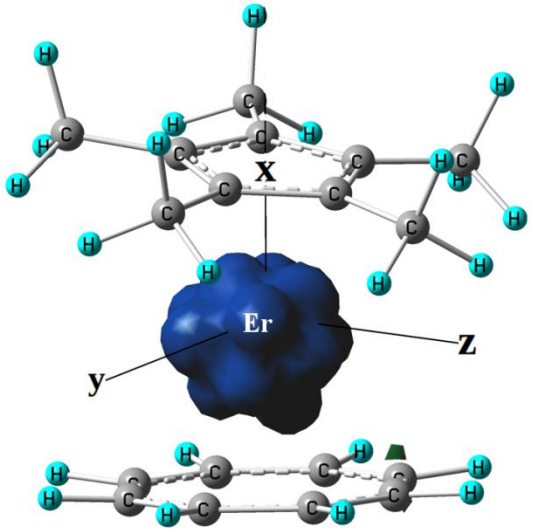

Figure 4.3: Spin density plot of the spin ground state (S=3/2) [Er(COT)(Cp*)] molecule. Blue and green regions indicate positive and negative spin density, respectively.

the major spin contribution appears from Er atom. The computed spin density map and molecular orbital picture clearly illustrate that the unpaired electrons are localized on the *f*-orbitals of Er ion. Out of seven, four *f*-orbitals (d-g, figure 4.4) of Er-atom are paired, while other three *f*-orbitals (a-c, figure 4.4) are singly occupied. These three singly occupied *f*-orbitals stabilize the molecule in a spin-ground state of S=3/2. Moreover, our study reveals that all occupied metal localized orbitals (including the unpaired electrons containing α-spin orbitals) are present much below in energy (for α-spin 7.85-8.62 eV and for β-spin 5.93-6.01 eV) than that of highest occupied MOs. The above results evidently prove the molecular paramagnetic nature.

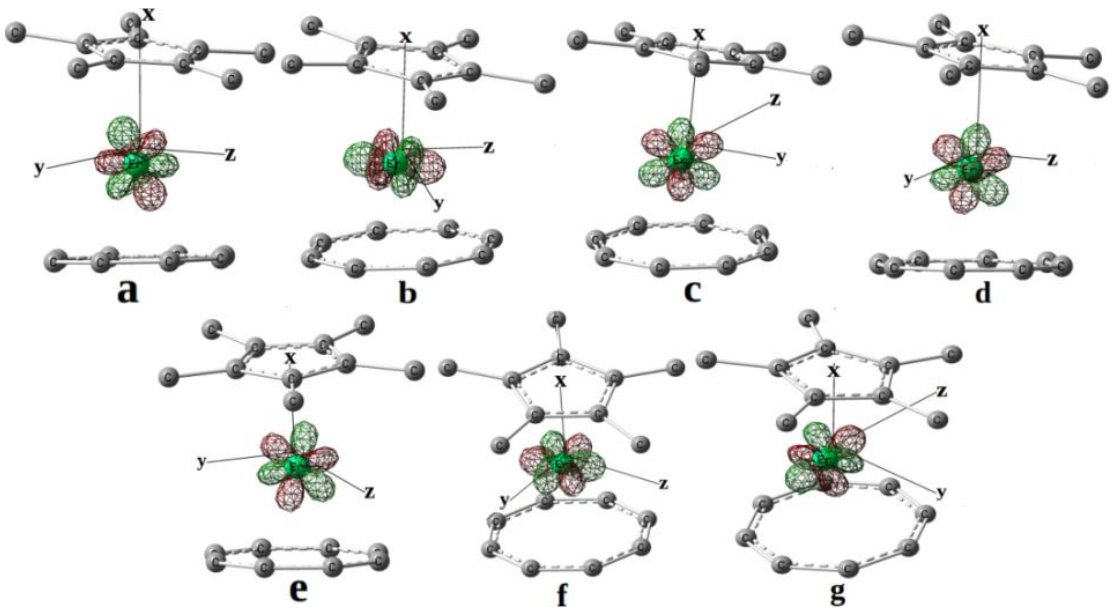

Figure 4.4: The computed natural localized MOs with f-localization of [Er(COT)(Cp*)] complex. MOs a-c are singly occupied, while MOs d-g are paired.

Finally, the application of this molecule in the spintronics is explored by understanding and computing its transport properties. Generally, electron transport occurs through the orbitals near the Fermi levels. In this account, the highest energy occupied and lowest energy unoccupied natural localized orbitals are computed and shown in the figure 4.5. The computed HOMO-LUMO gaps are found to be 3.73 eV and 2.66 eV for α-spin and β-spin, respectively. This type of unequal energy gap in two different spin channels is generally observed for the finite-size organometallic clusters.[98, 99] HOMO and HOMO-1 are delocalized over Er^{3+} ion and COT^{2-} ligand. Moreover, our computation shows that the three lowest singly unoccupied β-spin molecular orbitals (LSUMO, LSUMO+1 and LSUMO+2) are very close in energy (within 0.02 -0.06 eV energy difference, see figure 4.5).

To investigate the transport phenomenon of this complex, it has been placed in between the gold Au (111) electrodes. Molecules are anchored via thiol linker, [394, 395] where COT ligand in the molecule is anchored to the electrode *via* $–CH_2CH_2SH$ linker and Cp* *via* $–CH_2SH$ .To avoid molecule-molecule interaction in transverse directions (i.e. x- and y- direction here), a supercell of 8×4×4 containing 96 Au atoms have been chosen as electrodes. Initially, the geometry of free molecule with the spacer groups (i.e. $SHCH_2CH_2$-[COT-Er-Cp*]-CH_2SH) has been optimized using the DFT method. Then,

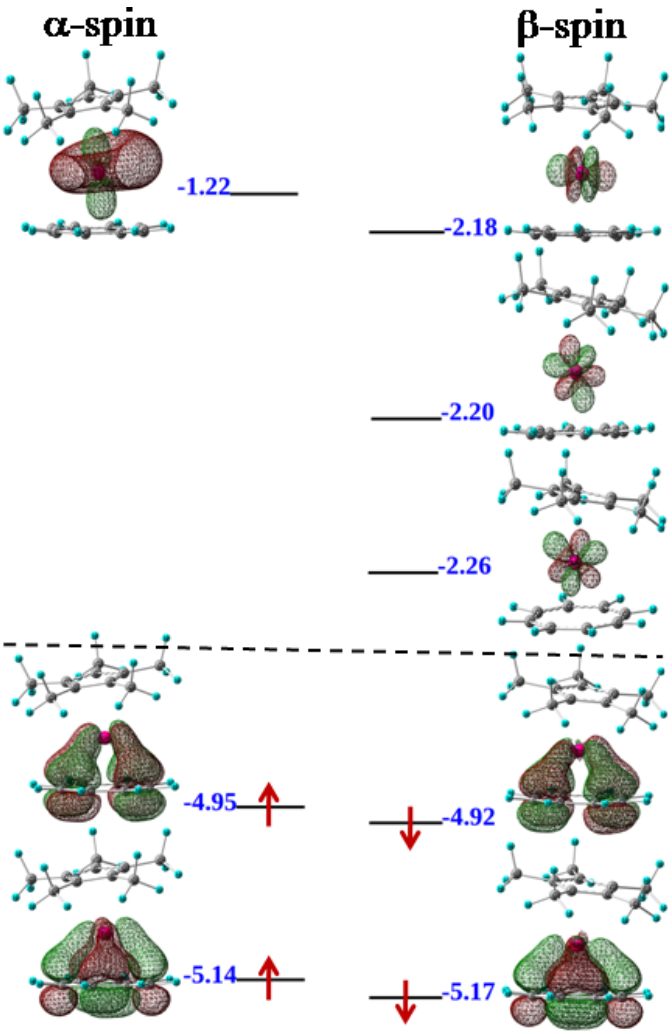

Figure 4.5: MO plots for HOMO and HOMO-1 for α and β-spin and LSUMO, LSUMO+1 and LSUMO+2 for β-spin. Energies of those MOs are given in eV. Black dotted line differentiates occupied and unoccupied energy levels.

hydrogen atoms attached to –S linker has been removed and molecule has been positioned in such a way that the –S atoms sit on top of the hollow site of Au(111) plane maintaining favorable Au–S distance[394, 395] at both sides. Finally, the whole structure has been optimized freezing the coordinate of Au atoms. We find that attachment of molecule to the Au electrode has a negligible impact on the geometry of the molecule.

In figure 4.6, spin polarized density of states are projected on to the molecular states (MDOS) and small-bias transmission function have been plotted. As can be seen, within a small energy window (-1 eV to 1eV) near Fermi level, strong transmission peaks

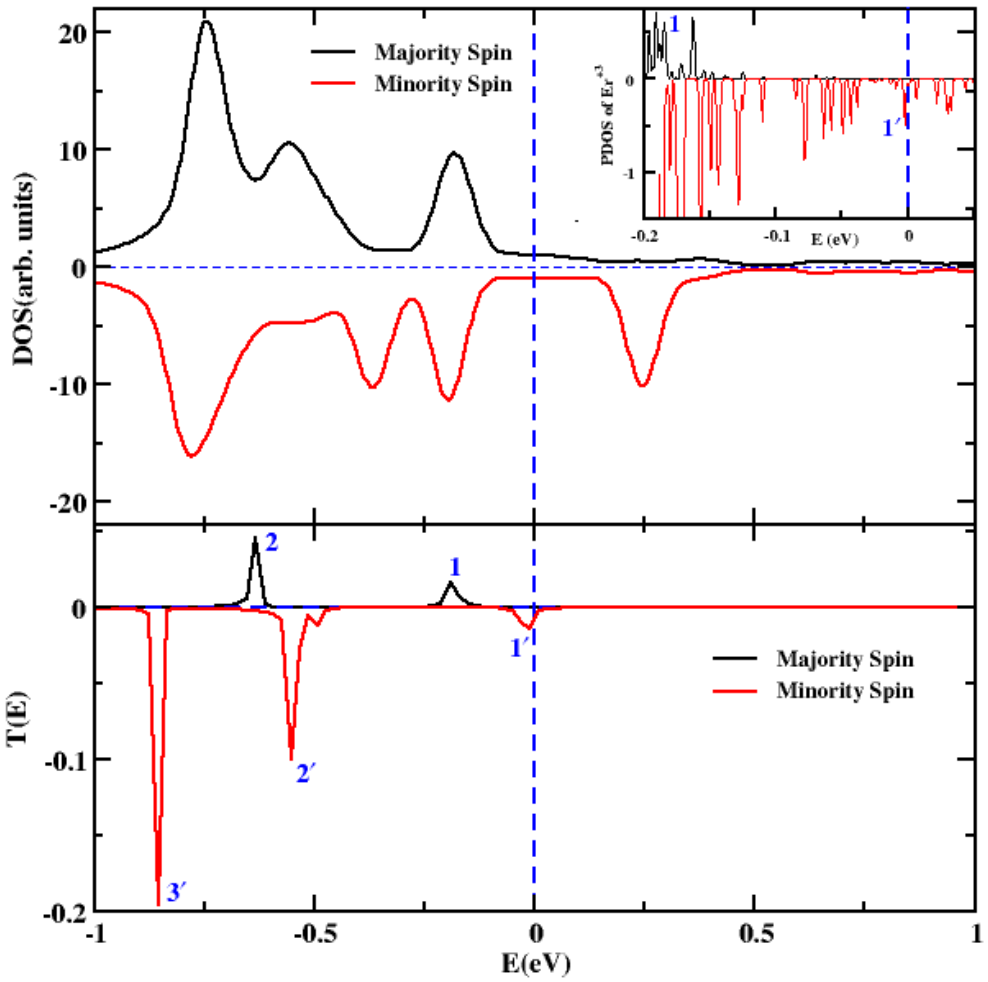

Figure 4.6: Spin polarized DOS and T(E) plot for Au-SCH_2CH_2-[COT-Er-Cp*]-CH_2S-Au. pDOS for Er^{+3} ion has been plotted in inset. All plots are scaled for E_F to lie at 0 eV. Important transmission peaks in the T(E) vs E plot and corresponding pDOS peaks of Er^{+3} have been labeled.

arise from minority spin electrons and hence transport is dominated by this particular spin channel. Specially, a transmission peak at Fermi level opens up a transport channel for minority spin electrons to pass through while the transport is blocked for the majority spin electrons and, hence, this complex can possibly be used as a spin filter component. Actually, these transmission peaks correspond to the resonant transmission through molecular states. Transmission shows a peak only when molecular states resonate with the states of the electrodes. Therefore, to observe a transmission peak at a particular energy, two basic criteria have to be fulfilled. Firstly, molecule must have a finite number of states at that energy and secondly, those molecular states have to be delocalized over whole electrode-molecule-electrode system.

To understand the transmission peaks (peaks 1 and 1' in the figure 4.6) very close to Fermi level, pDOS of Er^{+3} has been plotted in the inset of figure 4.6. As can be seen, the transmission peaks in both the spin channels are mainly guided by the corresponding peaks in the *f*-orbitals of Er^{+3}. From wave function plot (see figure 4.7), it can be confirmed that these *f*-orbitals are of the type, f_{xz}^{2} or f_{yz}^{2} for minority spin channel, whereas, f_{xyz} or $f_{z(x^2-3y^2)}$ type for majority spin channel. The orbitals corresponding to other two strong transmission peaks at E =-0.63 eV (peak 2 for majority spin) and at E =-0.55 eV (peak 2′ for minority spin) have also been plotted in figure 4.7. It is very clear that all these transport channels are delocalized over whole electrode-molecule-electrode system. Hence, these strong transmission peaks are governed by the strong resonance of molecular states with the states of electrodes. One can also clearly see that, several intense peaks in the molecular states remain inactive at small-bias transport (see figure 4.6). To understand this fact, corresponding wave functions have been plotted, where it can be seen that the wave functions are not fully delocalized over the whole molecule.

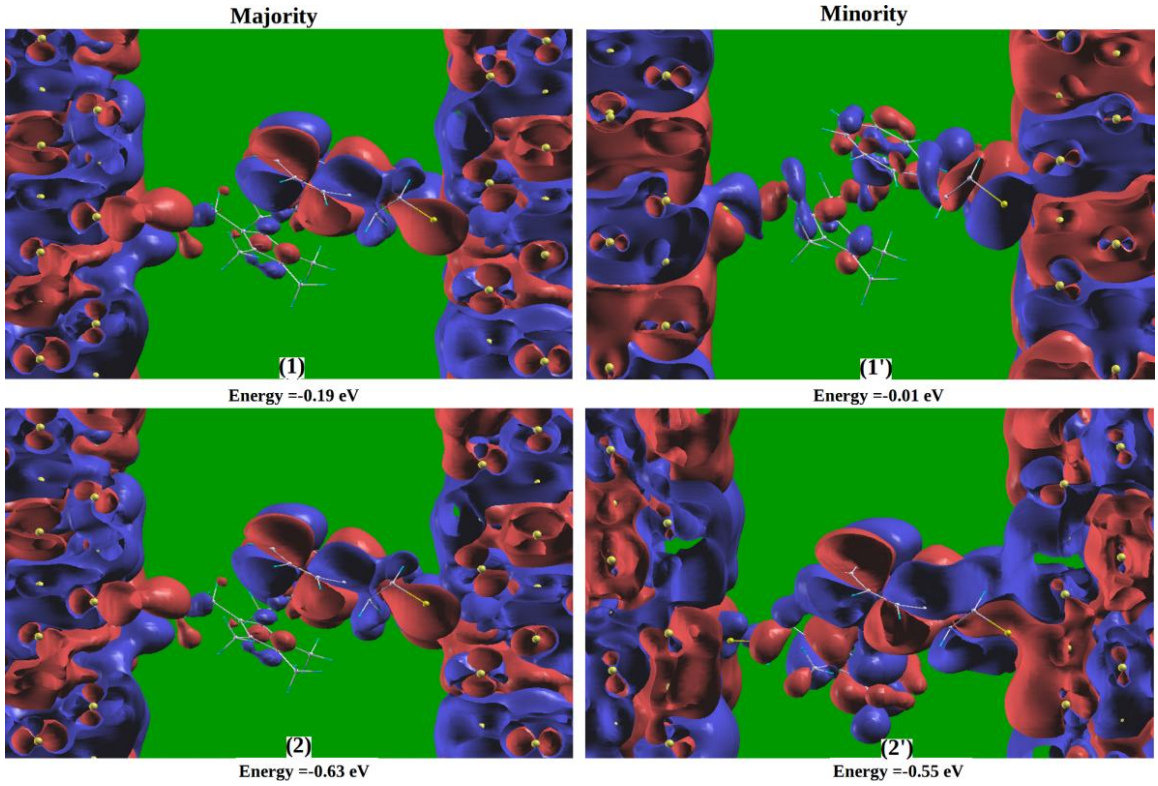

Figure 4.7: Wave function plots for the molecular states, situated in the energy levels correspond to the transmission peaks 1, 1′, 2 and 2′.

This is precisely the reason for the inertness of these states towards electronic conduction.

As the device works at finite bias, in figure 4.8, we present current-voltage (I-V) characteristics of the system. In a very small bias window, 0–0.45 V, (see the inset in figure 4.7), when bias increases current reaches several μA in minority spin component,

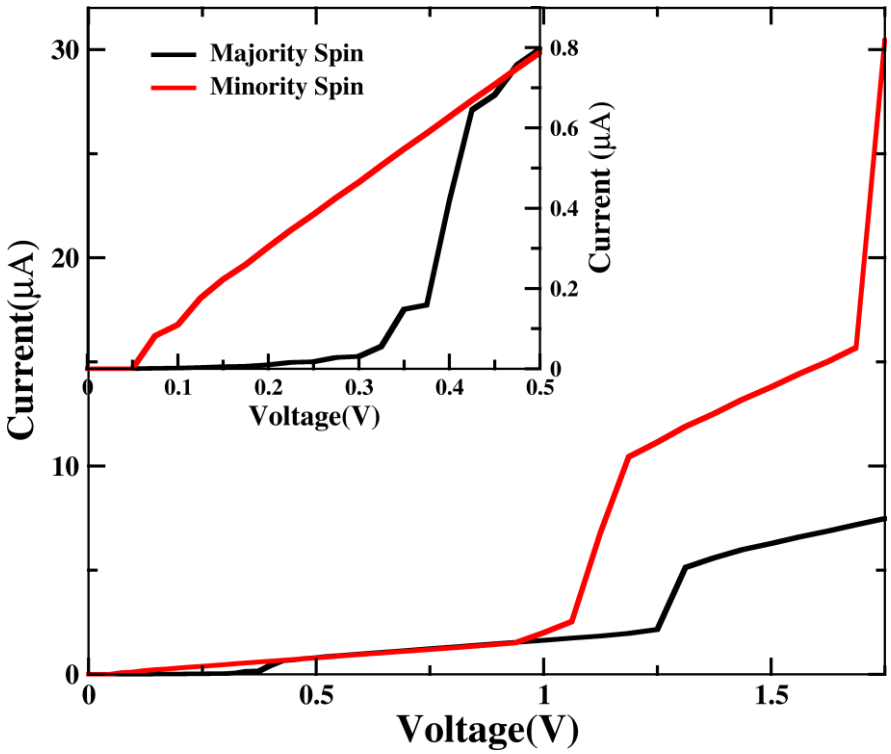

Figure 4.8: Current-Voltage characteristics for Au-SCH_2CH_2-[COT-Er-Cp*]-CH_2S-Au. The inset shows the same I-V characteristics zoomed in a small bias window. Code: black and red solid lines show I-V for majority and minority spin respectively.

however, remains almost zero for majority spin component, reflecting the efficient spin filter behavior. With further increase in bias, the current for both spin channels are equal and remain same in the bias window of 0.45-0.95V. This is because no new transmission peaks appear in that bias window and the current is only due to the transmission peaks 1, 1’ which are equal in magnitude for both the spin component. Interestingly, with further increase in bias and in the range of 0.95-1.75 V, the I-V shows again spin filter behavior which can be traced back to the large transmission coefficients of minority spin channel (2’ and 3’) compared to the majority spin channel (2).

4.4 Conclusion

To conclude, structural, electronic, magnetic and transport properties for [Er(COT)(Cp*)] have been investigated theoretically. This bent SIM are found to be more stable than its perfect stacked structure. The structural stability appears because of favorable ligand to metal charge transfer. It has a spin ground state of 3/2 where three unpaired electrons occupy three *f*-orbitals of Er atom. We believe that this complex can possibly be used as a spin-filter component in spintronic devices due to its fascinating spin polarized transport behavior.

References

[1] L. Degiorgi, *Strong interactions in low dimensions*, Springer, **2004**.
[2] M. J. Kelly, *Low-dimensional semiconductors:materials, physics, technology, devices*, **1995**.

[3] M. F. Crommie, C. P. Lutz, D. M. Eigler, *Science* **1993**, *262*, 218.
[4] G. D. Stucky, J. E. Macdougall, *Science* **1990**, *247*, 669.
[5] T. Takagahara, K. Takeda, *Phys. Rev. B* **1992**, *46*, 15578.
[6] B. Delley, E. F. Steigmeier, *Phys. Rev. B* **1993**, *47*, 1397.
[7] G. W. Bryant, *Phys. Rev. B* **1988**, *37*, 8763.
[8] M. V. R. Krishna, R. A. Friesner, *J. Chem. Phys.* **1991**, *95*, 8309.
[9] G. T. Einevoll, *Phys. Rev. B* **1992**, *45*, 3410.
[10] P. B. Wiegmann, *Phys. Rev. Lett.* **1988**, *60*, 821.
[11] Q. M. Si, S. Rabello, K. Ingersent, J. L. Smith, *Nature* **2001**, *413*, 804.
[12] E. Dagotto, *Science* **2005**, *309*, 257.
[13] M. Capone, M. Fabrizio, C. Castellani, E. Tosatti, *Science* **2002**, *296*, 2364.
[14] S. Chakravarty, M. P. Gelfand, S. Kivelson, *Science* **1991**, *254*, 970.
[15] O. Voskoboynikov, C. M. J. Wijers, J. L. Liu, C. P. Lee, *Europhys. Lett.* **2005**, *70*, 656.
[16] K. A. Matveev, A. I. Larkin, L. I. Glazman, *Phys. Rev. Lett.* **2002**, *89*, 096802.
[17] F. Miao, S. Wijeratne, Y. Zhang, U. C. Coskun, W. Bao, C. N. Lau, *Science* **2007**, *317*, 1530.
[18] R. Waser, M. Aono, *Nature Mater.* **2007**, *6*, 833.
[19] E. Coronado, J. R. Galan-Mascaros, C. J. Gomez-Garcia, V. Laukhin, *Nature* **2000**, *408*, 447.
[20] X. F. Wang, R. H. Liu, Z. Gui, Y. L. Xie, Y. J. Yan, J. J. Ying, X. G. Luo, X. H. Chen, *Nat. Commun.* **2011**, *2*.
[21] H. Jeong, A. M. Chang, M. R. Melloch, *Science* **2001**, *293*, 2221.
[22] W. J. Liang, M. P. Shores, M. Bockrath, J. R. Long, H. Park, *Nature* **2002**, *417*, 725.
[23] J. Nygard, D. H. Cobden, P. E. Lindelof, *Nature* **2000**, *408*, 342.
[24] J. Park, A. N. Pasupathy, J. I. Goldsmith, C. Chang, Y. Yaish, J. R. Petta, M. Rinkoski, J. P. Sethna, H. D. Abruna, P. L. McEuen, D. C. Ralph, *Nature* **2002**, *417*, 722.
[25] I. W. Lyo, P. Avouris, *Science* **1991**, *253*, 173.
[26] A. A. Dhirani, R. W. Zehner, R. P. Hsung, P. GuyotSionnest, L. R. Sita, *J. Am. Chem. Soc.* **1996**, *118*, 3319.
[27] T. A. Jung, R. R. Schlittler, J. K. Gimzewski, *Nature* **1997**, *386*, 696.
[28] C. Zhou, C. J. Muller, M. R. Deshpande, J. W. Sleight, M. A. Reed, *Appl. Phys. Lett.* **1995**, *67*, 1160.
[29] L. Fernandez-Seivane, V. M. Garcia-Suarez, J. Ferrer, *Phys. Rev. B* **2007**, *75*.
[30] F. J. Giessibl, *Science* **1995**, *267*, 68.
[31] M. Rief, F. Oesterhelt, B. Heymann, H. E. Gaub, *Science* **1997**, *275*, 1295.
[32] G. Meyer, N. M. Amer, *Appl. Phys. Lett.* **1988**, *53*, 1045.
[33] R. W. Carpick, M. Salmeron, *Chem. Rev.* **1997**, *97*, 1163.
[34] D. Rugar, P. Hansma, *Physics Today* **1990**, *43*, 23.

[35] M. T. Reetz, W. Helbig, S. A. Quaiser, U. Stimming, N. Breuer, R. Vogel, *Science* **1995**, *267*, 367.
[36] Z. L. Wang, *J. Phys. Chem. B* **2000**, *104*, 1153.
[37] J. R. Schrieffer, A. P. Kampf, *J. Phys. Chem. Solids* **1995**, *56*, 1673.
[38] C. G. Olson, R. Liu, A. B. Yang, D. W. Lynch, A. J. Arko, R. S. List, B. W. Veal, Y. C. Chang, P. Z. Jiang, A. P. Paulikas, *Science* **1989**, *245*, 731.
[39] F. J. Jongeneelen, *Ann. Occup. Hyg.* **2001**, *45*, 3.
[40] J. P. Incardona, T. L. Linbo, N. L. Scholz, *Toxicol. Appl. Pharmacol.* **2011**, *257*, 242.
[41] D. T. Sponza, O. Gok, *J. Hazard. Mater.* **2011**, *197*, 404.
[42] D. T. Sponza, R. Oztekin, *J Environ Eng-ASCE* **2011**, *137*, 1012.
[43] X. Feng, W. Pisula, K. Muellen, *Pure Appl. Chem.* **2009**, *81*, 2203.
[44] M. K. Cyranski, *Chem. Rev.* **2005**, *105*, 3773.
[45] Z. F. Chen, R. B. King, *Chem. Rev.* **2005**, *105*, 3613.
[46] J. Poater, X. Fradera, M. Duran, M. Sola`, *Chem. Eur. J* **2003**, *9*, 400.
[47] A. Mohajeri, A. Ashrafi, *Chem. Phys. Lett.* **2008**, *458*, 378.
[48] T. M. Krygowski, M. K. Cyranski, *Chem. Rev.* **2001**, *101*, 1385.
[49] J. R. Dias, *Tetrahedron* **1993**, *49*, 9207.
[50] I. Gutman, V. IvanovPetrovic, *J Mol Struc-THEOCHEM* **1997**, *389*, 227.
[51] Z. B. Maksic, D. Baric, T. Mueller, *J. Phys. Chem. A* **2006**, *110*, 10135.
[52] Y. Ruiz-Morales, *J. Phys. Chem. A* **2004**, *108*, 10873.
[53] G. Portella, J. Poater, M. Sola, *J. Phys. Org. Chem.* **2005**, *18*, 785.
[54] T. M. Krygowski, M. K. Cyranski, S. Czarnocki, G. Hafelinger, A. R. Katritzky, *Tetrahedron* **2000**, *56*, 1783.
[55] J. M. Schulman, R. L. Disch, *J. Phys. Chem. A* **1999**, *103*, 6669.
[56] G. Portella, J. Poater, J. M. Bofill, P. Alemany, M. Sola, *J. Org. Chem.* **2005**, *70*, 2509.
[57] R. W. A. Havenith, J. H. van Lenthe, F. Dijkstra, L. W. Jenneskens, *J. Phys. Chem. A* **2001**, *105*, 3838.
[58] I. Ashe, A. J., X. Fang, *Org. Lett.* **2000**, *2*, 2089.
[59] C. A. Jaska, D. J. H. Emslie, M. J. D. Bosdet, W. E. Piers, T. S. Sorensen, M. Parvez, *J. Am. Chem. Soc.* **2006**, *128*, 10885.
[60] M. J. D. Bosdet, W. E. Piers, T. S. Sorensen, M. Parvez, *Angew. Chem. Int. Ed.* **2007**, *46*, 4940.
[61] R. Islas, C. E., J. Robles, T. Heine, J. C. Santos, G. Merino, *Struct. Chem.* **2007**, *18*, 833.
[62] E. R. Abbey, L. N. Zakharov, S. Y. Liu, *J. Am. Chem. Soc.* **2008**, *130*, 7250.
[63] M. Munakata, L. P. Wu, G. L. Ning, T. Kuroda-Sowa, M. Maekawa, Y. Suenaga, N. Maeno, *J. Am. Chem. Soc.* **1999**, *121*, 4968.
[64] L. Brammer, J. C. M. Rivas, R. Atencio, S. Y. Fang, F. C. Pigge, *J. Chem. Soc. Dalton* **2000**, 3855.
[65] R. N. Grimes, *Coord. Chem. Rev.* **2000**, *200*, 773.
[66] T. J. Kealy, P. L. Pauson, *Nature* **1951**, *168*, 1039.
[67] A. Salzer, H. Werner, *Angew. Chem. Int. Ed.* **1972**, *11*, 930.
[68] H. Werner, *Angew. Chem. Int. Ed.* **1977**, *16*, 1.
[69] W. Siebert, *Angew. Chem. Int. Ed.* **1979**, *18*, 949.
[70] W. Siebert, *Angew. Chem. Int. Ed.* **1982**, *21*, 149.
[71] W. Siebert, *Angew. Chem. Int. Ed.* **1980**, *19*, 746.

[72] A. Nakajima, K. Kaya, *J. Phys. Chem. A* **1999**, *104*, 176.
[73] P. Weis, P. R. Kemper, M. T. Bowers, *J. Phys. Chem. A* **1997**, *101*, 8207.
[74] K. Hoshino, T. Kurikawa, H. Takeda, A. Nakajima, K. Kaya, *J. Phys. Chem.* **1995**, *99*, 3053.
[75] H. Akai, *Phys. Rev. Lett.* **1998**, *81*, 3002.
[76] A. E. Ashley, R. T. Cooper, G. G. Wildgoose, J. C. Green, D. O'Hare, *J. Am. Chem. Soc.* **2008**, *130*, 15662.
[77] K. Miyajima, M. B. Knickelbein, A. Nakajima, *J. Phys. Chem. A* **2008**, *112*, 366.
[78] K. Miyajima, A. Nakajima, S. Yabushita, M. B. Knickelbein, K. Kaya, *J. Am. Chem. Soc.* **2004**, *126*, 13202.
[79] K. Miyajima, S. Yabushita, M. B. Knickelbein, A. Nakajima, *J. Am. Chem. Soc.* **2007**, *129*, 8473.
[80] T. Kurikawa, H. Takeda, M. Hirano, K. Judai, T. Arita, S. Nagao, A. Nakajima, K. Kaya, *Organometallics* **1999**, *18*, 1430.
[81] Z. Zhang, X. Wu, W. Guo, X. C. Zeng, *J. Am. Chem. Soc.* **2010**, *132*, 10215.
[82] G. Balazs, F. G. N. Cloke, L. Gagliardi, J. C. Green, A. Harrison, P. B. Hitchcock, A. R. M. Shahi, O. T. Summerscales, *Organometallics* **2008**, *27*, 2013.
[83] R. Pandey, B. K. Rao, P. Jena, M. A. Blanco, *J. Am. Chem. Soc.* **2001**, *123*, 3799.
[84] L. Wang, Z. Cai, J. Wang, J. Lu, G. Luo, L. Lai, J. Zhou, R. Qin, Z. Gao, D. Yu, G. Li, W. N. Mei, S. Sanvito, *Nano Lett.* **2008**, *8*, 3640.
[85] V. V. Maslyuk, A. Bagrets, V. Meded, A. Arnold, F. Evers, M. Brandbyge, T. Bredow, I. Mertig, *Phys. Rev. Lett.* **2006**, *97*.
[86] R. Liu, S.-H. Ke, W. Yang, H. U. Baranger, *J. Chem. Phys.* **2007**, *127*.
[87] K. Xu, J. Huang, S. Lei, H. Su, F. Y. C. Boey, Q. Li, J. Yang, *J. Chem. Phys.* **2009**, *131*.
[88] S. A. Wolf, D. D. Awschalom, R. A. Buhrman, J. M. Daughton, S. von Molnar, M. L. Roukes, A. Y. Chtchelkanova, D. M. Treger, *Science* **2001**, *294*, 1488.
[89] I. Zutic, J. Fabian, S. Das Sarma, *Rev. Mod. Phys.* **2004**, *76*, 323.
[90] S. Sanvito, *Chem. Soc. Rev.* **2011**, *40*, 3336.
[91] S. Sanvito, A. R. Rocha, *J. Comput. Theor. Nanosci.* **2006**, *3*, 624.
[92] S. Sanvito, *Nature Mater.* **2007**, *6*, 803.
[93] S. Sanvito, *Nature Mater.* **2011**, *10*, 484.
[94] S. Sanvito, *Nature Phys.* **2010**, *6*, 562.
[95] G. Henkelman, A. Arnaldsson, H. Jónsson, *Comput. Mater. Sci.* **2006**, *36*, 254.
[96] R. Liu, S. H. Ke, H. U. Baranger, W. T. Yang, *Nano Lett.* **2005**, *5*, 1959.
[97] M. Koleini, M. Paulsson, M. Brandbyge, *Phys. Rev. Lett.* **2007**, *98*, 197202.
[98] S. S. Mallajosyula, P. Parida, S. K. Pati, *J. Mater. Chem.* **2009**, *19*, 1761.
[99] P. Parida, A. Kundu, S. K. Pati, *Phys. Chem. Chem. Phys.* **2010**, *12*, 6924.
[100] L. Zhou, S.-W. Yang, M.-F. Ng, M. B. Sullivan, V. B. C. Tan, L. Shen, *J. Am. Chem. Soc.* **2008**, *130*, 4023.
[101] H. J. Xiang, J. L. Yang, J. G. Hou, Q. S. Zhu, *J. Am. Chem. Soc.* **2006**, *128*, 2310.
[102] M. Urdampilleta, S. Klyatskaya, J. P. Cleuziou, M. Ruben, W. Wernsdorfer, *Nature Mater.* **2011**, *10*, 502.
[103] H. Schumann, J. A. Meese-Marktscheffel, L. Esser, *Chem. Rev.* **1995**, *95*, 865.
[104] F. T. Edelmann, D. M. M. Freckmann, H. Schumann, *Chem. Rev.* **2002**, *102*, 1851.
[105] W. J. Evans, M. S. Sollberger, J. L. Shreeve, J. M. Olofson, J. H. Hain, J. W. Ziller, *Inorg. Chem.* **1992**, *31*, 2492.

[106] J. K. Gibson, *J. Phys. Chem.* **1996**, *100*, 15688.
[107] W. J. Evans, L. A. Hughes, T. P. Hanusa, *J. Am. Chem. Soc.* **1984**, *106*, 4270.
[108] W. J. Evans, L. A. Hughes, T. P. Hanusa, *Organometallics* **1986**, *5*, 1285.
[109] T. V. Timofeeva, J.-H. Lii, N. L. Allinger, *J. Am. Chem. Soc.* **1995**, *117*, 7452.
[110] W. J. Evans, M. A. Johnston, R. D. Clark, J. W. Ziller, *J. Chem. Soc., Dalton Trans.* **2000**, 1609.
[111] N. Magnani, C. Apostolidis, A. Morgenstern, E. Colineau, J.-C. Griveau, H. Bolvin , O. Walter, R. Caciuffo, *Angew. Chem. Int. Ed.* **2011**, *50*, 1696.
[112] R. Sessoli, D. Gatteschi, A. Caneschi, M. A. Novak, *Nature* **1993**, *365*, 141.
[113] D. Gatteschi, A. Caneschi, L. Pardi, R. Sessoli, *Science* **1994**, *265*, 1054.
[114] R. Sessoli, A. K. Powell, *Coord. Chem. Rev.* **2009**, *253*, 2328.
[115] J. D. Rinehart, M. Fang, W. J. Evans, J. R. Long, *J. Am. Chem. Soc.* **2009**, *133*, 14236.
[116] N. Magnani, E. Colineau, R. Eloirdi, J. C. Griveau, R. Caciuffo, S. M. Cornet, I. May, C. A. Sharrad, D. Collison, R. E. P. Winpenny, *Phys. Rev. Lett.* **2010**, *104*, 197202.
[117] N. Ishikawa, M. Sugita, T. Ishikawa, S.-y. Koshihara, Y. Kaizu, *J. Am. Chem. Soc.* **2003**, *125*, 8694.
[118] N. Ishikawa, M. Sugita, W. Wernsdorfer, *J. Am. Chem. Soc.* **2005**, *127*, 3650.
[119] N. Ishikawa, M. Sugita, W. Wernsdorfer, *Angew. Chem. Int. Ed.* **2005**, *44*, 2931.
[120] F. Rostamzadeh Renani, G. Kirczenow, *Phys. Rev. B* **2011**, *84*, 180408.
[121] S. Barraza-Lopez, K. Park, V. Garcia-Suarez, J. Ferrer, *J. Appl. Phys.* **2009**, *105*, 07E309.
[122] S. Voss, M. Fonin, U. Rudiger, M. Burgert, U. Groth, *Appl. Phys. Lett.* **2007**, *90*, 133104.
[123] M. Misiorny, J. Barnas, *Phys. Rev. B* **2007**, *76*, 54448.
[124] A. W. Hofmann, *Proc. R. Soc. Lond.* **1856**, *8*, 1.
[125] P. v. R. Schleyer, j. H, *Pure Appl. Chem.* **1996**, *68*, 209.
[126] Z. F. Chen, C. S. Wannere, C. Corminboeuf, R. Puchta, P. V. Schleyer, *Chem. Rev.* **2005**, *105*, 3842.
[127] M. K. Cyranski, P. V. Schleyer, T. M. Krygowski, H. J. Jiao, G. Hohlneicher, *Tetrahedron* **2003**, *59*, 1657.
[128] T. M. Krygowski, M. K. Cyranski, Z. Czarnocki, G. Hafelinger, A. R. Katritzky, *Tetrahedron* **2000**, *56*, 1783.
[129] V. I. Minkin, M. N. Glukhovtsev, B. Y. Simkin, *Aromaticity and Antiaromaticity: Electronic and Structural Aspects;*, John Wiley & Sons., New York, **1994**.
[130] J. Poater, M. Duran, M. Sola, B. Silvi, *Chem. Rev.* **2005**, *105*, 3911.
[131] M. Guell, E. Matito, J. M. Luis, J. Poater, M. Sola, *J. Phys.Chem.A* **2006**, *110*, 11569.
[132] J. Gomes, R. B. Mallion, *Chem. Rev.* **2001**, *101*, 1349.
[133] V. J. Minkin, M. N. Glukhovtsev, B. Y. Simkin, *Aromaticity and Antiaromaticity: Electronic and Structural Aspects*, Wiley, New York, **1984**.
[134] L. Pauling, J. Sherman, *J. Chem. Phys.* **1933**, *1*, 606.
[135] G. B. Kistiakowsky, J. R. Ruhoff, H. A. Smith, W. E. Vaughan, *J. Am. Chem. Soc.* **1936**, *58*, 146.
[136] A. R. Katritzky, K. Jug, D. C. Oniciu, *Chem. Rev.* **2001**, *101*, 1421.
[137] H. Kollmar, *J. Am. Chem. Soc.* **1979**, *101*, 4832.
[138] D. Peters, D. Lewis, *Facts and theories of aromaticity*, **1975**.

[139] M. K. Cyrañski, T. M. Krygowski, A. R. Katritzky, P. v. R. Schleyer, *J. Org. Chem.* **2002**, *67*, 1333.
[140] M. K. Cyrański, P. v. R. Schleyer, T. M. Krygowski, H. Jiao, G. Hohlneicher, *Tetrahedron* **2003**, *59*, 1657.
[141] P. George, M. Trachtman, A. M. Brett, C. W. Bock, *J. Chem. Soc., Perkin Trans. 2* **1977**, 1036.
[142] W. J. Hehre, R. Ditchfield, L. Radom, J. A. Pople, *J. Am. Chem. Soc.* **1970**, *92*, 4796.
[143] J. A. Pople, L. Radom, W. J. Hehre, *J. Am. Chem. Soc.* **1971**, *93*, 289.
[144] W. J. Hehre, R. T. McIver, J. A. Pople, P. v. R. Schleyer, *J. Am. Chem. Soc.* **1974**, *96*, 7162.
[145] L. Radom, *J. Chem. Soc., Chem. Commun.* **1974**, 403.
[146] D. A. Ponomarev, V. V. Takhistov, *J. Chem. Educ.* **1997**, *74*, 201.
[147] P. George, M. Trachtman, C. W. Bock, A. M. Brett, *J. Chem. Soc., Perkin Trans. 2* **1976**, 1222.
[148] T. M. Krygowski, M. Cyranski, *Tetrahedron* **1996**, *52*, 10255.
[149] T. M. Krygowski, M. Cyranski, *Tetrahedron* **1996**, *52*, 10255.
[150] T. M. Krygowski, *J. Chem. Inf. Comput. Sci.* **1993**, *33*, 70.
[151] P. V. Schleyer, *Chem. Rev.* **2001**, *101*, 1115.
[152] I. D. Madura, T. M. Krygowski, M. Cyranski, *Tetrahedron* **1998**, *54*, 14913.
[153] L. Pauling, *J. Phys. Chem* **1936**, *4*, 673.
[154] J. Aihara, T. Horikawa, *Bull. Chem. Soc. Jpn.* **1983**, *56*, 1853.
[155] W. H. Flygare, R. C. Benson, *J. Am. Chem. Soc.* **1970**, *92*, 7523.
[156] W. H. Flygare, *Chem. Rev.* **1974**, *74*, 653.
[157] T. G. Schmalz, C. L. Norris, W. H. Flygare, *J. Am. Chem. Soc.* **1973**, *95*, 7961.
[158] P. C. M. Van Zijl, B. H. Ruessink, J. Bulthuis, C. MacLean, *Acc. Chem. Res.* **1984**, *17*, 172.
[159] T. G. Schmalz, T. D. Gierke, P. Beak, W. H. Flygare, *Tetrahedron Lett.* **1974**, *15*, 2885.
[160] H. J. Dauben, J. D. Wilson, J. L. Laity, *J. Am. Chem. Soc.* **1968**, *90*, 811.
[161] H. F. Hameka, *J. Chem. Phys.* **1961**, *34*, 1996.
[162] A. McNaught, A. Wilkinson, *Vol. 1997*, Blackwell Scientific Publications, Oxford, **1997**.
[163] B. C, *Fundamentals of molecular spectroscopy*, **1995**.
[164] F. Sondheimer, *Acc. Chem. Res.* **1972**, *5*, 81.
[165] M. Barfield, D. M. Grant, D. Ikenberry, *J. Am. Chem. Soc.* **1975**, *97*, 6956.
[166] J. C. Facelli, D. M. Grant, J. Michl, *Acc. Chem. Res.* **1987**, *20*, 152.
[167] N. D. Epiotis, W. R. Cherry, F. Bernardi, W. J. Hehre, *J. Am. Chem. Soc.* **1976**, *98*, 4361.
[168] A. J. Ashe, T. R. Diephouse, M. Y. El-Sheikh, *J. Am. Chem. Soc.* **1982**, *104*, 5693.
[169] P. v. R. Schleyer, C. Maerker, A. Dransfeld, H. Jiao, N. J. R. v. E. Hommes, *J. Am. Chem. Soc.* **1996**, *118*, 6317.
[170] P. v. R. Schleyer, H. Jiao, N. J. R. v. E. Hommes, V. G. Malkin, O. L. Malkina, *J. Am. Chem. Soc.* **1997**, *119*, 12669.
[171] P. von Ragué Schleyer, M. Manoharan, Z.-X. Wang, B. Kiran, H. Jiao, R. Puchta, N. J. R. van Eikema Hommes, *Org. Lett.* **2001**, *3*, 2465.

[172] C. Corminboeuf, T. Heine, G. Seifert, P. v. R. Schleyer, J. Weber, *Phys. Chem. Chem. Phys.* **2004**, *6*, 273.
[173] E. Hückel, *Z. Phys. A: Hadrons Nucl.* **1931**, *70*, 204.
[174] E. Hückel, *Z. Phys. A: Hadrons Nucl.* **1931**, *72*, 310.
[175] E. Hückel, *Z. Phys. A: Hadrons Nucl.* **1932**, *76*, 628.
[176] J. March, M. Smith, *March's Advanced Organic Chemistry: Reactions, Mechanisms, and Structure*, **2006**.
[177] X. Fradera, M. A. Austen, R. F. W. Bader, *J. Phys. Chem. A* **1998**, *103*, 304.
[178] D. B. Chesnut, L. J. Bartolotti, *Chem. Phys.* **2000**, *257*, 175.
[179] J. Poater, M. Solà, M. Duran, X. Fradera, *J. Phys. Chem A* **2001**, *105*, 2052.
[180] R. F. W. Bader, *Chem. Rev.* **1991**, *91*, 893.
[181] R. Bader, *Atoms in Molecules: A Quantum Theory*, **1990**.
[182] E. Matito, M. Duran, M. Sola, *J. Chem. Phys.* **2005**, *122*, 14109.
[183] P. v. R. Schleyer, M. Manoharan, H. Jiao, F. Stahl, *Org. Lett.* **2001**, *3*, 3643.
[184] H.-L. Liu, B. H. Hoff, T. Anthonsen, *J. Chem. Soc., Perkin Trans. 1* **2000**, 1767.
[185] Z. Zhou, R. G. Parr, J. F. Garst, *Tetrahedron Lett.* **1988**, *29*, 4843.
[186] R. G. Parr, P. K. Chattaraj, *J. Am. Chem. Soc.* **1991**, *113*, 1854.
[187] Z. Zhou, R. G. Parr, *J. Am. Chem. Soc.* **1989**, *111*, 7371.
[188] F. De Proft, P. Geerlings, *Phys. Chem. Chem. Phys.* **2004**, *6*, 242.
[189] G. Moore, *Electronics Magazine* **1965**.
[190] W. L. Chao, B. D. Harteneck, J. A. Liddle, E. H. Anderson, D. T. Attwood, *Nature* **2005**, *435*, 1210.
[191] T. A. J. Duke, R. H. Austin, *Phys. Rev. Lett.* **1998**, *80*, 1552.
[192] J. S. Foresi, P. R. Villeneuve, J. Ferrera, E. R. Thoen, G. Steinmeyer, S. Fan, J. D. Joannopoulos, L. C. Kimerling, H. I. Smith, E. P. Ippen, *Nature* **1997**, *390*, 143.
[193] T. Ito, S. Okazaki, *Nature* **2000**, *406*, 1027.
[194] J. C. McDonald, D. C. Duffy, J. R. Anderson, D. T. Chiu, H. K. Wu, O. J. A. Schueller, G. M. Whitesides, *Electrophoresis* **2000**, *21*, 27.
[195] M. A. Unger, H. P. Chou, T. Thorsen, A. Scherer, S. R. Quake, *Science* **2000**, *288*, 113.
[196] K. De Vos, I. Bartolozzi, E. Schacht, P. Bienstman, R. Baets, *Opt. Express* **2007**, *15*, 7610.
[197] A. Politi, M. J. Cryan, J. G. Rarity, S. Yu, J. L. O'Brien, *Science* **2008**, *320*, 646.
[198] M. Schulz, *Nature* **1999**, *399*, 729.
[199] S. V. F. Vashchenko V. A. , *Physical limitations of semiconductor devices*, Springer.
[200] J. D. Meindl, Q. Chen, J. A. Davis, *Science* **2001**, *293*, 2044.
[201] R. P. Feynman, *J. Microelectromech. Syst.* **1992**, *1*, 60.
[202] S. J. Tans, A. R. M. Verschueren, C. Dekker, *Nature* **1998**, *393*, 49.
[203] J. M. Tour, *Acc. Chem. Res.* **2000**, *33*, 791.
[204] A. R. Rocha, V. M. Garcia-Suarez, S. W. Bailey, C. J. Lambert, J. Ferrer, S. Sanvito, *Nature Materials* **2005**, *4*, 335.
[205] T. Rueckes, K. Kim, E. Joselevich, G. Y. Tseng, C. L. Cheung, C. M. Lieber, *Science* **2000**, *289*, 94.
[206] M. A. Reed, C. Zhou, C. J. Muller, T. P. Burgin, J. M. Tour, *Science* **1997**, *278*, 252.
[207] C. Joachim, J. K. Gimzewski, A. Aviram, *Nature* **2000**, *408*, 541.
[208] C. D. Dimitrakopoulos, P. R. L. Malenfant, *Adv. Mater.* **2002**, *14*, 99.

[209] E. Braun, Y. Eichen, U. Sivan, G. Ben-Yoseph, *Nature* **1998**, *391*, 775.
[210] M. Ratner, *Nature* **2000**, *404*, 137.
[211] M. Petty, *Molecular electronics:from principles to practice*, **2007**.
[212] A. Aviram, M. A. Ratner, *Chem. Phys. Lett.* **1974**, *29*, 277.
[213] R. Martel, T. Schmidt, H. R. Shea, T. Hertel, P. Avouris, *Appl. Phys. Lett.* **1998**, *73*, 2447.
[214] H. E. Katz, Z. Bao, *J. Phys. Chem. B* **1999**, *104*, 671.
[215] Z. J. Donhauser, B. A. Mantooth, K. F. Kelly, L. A. Bumm, J. D. Monnell, J. J. Stapleton, D. W. Price, A. M. Rawlett, D. L. Allara, J. M. Tour, P. S. Weiss, *Science* **2001**, *292*, 2303.
[216] C. P. Collier, G. Mattersteig, E. W. Wong, Y. Luo, K. Beverly, J. Sampaio, F. M. Raymo, J. F. Stoddart, J. R. Heath, *Science* **2000**, *289*, 1172.
[217] M. P. Samanta, W. Tian, S. Datta, J. I. Henderson, C. P. Kubiak, *Phys. Rev. B* **1996**, *53*, R7626.
[218] T. Rueckes, K. Kim, E. Joselevich, G. Y. Tseng, C.-L. Cheung, C. M. Lieber, *Science* **2000**, *289*, 94.
[219] D. Fichou, *J. Mater. Chem.* **2000**, *10*, 571.
[220] G. Raschke, S. Brogl, A. S. Susha, A. L. Rogach, T. A. Klar, J. Feldmann, B. Fieres, N. Petkov, T. Bein, A. Nichtl, K. Kürzinger, *Nano Lett.* **2004**, *4*, 1853.
[221] S. Datta, *Electronic Transport in Mesoscopic Systems*, **1995**.
[222] S. Datta, *Quantum Transport: Atom to Transistor*, **2006**.
[223] Landauer, *IBM J. Res. Dev.* **1957**, *1*, 223.
[224] I. Zutic, J. Fabian, S. Das Sarma, *Rev. Mod. Phys.* **2004**, *76*, 323.
[225] G. Szulczewski, S. Sanvito, M. Coey, *Nature Mater.* **2009**, *8*, 693.
[226] Z. Yi, X. Shen, L. Sun, Z. Shen, S. Hou, S. Sanvito, *ACS Nano* **2010**, *4*, 2274.
[227] G. Hummer, J. C. Rasaiah, J. P. Noworyta, *Nature* **2001**, *414*, 188.
[228] S. J. Tans, M. H. Devoret, H. J. Dai, A. Thess, R. E. Smalley, L. J. Geerligs, C. Dekker, *Nature* **1997**, *386*, 474.
[229] H. Ohnishi, Y. Kondo, K. Takayanagi, *Nature* **1998**, *395*, 780.
[230] D. J. Wold, C. D. Frisbie, *J. Am. Chem. Soc.* **2001**, *123*, 5549.
[231] P. Hohenberg, W. Kohn, *Phys. Rev.* **1964**, *136*, B864.
[232] W. Kohn, L. J. Sham, *Phys. Rev.* **1965**, *140*, A1133.
[233] D. M. Ceperley, B. J. Alder, *Phys. Rev. Lett.* **1980**, *45*, 566.
[234] J. P. Perdew, K. Burke, M. Ernzerhof, *Phys. Rev. Lett.***1996**, *77*, 3865.
[235] J. P. Perdew, Y. Wang, *Phys. Rev. B* **1992**, *45*, 13244.
[236] A. D. Becke, *Phys. Rev. A* **1988**, *38*, 3098.
[237] C. Lee, W. Yang, R. G. Parr, *Phys. Rev. B* **1988**, *37*, 785.
[238] F. A. Hamprecht, A. J. Cohen, D. J. Tozer, N. C. Handy, *J. Chem. Phys.* **1998**, *109*, 6264.
[239] G. B. Bachelet, D. R. Hamann, M. Schlüter, *Phys. Rev. B* **1982**, *26*, 4199.
[240] D. Vanderbilt, *Phys. Rev. B* **1990**, *41*, 7892.
[241] G. W. T. Frisch M. J., H. B. Schlegel, G. E. Scuseria, M. A. Robb, J. R. Cheeseman, G. Scalmani, V. Barone, B. Mennucci, G. A. Petersson, H. Nakatsuji, M. Caricato, X. Li, H. P. Hratchian, A. F. Izmaylov, J. Bloino, G. Zheng, J. L. Sonnenberg, M. Hada, M. Ehara, K. Toyota, R. Fukuda, J. Hasegawa, M. Ishida, T. Nakajima, Y. Honda, O. Kitao, H. Nakai, T. Vreven, J. A. Montgomery, Jr., J. E. Peralta, F. Ogliaro, M. Bearpark, J. J. Heyd, E. Brothers, K. N. Kudin, V. N. Staroverov, R. Kobayashi, J. Normand, K. Raghavachari, A. Rendell, J. C. Burant,

S. S. Iyengar, J. Tomasi, M. Cossi, N. Rega, J. M. Millam, M. Klene, J. E. Knox, J. B. Cross, V. Bakken, C. Adamo, J. Jaramillo, R. Gomperts, R. E. Stratmann, O. Yazyev, A. J. Austin, R. Cammi, C. Pomelli, J. W. Ochterski, R. L. Martin, K. Morokuma, V. G. Zakrzewski, G. A. Voth, P. Salvador, J. J. Dannenberg, S. Dapprich, A. D. Daniels, Ö. Farkas, J. B. Foresman, J. V. Ortiz, J. Cioslowski, and D. J. Fox, *Gaussian 09*, **2009**.

[242] M. W. Schmidt, K. K. Baldridge, J. A. Boatz, S. T. Elbert, M. S. Gordon, J. H. Jensen, S. Koseki, N. Matsunaga, K. A. Nguyen, S. Su, T. L. Windus, M. Dupuis, J. A. Montgomery, *J. Comput. Chem.* **1993**, *14*, 1347.

[243] G. te Velde, F. M. Bickelhaupt, E. J. Baerends, C. Fonseca Guerra, S. J. A. van Gisbergen, J. G. Snijders, T. Ziegler, *J. Comput. Chem.* **2001**, *22*, 931.

[244] J. M. Soler, E. Artacho, J. D. Gale, A. Garcia, J. Junquera, P. Ordejon, D. Sanchez-Portal, *J. Phys.: Condens. Matter* **2002**, *14*, 2745.

[245] G. Kresse, J. Furthmuller, *Phys. Rev. B* **1996**, *54*, 11169.

[246] G. Kresse, J. Furthmuller, *Comp. Mater. Sci.* **1996**, *6*, 15.

[247] G. Kresse, D. Joubert, *Phys. Rev. B* **1999**, *59*, 1758.

[248] J. Chen, M. A. Reed, A. M. Rawlett, J. M. Tour, *Science* **1999**, *286*, 1550.

[249] M. Brandbyge, J.-L. Mozos, P. Ordejón, J. Taylor, K. Stokbro, *Phys. Rev. B* **2002**, *65*, 165401.

[250] A. R. Rocha, V. M. García-Suárez, S. Bailey, C. Lambert, J. Ferrer, S. Sanvito, *Phys. Rev. B* **2006**, *73*, 085414.

[251] J. Taylor, H. Guo, J. Wang, *Phys. Rev. B* **2001**, *63*, 245407.

[252] P. Karamanis, G. Maroulis, *Chem. Phys. Lett.* **2003**, *376*, 403.

[253] G. Maroulis, *Theor. Chem. Acc.*, *129*, 437.

[254] P. Karamanis, G. Maroulis, *J. Phys. Org. Chem.*, *24*, 588.

[255] A. T. Balaban, *Pure Appl. Chem.* **1980**, *52*, 1409.

[256] P. J. Garrat, *Aromaticity*, Wiley, New York, **1986**.

[257] D. Lloyd, *J. Chem. Inf. Comput. Sci* **1996**, *36*, 442.

[258] T. M. Krygowski, M. K. Cyranski, Z. Czarnocki, G. Hafelinger, A. R. Katritzky, *Tetrahedron* **2000**, *56*, 1783.

[259] M. Randic, *Chem. Rev.* **2003**, *103*, 3449.

[260] M. Kertesz, C. H. Choi, S. J. Yang, *Chem. Rev.* **2005**, *105*, 3448.

[261] T. M. Krygowski, B. T. Stepien, *Chem. Rev.* **2005**, *105*, 3482.

[262] X. J. Feng, Q. S. Li, J. D. Gu, F. A. Cotton, Y. M. Xie, H. F. Schaefer, *J. Phys. Chem. A* **2009**, *113*, 887.

[263] A. I. Boldyrev, L. S. Wang, *Chem. Rev.* **2005**, *105*, 3716.

[264] A. Datta, N. S. John, G. U. Kulkarni, S. K. Pati, *J. Phys. Chem. A* **2005**, *109*, 11647.

[265] A. Datta, S. K. Pati, *J. Am. Chem. Soc.* **2005**, *127*, 3496.

[266] A. Datta, S. K. Pati, *Chem. Commun.* **2005**, 5032.

[267] A. Datta, S. S. Mallajosyula, S. K. Pati, *Acc. Chem. Res.* **2007**, *40*, 213.

[268] V. I. Minkin, R. M. Minyaev, *Chem. Rev.* **2001**, *101*, 1247.

[269] A. T. Balaban, D. C. Oniciu, A. R. Katritzky, *Chem. Rev.* **2004**, *104*, 2777.

[270] L. Nyulaszi, *Chem. Rev.* **2001**, *101*, 1229.

[271] G. Periyasamy, N. A. Burton, I. H. Hillier, M. A. Vincent, H. Disley, J. McMaster, C. D. Garner, *Faraday Discuss.* **2007**, *135*, 469.

[272] G. Periyasamy, N. A. Burton, I. H. Hillier, J. M. H. Thomas, *J. Phys. Chem. A* **2008**, *112*, 5960.

[273] H. S. Rzepa, *Chem. Rev.* **2005**, *105*, 3697.
[274] M. Buhl, A. Hirsch, *Chem. Rev.* **2001**, *101*, 1153.
[275] R. B. King, *Chem. Rev.* **2001**, *101*, 1119.
[276] X. Lu, Z. F. Chen, *Chem. Rev.* **2005**, *105*, 3643.
[277] A. K. Manna, S. K. Pati, *J. Phys. Chem. C* **2011**, *115*, 10842.
[278] R. H. Mitchell, *Chem. Rev.* **2001**, *101*, 1301.
[279] E. Stainer, P. W. Fowler, *Phys. Chem. Chem. Phys.* **2004**, *6*, 261.
[280] L. J. Schaad, B. A. Hess, *Chem. Rev.* **2001**, *101*, 1465.
[281] R. Z. Ma, D. Goldberg, Y. Bando, T. Sasaki, *Philos. T. Roy. Soc. A* **2004**, *362*, 2161.
[282] V. D. Khavryuchenko, O. V. Khavryuchenko, Y. A. Tarasenko, V. V. Lisnyak, *Chem. Phys.* **2008**, *352*, 231.
[283] A. J. V. Marwitz, M. H. Matus, L. N. Zakharov, D. A. Dixon, S. Y. Liu, *Angew. Chem. Int. Ed.* **2009**, *48*, 973.
[284] M. J. D. Bosdet, W. E. Piers, *Can. J. Chem.* **2009**, *87*, 8.
[285] J. E. Del Bene, M. Yanez, I. Alkorta, J. Elguero, *J. Chem. Theory Comput.* **2009**, *5*, 2239.
[286] E. R. Abbey, L. N. Zakharov, S. Y. Liu, *J. Am. Chem. Soc.* **2010**, *132*, 16340.
[287] M. J. D. Bosdet, W. E. Piers, T. S. Sorensen, M. Parvez, *Can. J. Chem.* **2010**, *88*, 426.
[288] P. G. Campbell, E. R. Abbey, D. Neiner, D. J. Grant, D. A. Dixon, S. Y. Liu, *J. Am. Chem. Soc.* **2010**, *132*, 18048.
[289] W. Kaim, N. S. Hosmane, *J. Chem. Sci.* **2010**, *122*, 7.
[290] S. M. Mansell, N. C. Norman, C. A. Russell, *Dalton Trans.* **2010**, *39*, 5084.
[291] M. Kranz, T. Clark, *J. Org. Chem* **1992**, *57*, 5492.
[292] J. R. Alvarez-Collado, *Theor. Chem. Acc.* **2011**, *128*, 223.
[293] R. F. W. Bader, A. Streitwieser, A. Neuhaus, K. E. Laidig, P. Speers, *J. Am. Chem. Soc.* **1996**, *118*, 4959.
[294] W. Langenaeker, F. Deproft, P. Geerlings, *J. Phys. Chem.* **1995**, *99*, 6424.
[295] T. M. Krygowski, M. Cyranski, *Tetrahedron* **1996**, *52*, 1713.
[296] F. De Proft, P. Geerlings, *Chem. Rev.* **2001**, *101*, 1451.
[297] D. M. Hudgins, S. A. Sandford, *J. Phys. Chem. A* **1998**, *102*, 329.
[298] A. D. Becke, *J. Chem. Phys.* **1993**, *98*, 5648.
[299] C. Lee, W. Yang, R. G. Parr, *Phys. Rev. B* **1988**, *37*, 785.
[300] R. G. Parr, W. Wang, *Density-Functional Theory of Atoms and Molecules*, Oxford University Press, New York, **1989**.
[301] M. J. Frisch, G. W. Trucks, H. B. Schlegel, G. E. Scuseria, M. A. Robb, J. R. Cheeseman, J. J. A. Montgomery, T. Vreven, K. N. Kudin, J. C. Burant, J. M. Millam, S. S. Iyengar, J. Tomasi, V. Barone, B. Mennucci, M. Cossi, G. Scalmani, N. Rega, G. A. Petersson, H. Nakatsuji, M. Hada, M. Ehara, K. Toyota, R. Fukuda, J. Hasegawa, M. Ishida, T. Nakajima, Y. Honda, O. Kitao, H. Nakai, M. Klene, X. Li, J. E. Knox, H. P. Hratchian, J. B. Cross, C. Adamo, J. Jaramillo, R. Gomperts, R. E. Stratmann, O. Yazyev, A. J. Austin, R. Cammi, C. Pomelli, J. W. Ochterski, P. Y. Ayala, K. Morokuma, G. A. Voth, P. Salvador, J. J. Dannenberg, V. G. Zakrzewski, S. Dapprich, A. D. Daniels, M. C. Strain, O. Farkas, D. K. Malick, A. D. Rabuck, K. Raghavachari, J. B. Foresman, J. V. Ortiz, Q. Cui, A. G. Baboul, S. Clifford, J. Cioslowski, B. B. Stefanov, G. Liu, A. Liashenko, P. Piskorz, I. Komaromi, R. L. Martin, D. J. Fox, T. Keith, M. A. Al-Laham, C. Y.

Peng, A. Nanayakkara, M. Challacombe, P. M. W. Gill, B. Johnson, W. Chen, M. W. Wong, C. Gonzalez, J. A. Pople, *Gaussian 03, Revision C.02*, **2003**.
[302] F. De Proft, P. K. Chattaraj, P. W. Ayers, M. Torrent-Sucarrat, M. Elango, V. Subramanian, S. Giri, P. Geerlings, *J. Chem. Theory Comput.* **2008**, *4*, 595.
[303] F. London, *J. Phys. Radium* **1937**, *8*, 397.
[304] R. McWeeny, *Phys. Rev.* **1962**, *126*, 1028.
[305] R. Ditchfield, *Mol. Phys* **1974**, *27*, 789.
[306] J. R. Cheeseman, G. W. Trucks, T. A. Keith, M. J. Frisch, *J. Chem. Phys.* **1996**, *104*, 5497.
[307] K. Wolinski, J. F. Hilton, P. Pulay, *J. Am. Chem. Soc.* **1990**, *112*, 8251.
[308] F.W. Biegler Konig, R.F.W. Bader, T. Tang, *J. Comput. Chem.* **1982**, *13*, 317.
[309] A. D. A Rehaman, Sairam S.M. and S. K. Pati, *J. Chem. Theory Comput.* **2006**, *2*, 30.
[310] S. P. Dash, S. Sharma, R. S. Patel, M. P. de Jong, R. Jansen, *Nature* **2009**, *462*, 491.
[311] D. A. Allwood, G. Xiong, C. C. Faulkner, D. Atkinson, D. Petit, R. P. Cowburn, *Science* **2005**, *309*, 1688.
[312] V. Dediu, M. Murgia, F. C. Matacotta, C. Taliani, S. Barbanera, *Solid State Commun.* **2002**, *122*, 181.
[313] Y.-W. Son, M. L. Cohen, S. G. Louie, *Nature* **2006**, *444*, 347.
[314] Z. H. Xiong, D. Wu, Z. V. Vardeny, J. Shi, *Nature* **2004**, *427*, 821.
[315] L. Wang, Z. Cai, J. Wang, J. Lu, G. Luo, L. Lai, J. Zhou, R. Qin, Z. Gao, D. Yu, G. Li, W. N. Mei, S. Sanvito, *Nano Lett.* **2008**, *8*, 3640.
[316] C. Herrmann, G. C. Solomon, M. A. Ratner, *J. Am. Chem. Soc.*, *132*, 3682.
[317] F. M. M. R. A. de Groot , P. G. van Engen and K. H. J. Buschow *Phys. Rev. Lett.* **1983**, *50*, 2024.
[318] H. Bea, M. Bibes, M. Sirena, G. Herranz, K. Bouzehouane, E. Jacquet, S. Fusil, P. Paruch, M. Dawber, J. P. Contour, A. Barthelemy, *Appl. Phys. Lett.* **2006**, *88*.
[319] R. Liu, S.-H. Ke, W. Yang, H. U. Baranger, *J. Chem. Phys.* **2007**, *127*.
[320] Y. Li, G. Zhou, J. Li, J. Wu, B.-L. Gu, W. Duan, *J. Phys. Chem. C*, **2011**, *115*, 7292.
[321] T. Kurikawa, Y. Negishi, F. Hayakawa, S. Nagao, K. Miyajima, A. Nakajima, K. Kaya, *J. Am. Chem. Soc.* **1998**, *120*, 11766.
[322] S. Dutta, T. K. Mandal, A. Datta, S. K. Pati, *Chem. Phys. Lett.* **2009**, *479*, 133.
[323] C. N. R. Rao, B. C. Satishkumar, A. Govindaraj, M. Nath, *ChemPhysChem* **2001**, *2*, 78.
[324] W.-Q. Han, H.-G. Yu, C. Zhi, J. Wang, Z. Liu, T. Sekiguchi, Y. Bando, *Nano Lett.* **2008**, *8*, 491.
[325] F. Zheng, G. Zhou, Z. Liu, J. Wu, W. Duan, B.-L. Gu, S. B. Zhang, *Phys. Rev. B* **2008**, *78*.
[326] Z. Yu, M. L. Hu, C. X. Zhang, C. Y. He, L. Z. Sun, J. Zhong, *J. Phys. Chem. C*, *115*, 10836.
[327] A. Du, Y. Chen, Z. Zhu, R. Amal, G. Q. Lu, S. C. Smith, *J. Am. Chem. Soc.* **2009**, *131*, 17354.
[328] D. Y. K. Il Seung Youn, N. Jiten Singh, Sung Woo Park, Jihee Youn, and Kwang S. Kim, *J. Chem. Theory Comput.* **2012**, *8*, 99.
[329] P. Giannozzi, S. Baroni, N. Bonini, M. Calandra, R. Car, C. Cavazzoni, D. Ceresoli, G. L. Chiarotti, M. Cococcioni, I. Dabo, A. Dal Corso, S. de Gironcoli,

S. Fabris, G. Fratesi, R. Gebauer, U. Gerstmann, C. Gougoussis, A. Kokalj, M. Lazzeri, L. Martin-Samos, N. Marzari, F. Mauri, R. Mazzarello, S. Paolini, A. Pasquarello, L. Paulatto, C. Sbraccia, S. Scandolo, G. Sclauzero, A. P. Seitsonen, A. Smogunov, P. Umari, R. M. Wentzcovitch, *J. Phys.: Condens. Matter* **2009**, *21*.
[330] M. Brandbyge, J. L. Mozos, P. Ordejon, J. Taylor, K. Stokbro, *Phys. Rev. B* **2002**, *65*.
[331] A. Yamashiro, Y. Shimoi, K. Harigaya, K. Wakabayashi, *Phys. Rev. B* **2003**, *68*.
[332] Z. Crljen, A. Grigoriev, G. Wendin, K. Stokbro, *Phys. Rev. B* **2005**, *71*.
[333] M. Fiebig, T. Lottermoser, D. Frohlich, A. V. Goltsev, R. V. Pisarev, *Nature* **2002**, *419*, 818.
[334] D. K. James, J. M. Tour, *Chem. Mater.* **2004**, *16*, 4423.
[335] S. C. Erwin, L. J. Zu, M. I. Haftel, A. L. Efros, T. A. Kennedy, D. J. Norris, *Nature* **2005**, *436*, 91.
[336] D. D. Awschalom, M. E. Flatte, *Nature Phys.* **2007**, *3*, 153.
[337] F. Maya, S. H. Chanteau, L. Cheng, M. P. Stewart, J. M. Tour, *Chem. Mater.* **2005**, *17*, 1331.
[338] J. R. Heath, M. A. Ratner, *Physics Today* **2003**, *56*, 43.
[339] C. Joachim, M. A. Ratner, *PNAS* **2005**, *102*, 8801.
[340] C. A. Mirkin, M. A. Ratner, *Annu. Rev. Phys. Chem.* **1992**, *43*, 719.
[341] F. Maya, A. K. Flatt, M. P. Stewart, D. E. Shen, J. M. Tour, *Chem. Mater.* **2004**, *16*, 2987.
[342] S. Lakshmi, S. Dutta, S. K. Pati, *J. Phys. Chem. C* **2008**, *112*, 14718.
[343] L. Bogani, W. Wernsdorfer, *Nature Mater.* **2008**, *7*, 179.
[344] J. Ferrer, V. M. Garcia-Suarez, *J. Mater. Chem.* **2009**, *19*, 1696.
[345] D. Pinkowicz, R. Podgajny, W. Nitek, M. Rams, A. M. Majcher, T. Nuida, S.-i. Ohkoshi, B. Sieklucka, *Chem. Mater.* **2011**, *23*, 21.
[346] G. Christou, *Polyhedron* **2005**, *24*, 2065.
[347] M. N. Leuenberger, D. Loss, *Nature* **2001**, *410*, 789.
[348] C. J. Milios, A. Vinslava, W. Wernsdorfer, S. Moggach, S. Parsons, S. P. Perlepes, G. Christou, E. K. Brechin, *J. Am. Chem. Soc.* **2007**, *129*, 2754.
[349] A. Ardavan, O. Rival, J. J. L. Morton, S. J. Blundell, A. M. Tyryshkin, G. A. Timco, R. E. P. Winpenny, *Phys. Rev. Lett.* **2007**, *98*, 057201.
[350] A. Scheybal, T. Ramsvik, R. Bertschinger, M. Putero, F. Nolting, T. A. Jung, *Chem. Phys. Lett.* **2005**, *411*, 214.
[351] A. J. Epstein, *MRS Bull.* **2003**, *28*, 492.
[352] D. Gatteschi, L. Bogani, A. Cornia, M. Mannini, L. Sorace, R. Sessoli, *Solid State Sci.* **2008**, *10*, 1701.
[353] S. R. Batten, R. Robson, *Angew. Chem. Int. Ed.* **1998**, *37*, 1460.
[354] A. Caneschi, D. Gatteschi, R. Sessoli, P. Rey, *Acc. Chem. Res.* **1989**, *22*, 392.
[355] S. Ferlay, T. Mallah, R. Ouahes, P. Veillet, M. Verdaguer, *Nature* **1995**, *378*, 701.
[356] J. S. Miller, A. J. Epstein, *Angew. Chem. Int. Ed.* **1994**, *33*, 385.
[357] H. Tamaki, Z. J. Zhong, N. Matsumoto, S. Kida, M. Koikawa, N. Achiwa, Y. Hashimoto, H. Okawa, *J. Am. Chem. Soc.* **1992**, *114*, 6974.
[358] G. Aromi, E. K. Brechin, in *Single-Molecule Magnets and Related Phenomena, Vol. 122* (Ed.: R. Winpenny), **2006**, pp. 1.
[359] M. Holynska, D. Premuzic, I.-R. Jeon, W. Wernsdorfer, R. Clerac, S. Dehnen, *Chem. Eur. J.* **2011**, *17*, 9605.

[360] M. Urdampilleta, N.-V. Nguyen, J.-P. Cleuziou, S. Klyatskaya, M. Ruben, W. Wernsdorfer, *Int. J. Mol. Sci.* **2011**, *12*, 6656.
[361] H. Hao, X. Zheng, L. Song, R. Wang, Z. Zeng, *Phys. Rev. Lett.* **2012**, *108*, 017202.
[362] C. Aronica, G. Pilet, G. Chastanet, W. Wernsdorfer, J. F. Jacquot, D. Luneau, *Angew. Chem. Int. Ed.* **2006**, *45*, 4659.
[363] J. P. Costes, S. Shova, W. Wernsdorfer, *Dalton Trans.* **2008**, *14*, 1843.
[364] A. L. Barra, A. Caneschi, A. Cornia, F. F. de Biani, D. Gatteschi, C. Sangregorio, R. Sessoli, L. Sorace, *J. Am. Chem. Soc.* **1999**, *121*, 5302.
[365] A. L. Barra, D. Gatteschi, R. Sessoli, *Chem. Eur. J.* **2000**, *6*, 1608.
[366] J. L. Manson, Q. Z. Huang, J. W. Lynn, H. J. Koo, M. H. Whangbo, R. Bateman, T. Otsuka, N. Wada, D. N. Argyriou, J. S. Miller, *J. Am. Chem. Soc.* **2001**, *123*, 162.
[367] E. C. Yang, D. N. Hendrickson, W. Wernsdorfer, M. Nakano, L. N. Zakharov, R. D. Sommer, A. L. Rheingold, M. Ledezma-Gairaud, G. Christou, *J. Appl. Phys.* **2002**, *91*, 7382.
[368] M. Jeletic, P.-H. Lin, J. J. Le Roy, I. Korobkov, S. I. Gorelsky, M. Murugesu, *J. Am. Chem. Soc.* **2011**, *133*, 19286.
[369] Y. Bi, Y.-N. Guo, L. Zhao, Y. Guo, S.-Y. Lin, S.-D. Jiang, J. Tang, B.-W. Wang, S. Gao, *Chem. Eur. J.* **2011**, *17*, 12476.
[370] P.-H. Lin, W.-B. Sun, M.-F. Yu, G.-M. Li, P.-F. Yan, M. Murugesu, *Chem. Commun.* **2011**, *47*, 10993.
[371] M. A. AlDamen, J. M. Clemente-Juan, E. Coronado, C. Marti-Gastaldo, A. Gaita-Arino, *J. Am. Chem. Soc.* **2008**, *130*, 8874.
[372] G. J. Chen, C. Y. Gao, J. L. Tian, J. K. Tang, W. Gu, X. Liu, S. P. Yan, D. Z. Liao, P. Cheng, *Dalton Trans.* **2011**, *40*, 5579.
[373] S.-D. Jiang, B.-W. Wang, H.-L. Sun, Z.-M. Wang, S. Gao, *J. Am. Chem. Soc.* **2011**, *133*, 4730.
[374] D.-P. Li, T.-W. Wang, C.-H. Li, D.-S. Liu, Y.-Z. Li, X.-Z. You, *Chem. Commun.*, *46*, 2929.
[375] J.-P. Zhao, B.-W. Hu, X.-F. Zhang, Q. Yang, M. S. El Fallah, J. Ribas, X.-H. Bu, *Inorg. Chem.* **2010**, *49*, 11325.
[376] Y. Wang, X.-L. Li, T.-W. Wang, Y. Song, X.-Z. You, *Inorg. Chem.* **2010**, *49*, 969.
[377] T. Jurca, A. Farghal, P.-H. Lin, I. Korobkov, M. Murugesu, D. S. Richeson, *J. Am. Chem. Soc.* **2011**, *133*, 15814.
[378] K. R. Meihaus, J. D. Rinehart, J. R. Long, *Inorg. Chem.* **2011**, *50*, 8484.
[379] J. D. Rinehart, K. R. Meihaus, J. R. Long, *J. Am. Chem. Soc.* **2010**, *132*, 7572.
[380] H. L. C. Feltham, Y. H. Lan, F. Klower, L. Ungur, L. F. Chibotaru, A. K. Powell, S. Brooker, *Chem. Eur. J.* **2011**, *17*, 4362.
[381] R. A. Layfield, J. J. W. McDouall, S. A. Sulway, F. Tuna, D. Collison, R. E. P. Winpenny, *Chem. Eur. J.* **2010**, *16*, 4442.
[382] D. P. Mills, F. Moro, J. McMaster, J. van Slageren, W. Lewis, A. J. Blake, S. T. Liddle, *Nature Chem.* **2011**, *3*, 454.
[383] N. Magnani, C. Apostolidis, A. Morgenstern, E. Colineau, J. C. Griveau, H. Bolvin, O. Walter, R. Caciuffo, *Angew. Chem. Int. Ed.* **2011**, *50*, 1696.
[384] M. Brandbyge, J. L. Mozos, P. Ordejon, J. Taylor, K. Stokbro, *Phys. Rev. B* **2002**, *65*, 165401.

[385] J. P. Perdew, K. Burke, M. Ernzerhof, *Phys. Rev. Lett.* **1996**, *77*, 3865.
[386] Y. Q. Xue, S. Datta, M. A. Ratner, *Chem. Phys.* **2002**, *281*, 151.
[387] J. M. Soler, E. Artacho, J. D. Gale, A. Garcia, J. Junquera, P. Ordejon, D. Sanchez-Portal, *J. Phys.: Condens. Matter.* **2002**, *14*, 2745.
[388] J. R. Cheeseman, G. W. Trucks, T. A. Keith, M. J. Frisch, *J. Chem. Phys.* **1996**, *104*, 5497.
[389] A. E. Reed, L. A. Curtiss, F. Weinhold, *Chem. Rev.* **1988**, *88*, 899.
[390] H. Schumann, R. D. Kohn, F. W. Reier, A. Dietrich, J. Pickardt, *Organometallics* **1989**, *8*, 1388.
[391] E. Di Santo, M. d. C. Michelini, N. Russo, *Organometallics* **2009**, *28*, 3716.
[392] W.P. Ma, Y.C. Wang, L.L. Lv, Y.Z. Jin, J.Y. Nian, D.F. Ji, C.L. Wang, M.J. La, X.B. Wang, Q. Wang, *J Mol Struc-THEOCHEM* **2011**, *977*, 69.
[393] L. Maron, D. Bourissou, *Organometallics* **2007**, *26*, 1100.
[394] Z. Crljen, G. Baranovic, *Phys. Rev. Lett.* **2007**, *98*, 116801.
[395] Z. Crljen, A. Grigoriev, G. Wendin, K. Stokbro, *Phys. Rev. B* **2005**, *71*, 165316.

List of Publications

1. *Density Functional Theoretical investigation of the aromatic nature of the BN substituted Benzene and four ring polyaromatic hydrocarbons*
   Dibyajyoti Ghosh, Ganga Periyasamy, and Swapan K Pati,
   Phys. Chem. Chem. Phys., **13**, 20627 - 20636 (2011)

2. *Electronic and magnetic structure of Fe_n-bis(n-acene) and its BN-analogue: A theoretical study*
   Dibyajyoti Ghosh, Prakash Parida, and Swapan K Pati
   (Submitted, 2012)

3. *Structural, Electronic, Magnetic and Transport Properties of Lanthanide-based Single Ion Magnet*
   Dibyajyoti Ghosh, Prakash Parida, Ganga Periyasamy and Swapan K Pati
   (Submitted, 2012)